Aramco Journal of Technology

WINTER 2023

page 2 /

First Industrial High Power Laser Perforation Deployment

Dr. Sameeh I. Batarseh, Dr. Damian P. San-Roman-Alerigi, Scott Marshall and Dr. Ramona M. Graves

page 30 /

Surfactants Structured by Nanoparticles to Stabilize CO_2 Foam at High Temperature

Prasad B. Karadkar, Dr. Shahid Ali, Tamim Alshehri, Dr. Bader G. Alharbi, Mohammed Alsakkaf, Dr. Muhammad Mansha and Dr. Safyan A. Khan

The *Aramco Journal of Technology* is published quarterly by the Saudi Arabian Oil Company, Dhahran, Saudi Arabia, to provide the company's scientific and engineering communities a forum for the exchange of ideas through the presentation of technical information aimed at advancing knowledge in the hydrocarbon industry.

Management

Amin Nasser
President & CEO, Saudi Aramco

Nabeel A. Al-Jama'
Executive Vice President, HR & Corporate Services

Editorial Advisors

Khalid M. Al-Abdulqader
Senior Vice President, Unconventional Resources

Waleed A. Al Mulhim
Senior Vice President, Petroleum Engineering & Development

Jumaan G. Zahrani
Senior Vice President, Northern Area Gas Operations

Ali A. Meshari
Senior Vice President, Technology Oversight and Coordination

Khaled A. Al Abdulgader
Vice President, Southern Area Drilling & Workover Operations

Najeed I. Abdulrahman
Vice President and Chief Drilling Engineer

Omar S. Al-Husaini
Vice President, Northern Area Drilling & Workover Operations

Faisal N. Al Nughaimish
Vice President and Chief Petroleum Engineer

Khalid Y. Al-Qahtani
Vice President and Chief Engineer

Gerald M. De Nazelle
Director, Research & Development Center

Ghaithan A. Muntasheri
Director, EXPEC Advanced Research Center

Editor

William E. Bradshaw
william.bradshaw.1@aramco.com.sa
tel: +966-013-876-0498

Production Coordination

Johnny Hanson
Corporate Publications, Aramco Americas

Design

Graphic Engine Design Studio
Austin, Texas, U.S.A.

No articles, including art and illustrations, in the *Aramco Journal of Technology* except those from copyrighted sources, may be reproduced or printed without the written permission of Saudi Aramco. Please submit requests for permission to reproduce items to the editor.

The *Aramco Journal of Technology* gratefully acknowledges the assistance, contribution and cooperation of numerous operating organizations throughout the company.

ISSN 1319-2388
© Copyright 2023 Aramco Services Company, all rights reserved.

Dear Reader,

After a publication run of 30 years, the *Aramco Journal of Technology* will end production with this issue.

It has been our pleasure to present the myriad articles across the oil, gas, and geological technologies over the years. We hope that you have enjoyed reading the articles as much as we have in publishing them.

Past editions can be found at: *www.saudiaramco.com/jot*.

Best Regards,

William E. Bradshaw,
Editor

Contents

p. 2 **First Industrial High Power Laser Perforation Deployment**

Dr. Sameeh I. Batarseh, Dr. Damian P. San-Roman-Alerigi, Scott Marshall and Dr. Ramona M. Graves

p. 11 **Wellhead Protective Measures during Well Stimulation Operations; Current Limitations and New Horizons**

Mohammed E. Mukhlifi, Mansour A. Al-Amer, Pandu Wirawan, Mohammed K. Muqri and Mohammad S. Al-Saeed

p. 18 **Combining Machine Learning and Multiphase Flow Model for Hybrid Virtual Flow Metering**

Dr. Anton Gryzlov, Dr. Sergey Safonov, Dr. Boris Krasnopolsky and Dr. Muhammad Arsalan

p. 30 **Surfactants Structured by Nanoparticles to Stabilize CO_2 Foam at High Temperatuer**

Prasad B. Karadkar, Dr. Shahid Ali, Tamim Alshehri, Dr. Bader G. Alharbi, Mohammed Alsakkaf, Dr. Muhammad Mansha and Dr. Safyan A. Khan

p. 38 **Water Hammering Evaluation in Perforation Efficiency for Variable Perforation Designs in Unconventional Horizontal Wells**

Abdulrahman M. Alowaid, Tayyar S. AlTayyar and Karim Mechkak

p. 48 **Ultra-High Speed High Gas Volume Fraction Pump Development**

Dr. Chidirim E. Ejim, Dr. Jinjiang Xiao, Dr. Anton Shakiro, Yaroslav Alexeev and Anton Shkolnyi

p. 54 **Chemical Treatment for Sustainable Acid Fracture Conductivity of Weak Carbonates**

Mahmoud Desouky, Dr. Murtada S. Al Jawad, Dr. Abduljamiu Amao, Dr. Dhafer A. Al-Shehri, Dr. Murtadha J. AlTammar and Dr. Khalid M. Alruwaili

p. 62 **Multilateral Completion Technology to Improve Reservoir Management**

Yousef W. Ameen, Abdulrakeeb Almasri, Abdullah Alsaleh and Mortada A. Alkadem

p. 72 **Use of Logging while Drilling Data and Machine Learning to Predict Maximum Borehole Diameter for Multistage Completion**

Khaqan Khan, Dr. Murtadha J. AlTammar, Rima T. Alfaraj and Rayan A. Alidi

p. 82 **Fracture Network Characterization Beyond Wellbores: A New Approach to Identify Water Corridors through Advanced Resistivity Analysis**

Ida Bagus Gede Hermawan Manuaba, Mohammad K. Aljishi, Gagok I. Santoso and James T. Dolan

First Industrial High Power Laser Perforation Deployment

Dr. Sameeh I. Batarseh, Dr. Damian P. San-Roman-Alerigi, Scott Marshall and Dr. Ramona M. Graves

Abstract /

This article presents the industry's first high power laser (HPL) field perforation and deployment — a successful HPL technology application. The innovative technology could perforate a well without affecting the substrate integrity and damage. The technology is safe, efficient, and cost-effective, providing a long-term alternative to shaped charge guns.

HPL technology has been tested and proven to effectively perforate in all rocks, regardless of strength and composition, including carbonate, shale, sandstones, and others. The success of the past two decades of intensive research has led to the development of the first HPL field system. The system's design is enclosed, providing a safe and environmentally friendly operation; it consists of a laser energy generator, nitrogen tank, coiled tubing (CT), and tool. The device's function is to control the size and shape of the beam that focuses on the targeted formation. The perforation process is done by utilizing the power of a laser to melt, spall, or vaporize the formation. The laser perforation tool can perforate through the casing, cementing into the formation.

The technology was deployed in a cased well. The well is logged pre- and post-laser perforation, and the CT is used to connect the fiber optic cable with the optical bottom-hole assembly (oBHA). The tool can perform multiple perforations in a single trip, with the azimuthal orientation controlled by rotating the head of the device. Laser perforation creates a nondamaging controlled perforation tunnel penetrating the casing, cement, and formation, and it is stress independent.

Introduction

Perforation and drilling are essential activities in energy extraction to connect reservoir rocks with the wellbore and surface production. Current techniques use chemical and explosive methods, which cause mechanical compaction and reduce permeability. Furthermore, these conventional techniques can account for about 4% of global greenhouse gas emissions[1].

An environmentally friendly alternative is to use lasers to drive rapid and localized thermomechanical processes that can alter the physical and chemical structure of the rocks and the fluids within them[2-4]. This technique utilizes a multikilowatt, continuous wave laser, typically in the near-infrared, to induce chemical and physical alterations, e.g., spallation, dissociation, melting, or vaporization of the rock, as well as catalysis of chemical reactions, which enable perforation, drilling, descaling, and fracturing among other applications. Laser methods could enhance the energy extraction's sustainability by dispensing with additives, water, and post-chemical treatment while reducing energy consumption.

Perforation is essential to establishing flow pathways from hydrocarbon-bearing formations to the wellbore. The conventional perforation technique is shaped charges, an explosive method that propels a bullet (shaped charge) through the casing and formation. The explosive nature of the process can generate a crushed zone, which is a cone-shaped volume of formation around the perforation hole and constitutes the region of the most significant damage around the perforated wellbore[5]. Debris from the shattered bullet can be embedded in this zone or remain in the tunnel along with crushed rocks[6].

These two effects combined could significantly decrease the permeability and flow properties of the tunnel. Additionally, the high-pressure and high temperature conditions generated by the explosion can cause damage to the cement sheath, or the debonding of the cement interfaces, resulting in fluid channeling during hydraulic fracturing treatment[7]. New methods have been developed to counter these effects, e.g., hydrajet, acid jetting, and back surging with maximum differential pressure; however, an inherent drawback of either explosive or chemical-based technique is that they can compromise the wellbore integrity by locally deforming and eroding the casing, which over time could lead to casing collapse and the loss of the wellbore[8, 9].

Addressing these challenges has led to the development of alternative technologies explicitly focusing on environmental sustainability. Of these, high power laser (HPL) technology has shown significant potential.

This method leverages dielectric heating to induce a localized phase change in the rock, e.g., dissociation, sublimation, melting, and evaporation. The process does not damage the formation, casing, or cement. Instead, it improves the permeabilities and porosities of the perforated rocks around the tunnel and adjacent zone, potentially improving production output.

Although the heat affected zone extends radially outwards into the metal and cement, the large heat sink provided by the tubing ensures the heat quickly dissipates into the surrounding unaffected volume, helping to prevent excessive heat buildup and maintaining the macroscopical integrity of the heat affected zone.

Note that depending on the HPL exposure at the microstructural level, the metal may undergo a process of solidification and recrystallization that changes its microstructure while preserving its structural integrity and original volume.

Finally, a unique attribute of laser perforation is its precise directional flexibility. Unlike traditional methods, which are often limited by the state of stress in the rock, laser perforations can propagate the perforation in any desired direction. This unique property is attributed to the electromagnetic-thermal-mechanical process during laser perforation, independent of the rocks' stresses. From an environmental perspective, the laser perforation method also shows clear advantages. It does not consume water or chemicals. Notably, it eliminates the need for chemical well cleanup because it does not leave any debris.

HPL Technology

Many HPLs are available in the market and research labs. The research and field-tests related to this article employed continuous wave near-infrared multimode lasers with multikilowatt outputs, i.e., $\lambda = 1064$ nm $\pm$ 10 nm, $P > 5$ *kW*. The term continuous wave in this context implies that the HPL beam has a constant amplitude and frequency from generation to operation. In all experiences, the illumination with the HPL beam is continuous or quasi-continuous, i.e., the exposure time is several orders of magnitude higher than the frequency of the laser light. The manuscript will use the terms HPL and laser indistinctively.

HPL perforation technology is an innovative alternative to conventional perforation methods, which use explosives or acids to perforate. The propagation of the laser beam depends on the electromagnetic thermal coupling between the subsurface material; therefore, unlike any mechanical process, the propagation direction of the laser, and consequently the perforation, is independent of the state of stresses of the formation. The user can target any wellbore region and create a tunnel in any orientation, thereby enabling complex perforation designs. The laser perforated tunnel has improved permeability and porosity with positive implications for flow assurance and productivity enhancement. The technology is cost-effective, environmentally friendly, waterless, chemical-free, and safe (thanks to electronic interlocks that prevent misfiring from occurring).

The deployment of a HPL tool into a live well in the field marked a significant milestone for the industry. This achievement demonstrated four key features: (1) the HPL generator can be operated reliably in field conditions; (2) it is possible to transmit an HPL beam through an fiber optic cable to a subterranean target hundreds of meters under the Earth; (3) it is possible to design optical bottom-hole assemblies (oBHAs) to direct that laser beam to a preselected region; and (4) HPL beams can be used to perforate (in situ) through multiple casing strings and formations without damaging the casing and improving the flow properties of the reservoir.

The operation's success built upon two decades of research and development, including fundamental analysis, technical demonstration, prototype tests, field trial, and field deployment.

Early Stage: Fundamental Research

This section discusses only the feasibility tests. It is not a summary of the last 20 years of research; instead, it provides an overview of the first experiments conducted by Batarseh (2001)[2], which proved that HPLs could pierce through any wellbore material. These experiments provided crucial insights into the efficiency and limitations of the process, ultimately informing the ever-evolving R&D roadmap to bring HPL tools to the field. The work involved many experiments with thousands of distinct rocks and conditions, including in situ (high-pressure, high temperature, saturation), casing simulations, and varying laser parameters (beam size, time on target, power, and purging fluid). Figure 1 presents the first reported results of the perforation experiments conducted on different rock samples using varying power levels (2 *kW*, 3 *kW*, and 6 *kW*).

The interaction of the HPL beam and the rock depends on different parameters. For example, depending on the power level and rock type, the process may benefit from adding a cooling time. Figure 2 illustrates this fact in Berea Gray sandstone and a 5 *kW* HPL. In this case, the findings suggested that maintaining a continuous beam for approximately 12 seconds, followed by a pause and repetition, was better than constant illumination[2]. In another set of experiments, various steel thicknesses ranging from 0.25" to 1" were exposed to a 5-*kW* laser with a 0.35" beam size, Fig. 2. The penetration time was recorded using air and nitrogen gases; the results are presented in Fig. 3.

Cement optimization experiments were performed on Class Y, Class G, and Class SY250 types of cement. The penetration depth was measured and displayed in Fig. 4.

The experiment was repeated on samples that had been cased and cemented. Figure 5 presents images of the rock samples

Fig. 1 *The rate of penetration (ft/hr) on Berea Gray sandstone (BG), limestone (Ls), shale (Sh), sandstone reservoir (Sst), Berea Yellow sandstone (BY), and granite white (GW) and granite feldspar (GF). The ROP extrapolation is for illustration only and not to scale[2].*

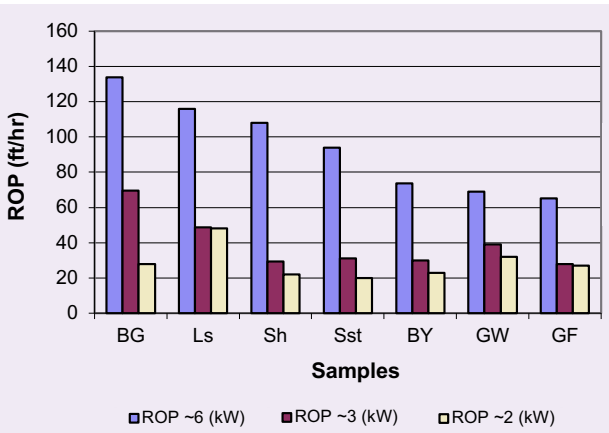
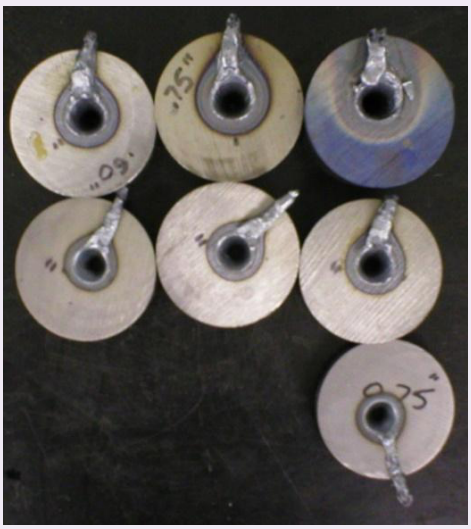


Fig. 2 *Examples of perforation through the simulated casing[2].*



after being exposed to 5-*kW* laser energy.

In situ conditions were simulated using a triaxial test cell for the cased samples. The experiments were conducted under downhole perforation conditions, and the results indicated an improvement in laser perforation at 2,000 psi stress, Fig. 6. Additionally, the sample was saturated with brine and oil during testing[10]. Specific energy is required to remove a unit of rock mass at some given condition.

Tool Development

This phase concerns the design, selection, and integration of optomechanical, optical, and hydraulic components. This phase is subject to continuous innovation. An essential outcome of this phase was establishing a process and platform that enabled constant improvement of design and fabrication.

The tool serves three purposes: (1) propagate the beam from the output of the laser or fiber to the target; (2) shape the beam for interaction; and (3) purvey the means to propagate the beam through the wellbore to the target, typically using a gas assist or purging. The tool integrates optical, mechanical, and electronic systems needed to attain these functions[10]:

- Outcouple the laser beam from the fiber.
- Transform the beam and its profile, e.g., focusing, defocusing, collimation, transformation.
- Control and guide purging fluids.
- Direct the laser beam to the target.
- Evaluate the interaction between the laser beam, the environment, and the rock.
- Monitor the environment.

The ultimate laser tool for the subsurface must be versatile, compact, reliable, sturdy, and efficient. The critical components and challenges in the tool design phase are:

1. Cable: Provides conveyance and isolation of the fiber optic and electric wires. The cable must keep the fibers locally straight and free of strain, either of which can seriously disrupt the HPL's propagation and lead to power or confinement loss.
2. Optics: Transmit, direct, and modify the beam as needed for the operation. High power optics require unique materials, antireflecting coatings, and constant cooling. The critical areas of concern are:
   - Optical materials: These are the essential building blocks of any optical component. These materials must satisfy two crucial demands: (1) be apt for high temperature and high-pressure environments, and (2) have low optical absorption and a high damage threshold within the frequency range of the laser.
   - Optical coatings: Protect the optics from damage and improve their transmission or reflection performance. These

Fig. 3 *Penetration time vs. depth in Berea Gray sandstone using two purge gases: air, and nitrogen[2].*

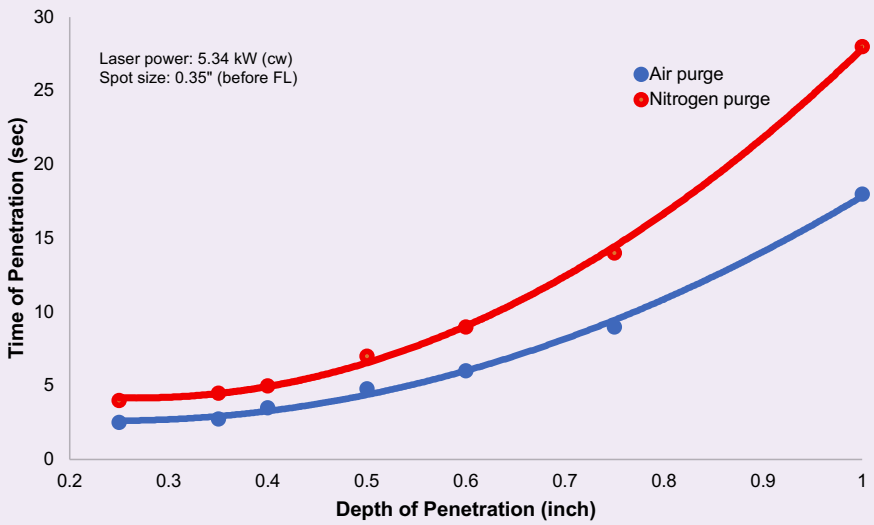
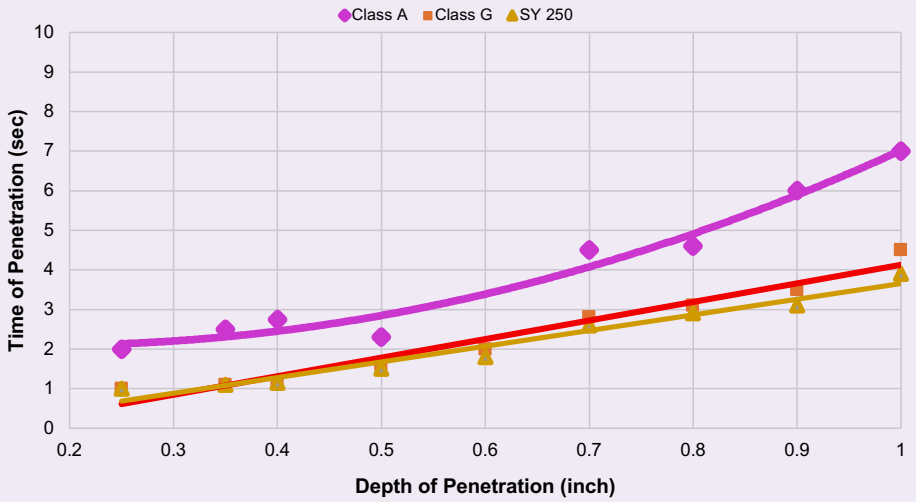


Fig. 4 *Penetration time vs. depth in different cement classes using air purge[2].*



coatings, however, can be easily damaged by temperature and debris.

- Thermal management: Ensures the optics' alignment and stability, impacting the laser's propagation quality. At the surface, water or air cooling is typically used; however, conveying water lines to the subsurface increases the complexity of deployment. Alternative cooling methods are still under investigation.

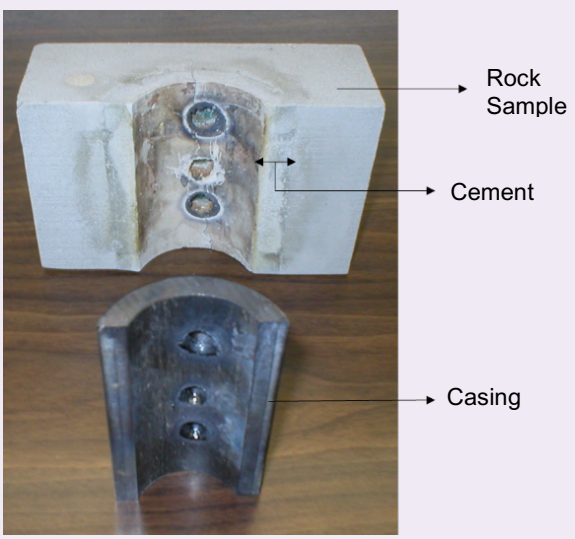
3. An optomechanical design is also vital to enable the precise control of the laser. These systems and their electronic components must be robust, reliable, and stable under various operational conditions. The key challenges are:

- Thermal management: Optomechanical devices control the position of the optical elements and assist in dissipating heat from the optics. Therefore, thermal management is crucial to ensure fast heat dissipation and the stability of the electronic and electromechanical systems. Similar to the optical elements, the complexity lies in providing efficient thermal management using passive and electrical methods.
- Vibration isolation: Active or passive control systems that safeguard the stability of the optical components, thereby ensuring the reliability and performance of the laser propagation.

4. Purging: High velocity and high-pressure fluid that provides a clear path for the laser propagation from the tool's output to the target. These fluids must be transparent or have a low optical loss at the wavelength range of the laser. Using near-infrared lasers implies that aqueous fluids and brines are unsuitable.

5. Enclosure: Protects the optical and electronic systems from the downhole environment. The tool must be lightweight, slim (typical outer diameter below 2½"), and robust.

Fig. 5 *A photo of three laser perforations pierced through a simulated cased wellbore consisting of the casing (stainless steel, 1"), cement (concrete, 2"), and rock (sandstone). The image shows that the casing is undeformed after the process[2].*



First Downhole Laser Tool

Figure 7 shows the design of the first HPL perforation tool with an optional centralization and casing collar locator. It was designed to pierce and cut through casing, cement, and rock formations. It is comprised of two subassemblies:

- The coil head assembly interfaces the coiled tubing (CT), laser perforation cutting head, dual flapper flow valves, hybrid fiber optic cable termination, and emergency mechanical disconnect.
- The laser cutting head consists of beam-forming optics, optomechanical components, a fiber optic cable connector, and an electrically driven rotating laser perforating head.

This tool uses nitrogen for cooling and purging. The downhole tool is conveyed via CT, employing the conventional pressure

Fig. 6 *A comparison of the specific energy needed to perforate sandstone and limestone under different confining pressures[2].*

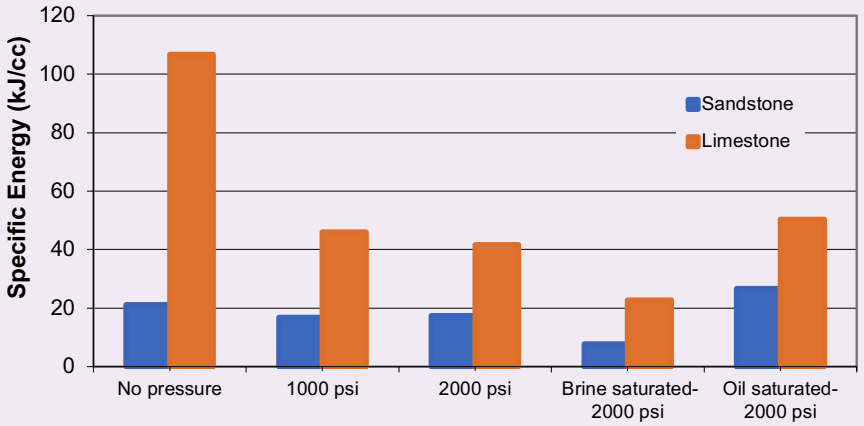


Fig. 7 *The HPL perforation tool at the yard test, showing the tool's rotational head and beam port connected to the CT.*



control equipment at the wellhead. Once deployed to the preferred target depth for perforation, the laser perforation cutting head directs the HPL beam to create single-shot holes at various phase angles or custom-length radial slots. The interaction between the laser and each of the materials in the target zone — casing, cement, and rock formation — is a function of the properties of the HPL beam (transversal energy distribution, wavelength, polarization) and each material (mainly thermal and electromagnetic).

The coupling between them heats the illuminated area, which supports each material's controlled phase or chemical change, including retorting, annealing, and removal through melting, evaporation, sublimation, dissociation, and spallation, i.e., perforation.

Field Integration, Yard Test, and Field Deployment

The third step focused on field system integration of the HPL generator, chiller, control unit, cable conveyance, CT, and all ancillary systems. The packaged fiber optics and the cables were spooled in the CT reel. Figures 8 and 9 show the laser tool and its components, respectively. Figure 10 shows the integrated system during yard testing.

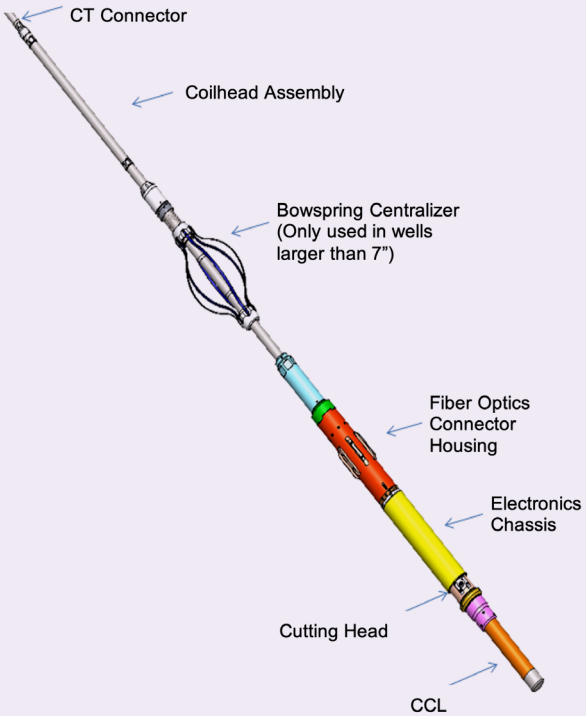
Surface System and Auxiliary Equipment

Laser skid: Figure 11 shows the portable steel frame and climate-controlled units that house a 20-*kW* HPL with the fiber optic coupler and the chiller. The laser beam is coupled first to the surface fiber optic cable and then to the hybrid fiber optic cable for conveyance to the downhole. The hybrid cable includes the primary and backup fiber optic and electric wires.

Chiller Skid: The chiller skid is a portable steel frame with a 243,000 Btu water chiller installed. This chiller unit circulates coolant fluid (water) to the laser, inside the laser skid, via 1.5" supply hoses.

The system utilizes up hole and downhole telemetry hardware to provide real-time tool control and to track the overall

Fig. 8 *A diagram of the oBHA. From top to bottom, is a CT connector, coil head assembly, bowspring centralizer, fiber optic and connector housing, electronics, cutting head, and the casing collar locator.*



system integrity via pressure, temperature, and optical sensors. In addition, this system offers a lock-out safety system for HPL functions.

CT unit: The downhole laser perforation tool is deployed via a conventional CT unit, which consists of a CT reel, hydraulic injector, hydraulic power unit, and coil control room. Spooled onto the CT drum is a unique CT string. A hybrid fiber optic cable has been installed within the CT string, consisting of a fiber optic cable, electrical power/signal to the tool, and mechanical cable integrity functionality.

Power generation: A 200-*kW* portable generator is required to provide 480 V/3 Phase power to the laser, chiller, and downhole laser tool. The generator is installed by interconnecting the laser and chiller directly to the output lugs and can provide 220 V/120 V ancillary power to other components.

Nitrogen pumping system: The liquid nitrogen pumping system is utilized to produce nitrogen gas for the downhole tool to cool the optic components, provide clean gas across the optical pressure window interface, as well as provide a path for the laser beam to travel through the downhole liquids and move any molten material out of the way.

The pumping system comprises a nitrogen liquid storage tank, triplex pump, heat recovery system, and control panel.

Field Trial Operation

The objectives of the field-test were fourfold: First, to ensure the reliable operation of the HPL generator in field conditions. Second, to demonstrate the transmission of the HPL beam through a fiber optic cable to a target deep underground. Third, to design and test the oBHA capable of directing the laser beam to a specific region of interest. Last, to prove that the HPL beam

Fig. 9 *Photos of the conveyance cable mounted on a CT rig at the yard. The cable carries the fiber optics and electrical wires required to operate the oBHA. The cable may include more than one fiber and conductor, depending on the application. The cable provides mechanical and environmental isolation to the fiber optics.*

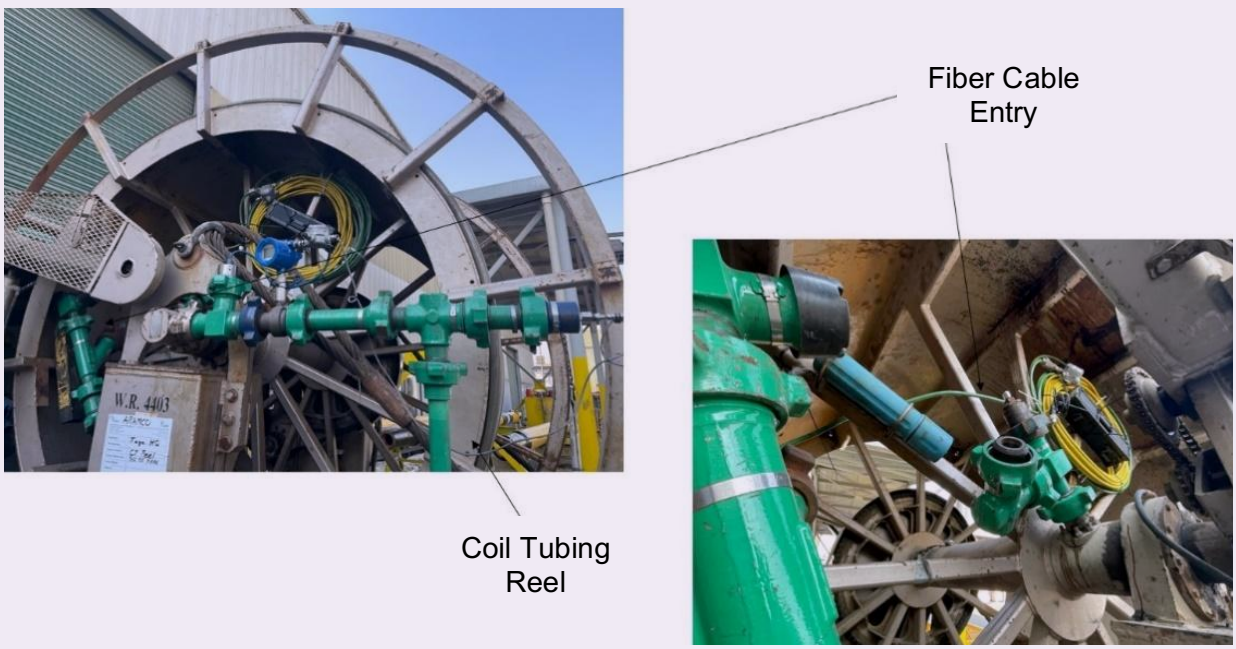


Fig. 10 *A photo of the integrated laser system at the yard. The image was taken during the yard and function test of the system.*



Fig. 11 *A photo of the laser (left) and chiller (right) skids designed for field operation.*





can effectively perforate through multiple casing strings and formations, enhancing the flow properties of the rock. Therefore, quantitative and qualitative assessments are vital at each phase.

The perforation technology's performance was verified in three stages: pre-job, operation, and post-perforation. Pre- and post-analysis involved using downhole video, ultrasound, and caliper logs. The procedure was monitored through backscattered luminosity, component temperatures, and wellhead pressure. The luminosity acts as a crucial indicator of the perforation process, ensuring operators that material removal is occurring. Temperature readings provide insights into the health of the optical elements. Any sudden temperature increases the telltale signs of malfunction in the optical assembly or its components. The bottom well pressure sensor is a qualitative indicator of successful piercing; any reduction signals a breakthrough.

The deployment process is similar to any other CT tool except for monitoring the speed to avoid building stresses or strain in the cable. Nitrogen gas was continuously injected during the perforation operation. Three scenarios were demonstrated: (1) a straight shot, (2) two shots at 180°, and (3) creating a slot by slightly rotating the tool's head during perforation.

In the first scenario, the HPL power gradually increased from zero to 12 *kW* while monitoring wellhead pressure, reflection, and temperature. The luminosity and pressure sensors confirmed the

successful perforation. The second scenario involved initiating two perforation shots at 180° facing; this is done by rotating the head to create the oriented shot. The third scenario entailed creating a slot by initiating a perforation and rotating axially 2°.

The successful deployment of HPLs in a live well showcases the potential of this advanced technology in the oil and gas industry. By utilizing HPLs, operators can achieve more precise and efficient drilling operations, reduce the environmental impact, and enhance overall well productivity.

Conclusions

The HPL perforation tool offers several advantages over traditional methods. It is a contactless, nondamaging, and nonexplosive technique. The laser beam can be precisely targeted to any desired wellbore region at any angle. The laser perforated tunnel has improved permeability and porosity, positively impacting flow assurance and productivity while being cost-effective, environmentally friendly, and devoid of water usage or chemical additives.

The advantages of HPL perforation have revolutionized perforation operations in several ways:

- Nonexplosive technology: HPL perforation utilizes diode laser-based technology, ensuring safe operation. The energy is transmitted to the tool through a fiber optic cable, making it safe to handle both at the surface and during the process.
- Controlled operation: With built-in engineering controls such as sensors and interlocks, there is no chance of misfiring. Multiple sequential steps must be enabled before the laser perforation tool can be fired, ensuring a controlled and safe operation.
- Precise perforation shape: HPLs precisely control the perforation tunnel's shape, depth, and size. The laser power can be tuned from the surface, allowing real-time control over the perforation depth.
- Stress independence: HPLs can perforate in any direction, regardless of the state of stresses in the near wellbore region and formation. This capability ensures flexibility and efficiency in the perforation process.
- Perforation in any formation: HPL perforation is effective in perforating any formation, regardless of its compressive strength. This versatility eliminates the need for specialized tools for diverse types of formations.
- Multiple shots in one trip: The on-off functionality of the laser enables multiple perforation shots in a single trip. This feature eliminates the need for repeated trips in and out of the wellbore, saving time and resources.
- Orientation control: The laser perforation tool features a rotational head that can turn 360°, allowing for shots at different azimuthal orientations. This flexibility enhances the precision and effectiveness of the perforation process.
- Formation structure independence: Laser perforation is independent of the formation's structure, including fractures, laminations, and heterogeneity. The laser can effectively perforate through such formations, ensuring consistent results.
- Enhanced tunnel permeability: HPL perforation improves the permeability of the tunnel. The contactless laser enhances the tunnel permeability by operating without physical impact, improving flow dynamics.
- Phase control: Laser parameters such as power and time can be controlled to manipulate the phase of the rock. The laser can melt, spall, or vaporize the formation, providing further control and customization in the perforation process.

The field trials were a crucial milestone of the technology development, attesting to its reliability, efficacy, and environmental benefits, while providing key insights and data for engineering the next generation of tools and subsystems. The successful deployment of a HPL tool to perforate wells signifies a noteworthy advancement in the oil and gas industry. This technology's benefits — from improved permeability and reduced formation damage to environmental friendliness — suggest that laser perforation could be a game changer in the industry's quest for efficient, sustainable production techniques.

Acknowledgments

This article was presented at the SPE Annual Technical Conference and Exhibition, San Antonio, Texas, October 16-18, 2023.

References

1. Beck, C., Rashidbeigi, S., Roelofsen, O. and Speelman, E.: "The Future is Now: How Oil and Gas Companies can Decarbonize," McKinsey Company, January 2020, 7 p.
2. Batarseh, S.I.: "Application of Laser Technology in the Oil and Gas Industry: An Analysis of High Power Laser-Rock Interaction and its Effect on Altering Rock Properties and Behavior," Ph.D. thesis, Colorado School of Mines, 2001, 214 p.
3. Batarseh, S.I., Gahan, B.C., Graves, R.M. and Parker, R.A.: "Well Perforation Using High Power Lasers," SPE paper 84418, presented at the SPE Annual Technical Conference and Exhibition, Denver, Colorado, October 5-8, 2003.
4. Salavati, S.: "Applied High Power Laser in Drilling Oil and Gas Wells," *SPIE Proceedings*, Vol. 11981, Fiber Lasers XIX: Technology and Systems, March 2022.
5. Asadi, M. and Preston, F.W.: "Characterization of the Jet Perforation Crushed Zone by SEM and Image Analysis," *SPE Formation Evaluation*, Vol. 9, Issue 2, June 1994, pp. 135-139.
6. Campos, H., Martinez, S., Pizarro, H., Kessler, C., et al.: "Geomechanical Applications for Near-Balance and Dynamic Underbalance Perforating Technique in Overpressured Gas Zones in Burgos Basin," SPE paper 108480, presented at the International Oil Conference and Exhibition in Mexico, Veracruz, Mexico, June 27-30, 2007.
7. Yan, Y., Guan, Z., Yan, W. and Wang, H.: "Analysis Method of Cement Sheath Damage Zone After Perforation," SPE paper 196556, presented at the SPE/IATMI Asia Pacific Oil and Gas Conference and Exhibition, Bali, Indonesia, October 29-31, 2019.
8. Littleford, T., Battistel, A., Simpson, G. and Wardynski, K.: "High Resolution Solid-State Acoustic Imaging for Advanced Well Integrity and Deformation Assessments in Conventional and Unconventional Wells," SPE paper 205933, presented at the SPE Annual Technical Conference and Exhibition, Dubai, UAE, September 21-23, 2021.
9. Littleford, T., Wardynski, K., Battistel, A. and Simpson, G.: "High Resolution Acoustic Imaging for Geometric Quantification of Eroded Perforations in Hydraulically Fractured Wells," paper presented at the Unconventional Resources Technology Conference, Houston, Texas, July 26-28, 2021.
10. Batarseh, S.I., Graves, R.M., San-Roman-Alerigi, D.P. and Chand, K.: "Laser Perforation: Lab to the Field," SPE paper 188729, presented at the Abu Dhabi International Petroleum Exhibition and Conference, Abu Dhabi, UAE, November 13-16, 2017.

About the Authors

Dr. Sameeh I. Batarseh

Ph.D. in Petroleum Engineering, Colorado School of Mines

Dr. Sameeh I. Batarseh is a Petroleum Engineering Consultant working with the Production Technology Team of Saudi Aramco's Exploration and Petroleum Engineering Center – Advanced Research Center (EXPEC ARC). Currently, he is the Focus Area Champion of the Unconventional Resources leading the High-Power Laser Program. Sameeh's area of interest is to develop an in situ laser application in drilling, perforation and fracturing, among many other applications with a focus on unconventional reservoirs.

He is an active member of the Society of Petroleum Engineers (SPE), serving the society since 1992 while holding different positions, including sitting on the SPE Executive Advisory Committee, ATCE Program Committees (Chairperson), subcommittees (chair and member). Sameeh was also on the board and Vice Chair for the Western Region USA San Joaquin Valley chapter. His service is recognized worldwide as he received the SPE President Section Award of Excellence, Regional Service Award, and is a SPE Distinguished Lecturer, Distinguished Member and Editorial Review Committee Technical Editor. He has organized over 54 SPE technical workshops.

Sameeh has authored or coauthored more than 92 articles with high-impact publications, and has an H-Index of 42. He holds 96 patents (44 granted patents and 52 patents in progress).

Sameeh received his Ph.D. degree in Petroleum Engineering from the Colorado School of Mines, Golden, CO.

Dr. Damian P. San-Roman-Alerigi

Ph.D. in Electrical Engineering, King Abdullah University of Science and Technology

Dr. Damian P. San-Roman-Alerigi is a Petroleum Scientist working with the Production Technology Team of Saudi Aramco's Exploration and Petroleum Engineering Center – Advanced Research Center (EXPEC ARC). His focus is on developing the next generation of subsurface photonic and electromagnetic tools.

Damian's previous research focused on the interaction of waves with complex media and its application to subsurface technologies. His work encompasses different areas of science and engineering, from oil and gas to applied mathematics. He has published papers in various international journals and conferences around the world.

Damian received his B.S. degree in Physics from the National Autonomous University of Mexico, Mexico City, Mexico. In 2008, he enrolled in King Abdullah University of Science and Technology (KAUST) as a founding class student where he completed his M.S. degree in 2010, and his Ph.D. degree in 2014, both in Electrical Engineering.

Scott Marshall

B.S. in Mechanical Engineering, Louisiana State University

Scott Marshall is the Vice President of Operations for Foro Energy, where since 2011 he has served as a Program Manager, Product Champion, and most recently, as Global Decommissioning Manager.

Scott's focus has been on developing new material removal processes and tools using Foro Energy's proprietary laser cutting technology. These advances in laser material removal applications will be utilized in a wide range of offshore and onshore tools, which will be implemented in intervention, production enhancement, as well as plug and abandonment programs worldwide.

He has been involved in the oil field service industry for 18 years in a variety of operational, technical, and service roles. Prior to joining Foro Energy, Scott was a Project Manager for Ocean Subsea Services, Norse Cutting (NCA) and Oceaneering, where he was responsible for the planning and execution of subsea and surface tooling utilized in conductor and platform removal campaigns.

Scott received his B.S. degree in Mechanical Engineering from Louisiana State University, Baton Rouge, LA.

Dr. Ramona M. Graves

Ph.D. in Petroleum Engineering, Colorado School of Mines

Dr. Ramona M. Graves is the retired Vice Provost for International Initiatives, the retired Dean of the College of Earth Resource Sciences and Engineering and an Emeritus Professor of Petroleum Engineering at the Colorado School of Mines in Golden, CO.

In 2006, she was awarded an Honorary Doctorate from the Mining University of Leoben, Austria. The commendation reads "... recognition of her significant scientific achievements in the area of laser/rock interaction." Ramona is the first woman to receive this honor in the 166-year history of the university. Previous recipients include Herbert C. Hoover, former U.S. president; Hans Hoefer, the pioneer of petroleum engineering in the Austrian-Hungarian Empire; and Ahmed Z. Yamani, the former Minister of Petroleum and Mineral Resources of Saudi Arabia.

She has an extensive background in multidisciplinary reservoir characterization, rock mechanics, environmental issues in petroleum development and production, and high power laser-rock fluid interaction.

During Ramona's career, she has been an active member of the Society of Petroleum Engineers (SPE), serving on and chairing many international SPE committees as well as being on the SPE Board of Directors as the Director of Academia (2018-2020). In addition, she is an active member of seven other professional societies, which relate to her areas of expertise.

Ramona received her Ph.D. in Petroleum Engineering from the Colorado School of Mines, Golden, CO.

Wellhead Protective Measures during Well Stimulation Operations; Current Limitations and New Horizons

Mohammed E. Mukhlifi, Mansour A. Al-Amer, Pandu Wirawan, Mohammed K. Muqri and Mohammad S. Al-Saeed

Abstract /

Wellhead and production trees are the primary safety barriers on any gas, oil, and water wells. Such wells may require flowing corrosive or abrasive fluids through the permanent wellhead components as part of well stimulation to restore well productivity.

This article describes the limitations of the available methods to protect wellhead equipment during acid stimulation jobs and proposes a new solution that will provide the required protection and field operation optimization.

Current wellhead protection solutions during well stimulation activities fall under two methods: utilizing sacrificial equipment during well stimulation or utilizing tree savers on permanent wellhead equipment. Both approaches have their drawbacks. The former involves additional operational cost to install and remove the sacrificial equipment. Furthermore, well securement involves killing the well, which will diminish the effectiveness of the stimulation job. The latter utilizes proprietary technology that is limited by well completion size and does not offer protection for all production tree sizes.

The proposed solution involves setting an isolation sleeve across the permanent wellhead equipment. A sacrificial setup is installed on top of the permanent production tree to facilitate isolation sleeve installation, well stimulation activities and maintain well control requirements. The sleeve will be retrieved and the sacrificial setup removed once the stimulation operations are concluded.

This technology bypasses the limitations of the available methods. It provides full protection from the production tree to the tubing hanger from abrasive fluids pumped, and pressure during well stimulation jobs. Furthermore, it does not require killing the well to remove the sacrificial setup, resulting in optimizing rig operations and maximizing the benefit of well stimulations. Finally, it has no limitations to production tree size, unlike the existing solutions.

The methodology presented in this article provides a novel solution to ensure complete protection to the wellhead equipment during well stimulation, minimize operation costs, and bypass the current limitations from the available solutions in the market.

Introduction

Well stimulation is defined as "treatment performed to restore or enhance the productivity of a well." This involves pumping special fluids at high pumping pressures to fracture the hydrocarbon reservoir or remove formation damage. The treatment fluids can involve acids, which are very abrasive to the wellhead equipment — mainly the production tree and tubing bonnet. If not done properly, the well integrity will be compromised and workover operations will be required to replace the damaged wellhead components.

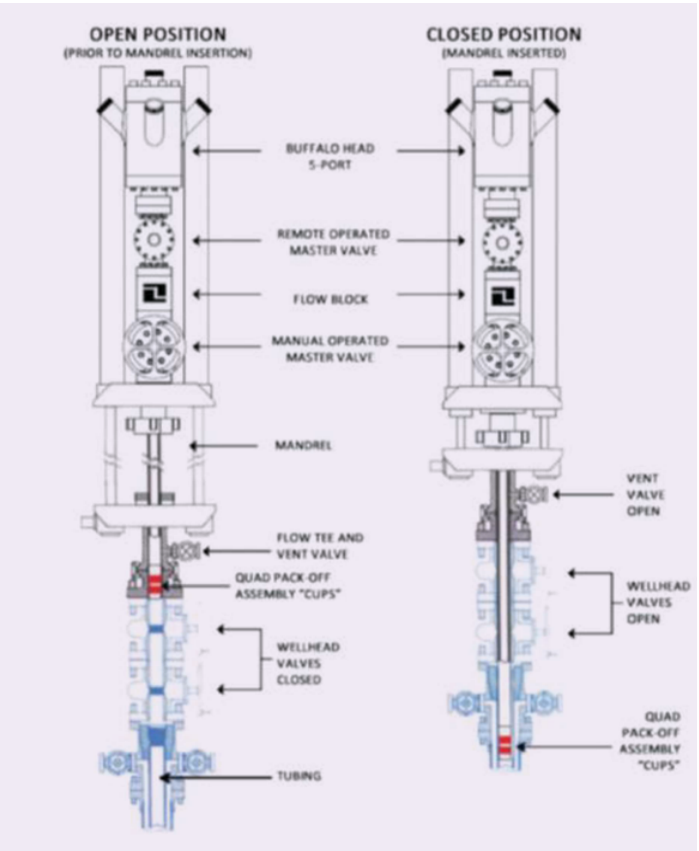
The industry has developed several methods to protect these components. Moreover, there are gaps in the available solutions due to scaling and effectiveness issues. Accordingly, it was identified that there is a need for a new solution that address these challenges. The main groundwork for the solution was based on available technologies from the industry and the American Petroleum Institute's (API) SPEC 6A[1] design validation method to make it easily adaptable regardless of the wellhead configuration.

This article proposes a new method for protecting the permanent tree and bonnet while conducting acid stimulation jobs. Although the solution is presented on a theoretical case of a large completion size with high-pressure rating, it can be adapted to cover any scenario regardless of the well completion size and pressure rating. While the solution does not address every well stimulation scenario, it shows that there is a potential to further optimize these operations and enhance wellhead protection methods.

Current Solutions; Current Challenges

Wellhead protection methods during well stimulation activities fall under the following categories:

Fig. 1 *The setup of a generic tree saver.*



- Tree savers.
- Utilization of sacrificial equipment.
- Pumping acid through the permanent production tree.

A tree saver is a hollow mandrel inserted through the top of the tree on the wellhead and the seal down below the tubing hanger, Fig. 1. The acidizing or fracking fluid is then pumped downhole through the tree saver, which acts as a protective liner taking the full pressure and preventing the fluid from contacting the tree, tubing bonnet, and hanger components. While this method is widely utilized in the industry[2], it has some limitations. First, the available tree savers do not cover completions larger than 5½". Furthermore, tree savers utilize proprietary technologies, which makes scaling it to larger sizes a challenge. Finally, they are not optimized for flow back operations as they impose a restriction in the tree's internal diameter.

An alternate method is to utilize a sacrificial tree. The tree will be exposed to the abrasive fluids — both live and spent acids — during the stimulation activities. Once the job is completed, the temporary tree is removed and a permanent tree is installed. The sacrificial tree can be serviced and utilized for future well stimulations. The main drawback of this method is that it is time-consuming. Additional time and special operations are required to secure the well to safely remove the sacrificial tree and install the permanent equipment.

This involves displacing the well with high density fluids and installing downhole plugs. Additionally, these operations can reduce the effectiveness of the well's stimulation by damaging the reservoir and reducing the well's productivity. Finally, there is the associated cost of utilizing sacrificial equipment, as it is commonly supplied on a rental basis.

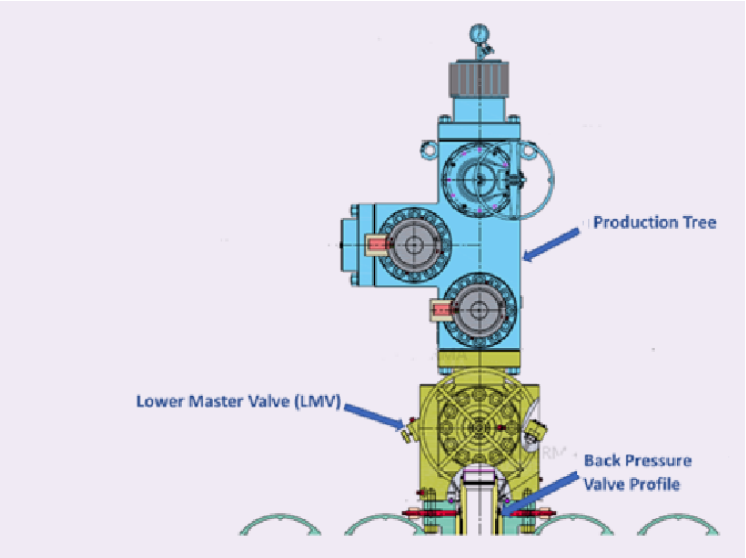
The last option is to conduct the acid operations through the permanent tree. Steps such as pumping chemicals that neutralizes the acid, flushing and greasing the tree prior to and after the acid job, can be implemented to mitigate the risk of damaging the tree. Acidization through the production tree constitutes a very high risk for compromising the seal's integrity of the gate valves, due to the entrapped live acid or spent acid in the valves' cavities. Live acid or spent acid can be highly corrosive to metals[3].

After the acid treatment, the spent acid is flushed out of the formation and the production equipment. The composition of the spent acid coming back out of the well is a bit different than what went in because of its mineral content. Even though the pH will become higher as the acid dissolves the minerals in the formation, the spent acid is still strongly acidic. It will contain a great deal of contamination. The spent acid will have a high concentration of chloride from the hydrochloric acid and is very corrosive. Unlike live acid, it does not contain corrosion inhibitors, which increases its effect on the exposed equipment[4]. The effect of the corrosion is a function of the type of acid utilized, acid concentration, and the exposed material[5].

Fig. 2 *Images of acid pitting on the gate valve seat.*



Fig. 3 *A drawing of the generic wellhead configuration utilized for the proposed solution.*



Corrosion damage due to acidizing is generally the result of the pumped and spent acids, Fig. 2, which are very difficult to flush, therefore, the acid or spent acid may become trapped in these cavities. This will result in severe seat or seat pocket pitting and losing the valve seal integrity over a short period of time. Furthermore, pumping stimulation fluid with proppants through the tree can affect its valves' functionality and risk damaging their internal components[6].

Design Criteria

A new method was developed with the following design guidelines:

- The design can be easily scaled to accommodate any well design regardless of the completion size or pressure rating.
- The sealing elements need to provide full protection for the wellhead equipment, and should be rated to the wellhead equipment rated working pressure.
- The protection tool should have a maximized internal diameter to not interfere with the stimulation and flow back operations.
- The system needs to maintain sufficient mechanical barriers (sacrificial valves) to eliminate the need for conducting well killing operations.
- The system needs to incorporate proven and available technologies, e.g., standard gate valve, tree and hydraulic lubricator.

The proposed solution was considered for a generic well with a large completion size, high-pressure rating, and wellhead configuration, Fig. 3. The relevant wellhead section is comprised of a production tree, tubing bonnet, with integral gate valve (it will be referred to as a lower master valve (LMV) from this point onwards), and a tubing hanger with back pressure valve (BPV) profile.

The design was based on API SPEC 6A[1]. This global standard is implemented by many wellhead suppliers and specifies the requirements and recommendations for design, equipment interchangeability, material selection, manufacturing processes, testing requirements, quality control, inspection, marking, and handling of wellhead and tree equipment. This enabled a new solution to be developed based on field proven technologies.

A key methodology that was adapted from the standard is the design validation procedures for wellhead equipment under API[1] performance requirement (PR) level-2 — also designated as PR2F level. The process validates material, seals performance (metallic and nonmetallic), load-bearing components, wellhead accessories, and equipment structural integrity. API proposed it

Fig. 4 *The pressure and temperature cyclic testing as proposed by API SPEC 6A[1].*

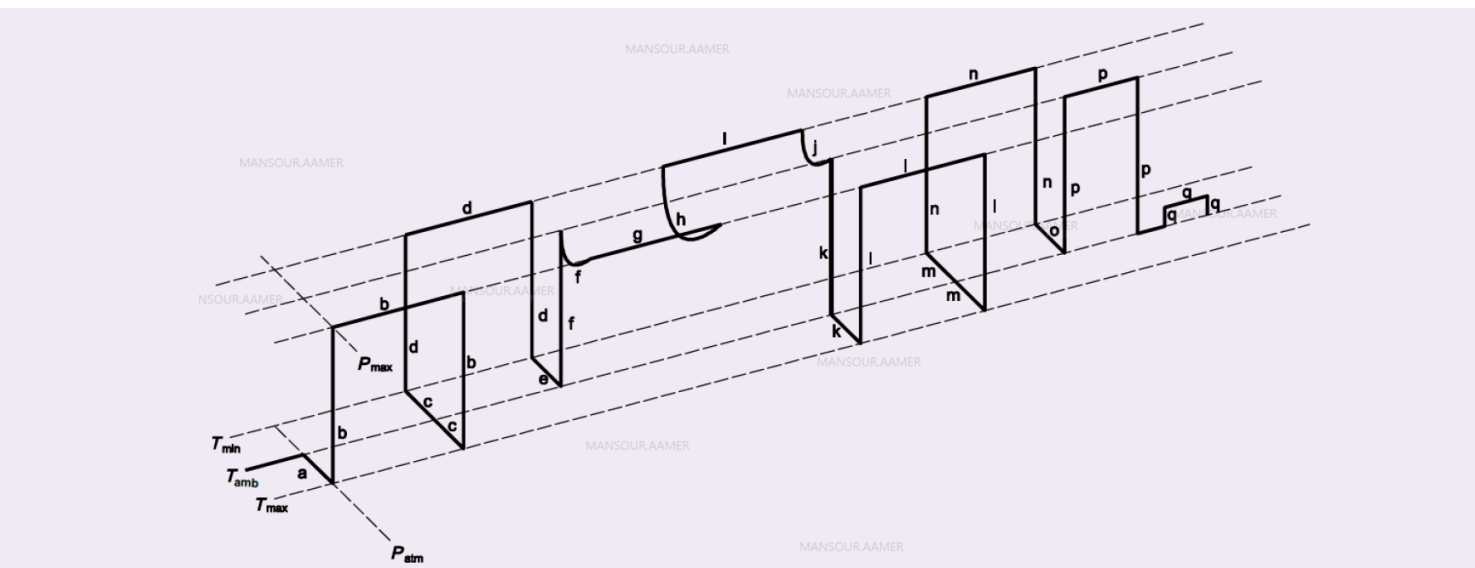
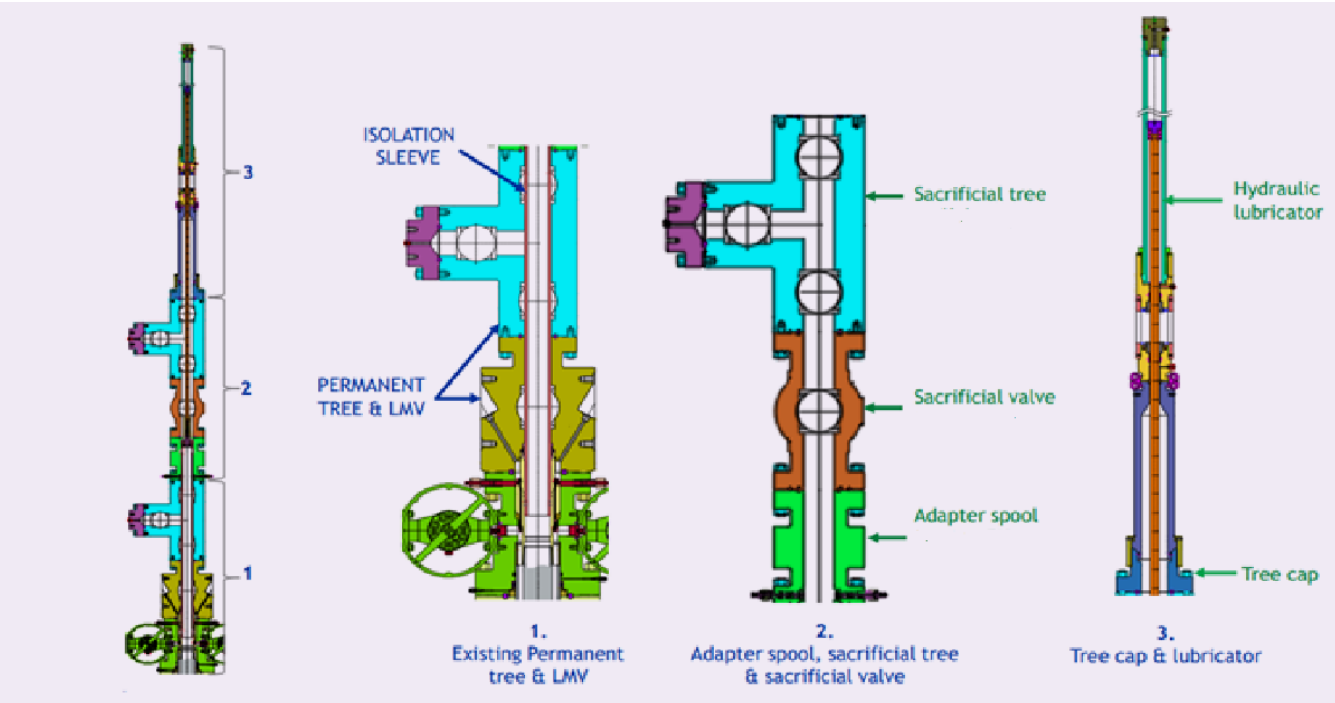


Fig. 5 *The general layout of the protection system.*



as an optional method for the end user to evaluate the wellhead suppliers' equipment fit, form, function, and material selection based their requirements (well pressure, temperature, casing loads, effluent, etc.).

Implementing this approach for the proposed solution mitigates the risk regarding field implementation and ensures comparable performance to the permanent wellhead equipment in terms of material, seal reliability, pressure and temperature ratings.

For pressure containing and controlling components, API SPEC 6A[1] specifies the pressure and temperature testing required to validate the design. The pressure and temperature ranges are based on the required wellhead rated working pressure and temperature classes as specified in the standard. Figure 4 is a visual representation of the testing process. It involves cyclic testing of the equipment at the required testing pressure under the temperature range (minimum, maximum, and ambient). The testing medium can be either hydro or gas, depending on the pressure rating of the equipment. API SPEC 6A[1] mandates gas testing for wellhead equipment rated 10,000 psi and above.

The sealing elements for the solution were based on nonmetallic material. For such components, API PR2F includes immersion testing to confirm on the seal compound compatibility with hydrocarbon gas, hydrogen sulfide and carbon dioxide based on the material class and pressure ratings. The parameters for qualifying the system's design are carefully selected to meet the well pressure, temperature fluid parameters. Adapting this approach will ensure that the sealing capability of the new system will be aligned with the performance of the wellhead seals.

Proposed Solution

The protection system is comprised of three main components: (1) an adaptor, (2) an isolation sleeve, and (3) a well control configuration, Fig. 5. The adaptor is installed on top of the production tree and is equipped with a sealing profile and locking mechanism or segments to retain the isolation sleeve in place. The adaptor comes with a flanged connection per API SPEC 6A[1] standard, which is similar to the wellhead equipment. Additionally, it does facilitate pressure testing the isolation sleeve seals.

Fig. 6 *The isolation sleeve design.*

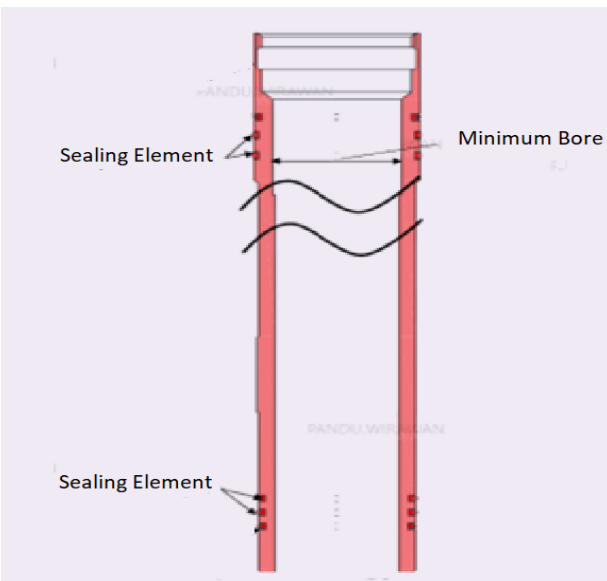
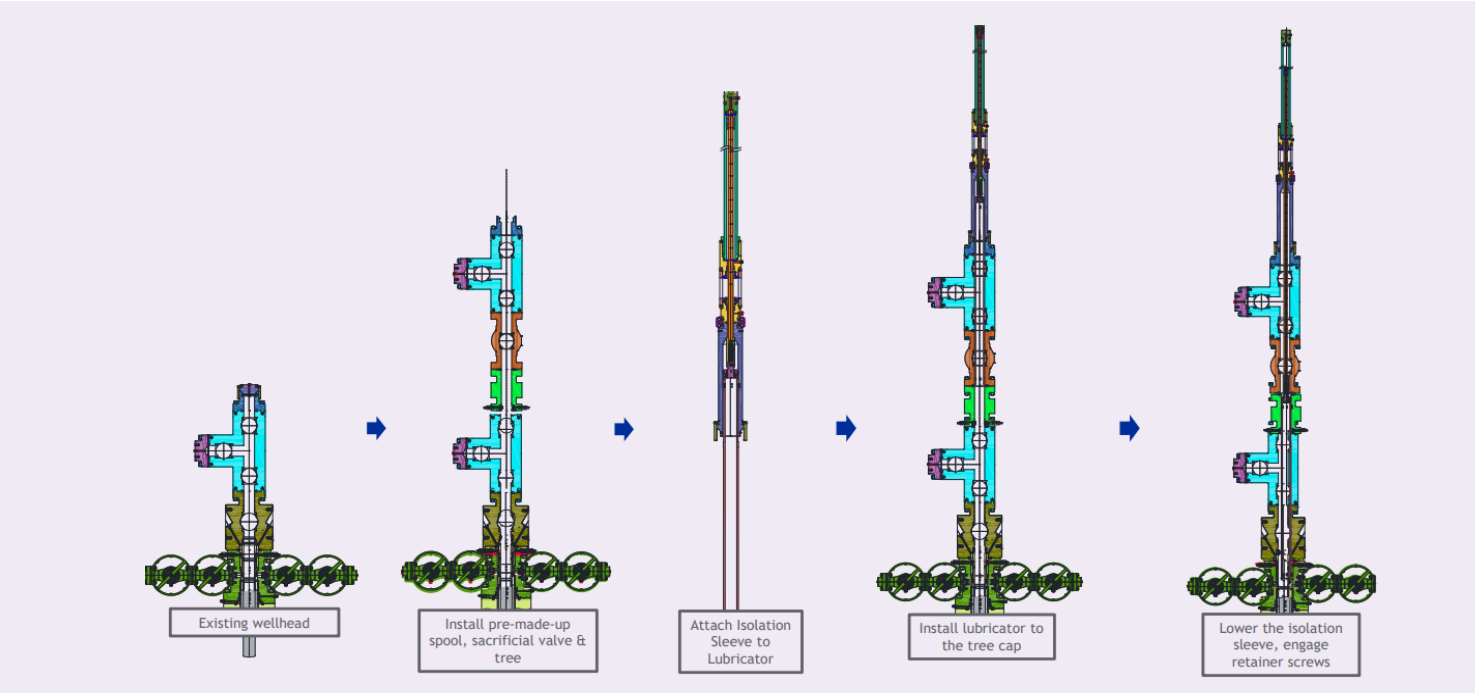


Fig. 7 *The installation steps for the isolation sleeve.*



The isolation sleeve, Fig. 6, is a cylindrical hallow body with the following characteristics:

- It has sealing elements on the adaptor and inside the tubing hanger (above the BPV profile). The sleeve can also include wiper seals to clean the sealing surfaces on the adaptor and tubing hanger.
- The isolation sleeve will have a running profile to engage the running tool. The profile and the running tool follow similar designs utilized on the wellhead spools bowl protector.
- The sleeve is run by a BPV lubricator. This will ensure well containment during the installation process and will result in an efficient and cost-effective running method.

The final component is the well control configuration, a customizable assembly of temporary trees and/or loose valves that are installed on top of this adaptor to provide the required well control capability, allow the installation of the isolation sleeve and offer the well control (in and out) capability.

System Installation Steps

The system installation method follows the following steps, Fig. 7.

The isolation sleeve adaptor is installed directly on top of the permanent tree. This will assist in minimizing the length of the isolation sleeve. Next is the installation of the well control configuration on the adaptor. The configuration can be arranged per the end user's well control requirements. For this article, the configuration is shown to consist of a sacrificial valve and tree. Subsequently, the lubricator is installed on top of the well control configuration and the isolation sleeve is run and set into position via the adaptor's retaining screws.

The BPV profile should have a positive stop to act as a landing point for the sleeve. At this point, the area from the top of the permanent production tree, the LMV and tubing hanger (above the BPV profile), is fully isolated from pressure and any abrasive fluids pumped during the stimulation operations. The stimulation setup is rigged on top of the well control configuration and the acid job can be conducted.

Once the job is completed, the temporary equipment is removed and the well is ready for production.

Potential Benefits

The proposed system described in this article provides several benefits. It offers complete protection to the permanent production tree, LMV, and tubing hanger while conducting well stimulation work.

The concept utilizes available technology from the industry. The adaptor's connection interface is based on the API SPEC 6A[1] standard. The wellhead control configuration is customizable and utilizes API SPEC 6A[1] gate valves, which are widely available in the market. The isolation sleeve utilizes qualified sealing technology per the API SPEC 6A[1] design validation method, ensuring equivalent performance to the wellhead seals. The isolation sleeve running profile can be run via standard lubricator — such as a BPV lubricator.

By utilizing this method, the only components that need to be designed are the isolation sleeve and its adaptor. Accordingly, it is easily scalable, it does not have size limitations as with the current solutions and can be designed to fit all production tree sizes. Furthermore, it will have operational cost savings as it does not require the installation of downhole well control barriers to remove the sacrificial equipment.

The Way Forward

There is a gap in the oil and gas industry when it comes to

wellhead protection methods during well stimulation activities. This is due to either design availability, e.g., no tree savers available for sizes greater than 5½" completion sizes, or having to rely on time-consuming and costly extensive solutions, i.e., utilization of sacrificial equipment.

The developed solution bypasses some of those limitations for acid stimulation by being reliable, efficient, and cost-effective. This was mainly achieved by relying on field proven technologies, international design validation processes, and minimizing the use of proprietary solutions. The next step is to turn this concept into reality and conduct a field trial.

Subsequently, the solution presented in this article does not address all of the challenges when it comes to well stimulation. It assumes that the scope of the equipment to be protected are the permanent tree and LMV. Additionally, the system is only rated to the working pressure of the wellhead equipment. This is not always the case with well stimulation. For frac operations (either single or multistage), it is a common practice to utilize a dedicated tree with a working pressure greater than the permanent wellhead equipment. It was identified that there is an opportunity to further optimize this process with a reliable and cost-effective solution.

Acknowledgments

This article was presented at the Middle East Oil, Gas and Geosciences Show, Manama, Kingdom of Bahrain, February 19-21, 2023.

References

1. API: *API Specification 6A, Wellhead and Tree Equipment*, 21st edition, Standard, November 2018, 412 p.
2. Craig, C.H.: "Mechanical Design Considerations for Fracture-Treating Down Casing Strings," *SPE Drilling Engineering*, Vol. 2, Issue 2, June 1987, pp. 116-126.
3. Schutz, R.W. and Walker, H.W.: "Behavior of Titanium Exposed to Fresh and Spent Dilute HF Acid Well Stimulation Fluids," paper presented at CORROSION 2018, Phoenix, Arizona, April 15-19, 2018.
4. Hernandez, S., Goodman, L., Knobles, M. and Schutz, R.W.: "Materials and Corrosion Risk Mitigation Associated with Flowback of Acid Stimulation Fluids," paper presented at CORROSION 2017, New Orleans, Louisiana, March 26-30, 2017.
5. Morgenthaler, L.N., Rhodes, P.R. and Wheaton. L.L.: "Testing the Corrosivity of Spent HCl/HF Acid to 22 Cr and 13 Cr Stainless Steels," SPE paper 37278, presented at the International Symposium on Oil Field Chemistry, Houston, Texas, February 18-21, 1997.
6. Garvin, T.: "Low-Pressure Wellhead for High-Pressure Stimulation," *Journal of Petroleum Technology*, Vol. 46, Issue 5, May 1994.

About the Authors

Mohammed E. Mukhlifi

Master of Business Administration, Open University Malaysia

Mohammed E. Mukhlifi is a Drilling Engineering Consultant with 25 years of experience with Saudi Aramco. He is a wellhead subject matter expert, working in the Drilling Technical Pressure Control Unit of Saudi Aramco's Drilling Technical Department.

Mohammed's main roles are handling wellhead suppliers' qualifications, conducting failure investigations, extending field support, and representing Saudi Aramco as the primary voting member in the American Petroleum Institute Subcommittee 6 — related to wellhead equipment specifications (API SPEC 6A).

He has contributed to several patents that address major challenges related to wellhead equipment.

Mohammed received his B.S. degree in Mechanical Engineering from King Fahd University of Petroleum and Minerals (KFUPM), Dhahran, Saudi Arabia, and his MBA degree from Open University Malaysia, Manama, Bahrain.

Mansour A. Al-Amer

M.S. in Petroleum Engineering, University of Oklahoma

Mansour A. Al-Amer is a Senior Drilling Engineer with 17 years of experience with Saudi Aramco. He is a wellhead subject matter expert, working in the Drilling Technical Pressure Control Unit of Saudi Aramco's Drilling Technical Department.

Mansour's main roles are handling wellhead suppliers' qualifications, conducting failure investigations, extending field support, and representing Saudi Aramco as a back-up voting member in the American Petroleum Institute Subcommittee 6 to develop the wellhead standard (API SPEC 6A).

He has contributed to several patents that address major challenges related to wellhead equipment.

Mansour received his B.S. degree in Petroleum Engineering from King Fahd University of Petroleum and Minerals (KFUPM), Dhahran, Saudi Arabia, and his M.S. degree in Petroleum Engineering from the University of Oklahoma, Norman, OK.

Pandu Wirawan

M.S. in Systems and Project Management, Nanyang Technological University

Pandu Wirawan is a Senior Drilling Engineer with 16 years of experience in the oil and gas industry. Throughout his career, he has worked as a Wellhead Design Engineer as well as managing wellhead research and development test centers for major wellhead manufacturers in Asia.

Pandu joined Saudi Aramco in 2020 and is currently working as a wellhead subject matter expert in the Drilling Technical Pressure Control Unit of Saudi Aramco's Drilling Technical Department. In his current role, he has contributed in improving the design and reliability of various wellhead components.

Pandu is a member of the Society of Petroleum Engineers (SPE), and has filed several patents and coauthored several published papers.

In 2007, Pandu received his B.S. degree in Industrial Engineering from Diponegoro University, Semarang, Indonesia, and his M.S. degree in Systems and Project Management from Nanyang Technological University, Singapore.

Mohammed K. Muqri

B.S. in Mechanical Engineering, University of Nottingham

Mohammed K. Muqri is a Senior Drilling Engineer, currently working as a wellhead subject matter expert in the Drilling Technical Pressure Control Unit of Saudi Aramco's Drilling Technical Department.

He has been extending support to all Saudi Aramco operations related to wellhead equipment, either in Drilling or Production.

Mohammed has contributed to several initiatives and patents that resolved major challenges faced by Saudi Aramco.

In 2013, he received his B.S. degree in Mechanical Engineering from the University of Nottingham, Nottingham, U.K.

Mohammad S. Al-Saeed

B.S. in Petroleum Engineering, King Fahd University of Petroleum and Minerals

Mohammad S. Al-Saeed is a Senior Drilling Engineer, currently working as a wellhead subject matter expert in the Drilling Technical Pressure Control Unit of Saudi Aramco's Drilling Technical Department.

During his career, he has held several technical positions in Drilling Engineering, Operations, and also worked as a Material Advisor with the Wellhead Forecasting and Procurement Team.

Mohammad is a member of the Society of Petroleum Engineers (SPE), and has several contributions, technical papers, and patents in the wellhead field.

In 2011, he received his B.S. degree in Petroleum Engineering from King Fahd University of Petroleum and Minerals (KFUPM), Dhahran, Saudi Arabia.

Combining Machine Learning and Multiphase Flow Model for Hybrid Virtual Flow Metering

Dr. Anton Gryzlov, Dr. Sergey Safonov, Dr. Boris Krasnopolsky and Dr. Muhammad Arsalan

Abstract /

Virtual flow metering is a technology for indirect estimation of multiphase production rates. The most straightforward approach to obtain virtual measurements is to apply machine learning models, which enable fast but not necessarily an accurate prediction of flow rates. To overcome any related limitations, machine learning methods can be combined with physical conservation laws of mass, momentum, and energy. The resulting hybrid virtual flow metering approach strongly relies on the capabilities of the underlying physical simulator.

In this work, various approaches of combining measurements with multiphase flow models are investigated. It is demonstrated that a wellbore flow model has a central role in any type of hybridization scheme, which connects the available measurements to the target flow rates. Due to specific requirements of the virtual flow metering applications, this simulator has to be fast and accurate enough to qualitatively describe the flow in wellbores and pipelines.

In this work, such a simulator is presented, which is based on a 1D formulation for mass and momentum conservation, but contrary to other commercially available options, the current development is based on a drift-flux approach, which is less demanding on the interfacial closure terms and can be more easily tuned with field data. The performance of the simulator has been evaluated using a set of transient benchmark scenarios, where the reasonable match against the reference data has been demonstrated.

The simulator is applicable to a wide range of multiphase flow problems of practical interest and uses advanced numerical algorithms to ensure robustness and performance. The closure relationships can be adjusted to improve the performance for a particular well. In addition, a dedicated graphical user interphase enables user-friendly interaction for setting up the computational case and processing the output production data.

Introduction

Hydrocarbon production is characterized by multiphase flow, which in petroleum nomenclature refers to a simultaneous transport of oil, gas, and water. Multiphase flow can exist in any location of a production system: inflows from a reservoir to a producing wellbore, flows in the wellbore from a bottom to a wellhead, and fluid transportation in surface pipelines. It is then important to ensure that hydrocarbon fluids are transported economically and safely from a reservoir to the processing facilities, which can be analyzed through production engineering techniques.

These techniques are intended to describe complex transient flow phenomena, which are dependent on wellbore geometry, fluid properties, operating conditions, and multiphase flow regimes. While initially the analysis of multiphase flow problems has been performed with using empirical and engineering models, the state-of-the-art approach relies on the computational fluid dynamics tools, which are tuned by means of experimental data.

The general approach for numerical modeling of wellbore and pipeline flows is to formulate the conservation of mass, momentum, and energy for each fluid in a multiphase mixture. These equations are supplemented by proper boundary and initial conditions and solved numerically in a simulation domain discretized by a computational grid. In practice, reduced order models are frequently used, which facilitate fast-response analysis and real-time applications.

This approach has first been introduced by Bendiksen et al. (1991)[1], who developed a 1D multiphase flow model based on multifluid simulation. This model has eventually evolved into the commercial flow assurance software OLGA (2014)[2]. LedaFlow[3] is another prominent commercial multiphase wellbore simulator, where mass balances are formulated for both continuous and dispersed phases in a multifield approach. These computational tools can be considered as general-purpose simulators capable of providing a stable numerical

solution at a wide range of operating conditions for various types of flow-related problems.

The use of advanced numerical algorithms combined with modern computational hardware generally allows the running of these simulations easily in real-time or close to real-time mode. Nevertheless, significant efforts have also been devoted for further simplifications of flow models, which could further increase their computational efficiency and potentially facilitate implementation for particular tasks. Such fit-for-purpose models may be used for control of drilling operations[4], online estimation of multiphase model parameters[5] or describing transport of mixtures with carbon dioxide[6].

Following the same concept, it is proposed to utilize the power of numerical flow modeling to improve robustness and performance of virtual flow metering technology, where the multiphase flow rates are estimated from indirect measurements. By means of combining the outputs from the numerical simulator with data from several installed sensors, the unmeasured quantities, such as multiphase rates, can be inferred. The employed mathematical model is expected to have a certain balance between complexity and efficiency and can describe qualitatively wellbore dynamics and provide a real-time simulation response. This article describes the development of such a fast simulator.

Hybrid Virtual Flow Metering

Multiphase flow metering is a technology for inline measurements of production rates of oil, gas, and water without separation of flowing phases. The measurement principle implies the installation of several sensors for velocity and composition determination in a single meter body, which values can be consequently recalculated into the values of multiphase flow rates using complex interpretation approaches.

The evolution of multiphase metering technology was driven by the rapidly changing requirements toward better accuracy of the measurements, constrained by the reducing costs and safety improvement issues. Alternatively, all these demands can be met by using indirect measurements, where the multiphase flow rates are estimated by combining data from preinstalled field instrumentation and a process model of multiphase fluid flow. This approach, known as virtual flow metering or soft-sensing, is considered as a digital counterpart of conventional flow metering technology. A complete classification of all flow estimation methods is available[7], where two distinct approaches are outlined: physics-based virtual flow metering and data-driven virtual flow metering.

A physics-driven approach requires application of a hydrodynamical numerical simulator, which describes the conservation of mass, momentum, and energy of multiphase flow in a production system. This approach requires a strong domain knowledge and experience, as it is necessary to formulate the first principles governing equations, provide the exact details of a wellbore geometry, define the correct values of numerous input parameters, and choose a proper numerical method.

Since any physical model is only an approximation of reality, the results of numerical modeling tend to provide inaccurate calculation of multiphase rates. The associated uncertainty is mainly caused by the physical properties of fluids and closure relationships, which are known to a limited extent. Such models provide a transparent understanding on how various components affect the dynamics of hydrocarbon production and set up the correct trends, even if the results are not perfect.

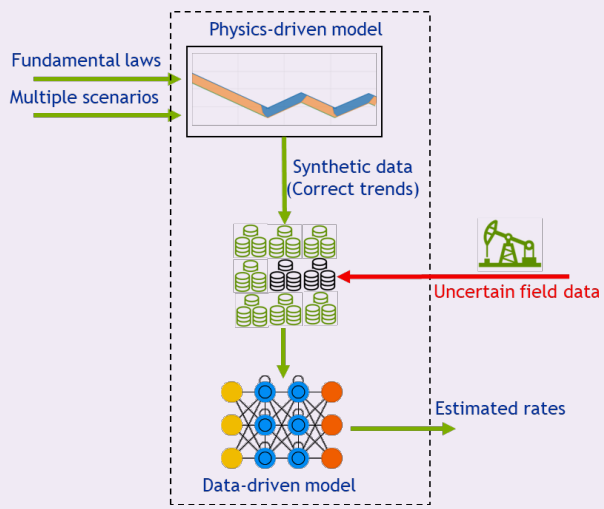
In contrast, a data-driven approach does not require any prior information on underlying physics. Rather it is based on accumulating all the available measurements and identifying the hidden relationship between these measurements and target flow rates through some computational model. Data-driven virtual flow metering can be considered as the system identification method, where multiphase flow dynamics is estimated from the input/output data rather than trying to rigorously describe it using physics-based simulations. In addition, the physical properties of fluids are being accounted for by the available data, which makes machine learning models extremely adaptive to the certain flow conditions.

The main disadvantage of the data-driven approach is the lack of generality and the associated problems with extrapolation to the data outside the training range. More importantly, data-driven models are considered as a black box, where all the internal interpretation mechanisms are hidden. Therefore, updating such a model with newly acquired data is basically equivalent to formulating it all over again.

Since both data and the physical model are never perfect, it is natural to look for some intermediate solution, where the data and physics are combined in a certain way, which strives to mitigate the shortcomings of both approaches if they are used separately. Depending on a degree of wellbore instrumentation, and therefore, the amount of data available or the level of confidence of the multiphase dynamic model used, a hybrid approach is suggested, where the balance between modeling and the data can be adjusted for each considered well. A hybrid model can be data centric or physics centric, the distinction is based on the availability of the data against the anticipated model uncertainty.

Figure 1 illustrates an example of a data-centric hybrid model. It is applicable for scenarios with very limited field data availability, and the data alone are not sufficient to create an accurate machine learning model. Then the physical model, which is assumed to describe accurate production dynamics, is used to

Fig. 1 *An example of a data-centric hybrid model.*



generate additional synthetic data to complement all the possible scenarios of wellbore operation.

Afterwards, both field and simulated data are combined into an extended dataset, which is further used to create a predictive model using any regression technique. Ultimately, such an approach can be used even without any field data, when the dataset is represented fully by the synthetic simulation results. In this case, the obtained data-driven model is basically a low order projection of the original conservation laws, which is characterized by a significantly faster computational capability compared to the numerical solution of partial differential equations. The example of creating such a fast proxy model can be found in Gryzlov et al. (2022)[8].

Figure 2 provides another example of data-centric hybridization, where the performance of a machine learning model is enhanced by introducing physically engineered features. In this approach, it is suggested to transform available raw measurements into physically meaningful features. This is performed by analyzing components of the production system, such as an electric submersible pump, a topside choke, reservoir inflow zones, and identifying corresponding first-principle models for each component of the system. These models are normally described by relatively simple relationships, e.g., the Bernoulli equation, which do not provide a quantitative description of the process, but contain a general understanding about the behavior of a target variable. Eventually, the combination of the original production data and physically processed features is used with a supervised machine learning technique.

More details on how feature engineering can improve virtual flow metering solutions can be found in Bikmukhametov (2020)[9]. Hotvedt et al. (2022)[10] discusses how the data can improve the fidelity of a mechanistic model via a gray box approach.

Physics-based hybridization assumes that a first-principle model is a core component of the virtual flow metering system, while data is used to refine the model prediction by reducing the uncertainty. The model of a production system is always an approximation of reality where multiphase flow is treated as 1D. These models follow the main conservation laws, although they rely heavily on the empirical correlations obtained from the lab experiments[11].

By default, such models never describe the production system perfectly, and therefore, require refinement or tuning. This can be done in a most straightforward manner where the data from the particular well or flow loop type experiments is used to update the critical model parameters. Since it is extremely difficult to distinguish the contribution of individual components, a special optimization routine is suggested, which finds an optimal set of model parameters to match the available data. The field/flow loop data is collected over certain time interval afterwards, and is processed in a single batch to refine the model, Fig. 3.

Unfortunately, the target variables are not always provided by a simulator. For example, the inflow from a reservoir to the wellbore is needed to initialize the simulations, and therefore, it affects the estimates of downhole rates even if other model parameters are perfectly defined. Moreover, there is a strong connection between the unknown flow rates and the readings from available sensors. Some measurements can be more easily obtained at the surface conditions rather than downhole, although the latter are usually accessible only at a few locations in the wellbore.

In case of the closed loop physics-driven hybrid model, the algorithm sequentially compares the prediction of the flow model with measurements, instantly, each time when data becomes available. Then, the mismatch between the model and the measurements is minimized using an optimization technique making this kind of hybrid model perform as an inverse problem solution, Fig. 4. Contrary to the open loop framework, where the model is tuned only once, before the application, the closed loop approach corrects its behavior every time if there is a significant deviation of the model results from the measurements. The example of such a closed loop approach is given in Gryzlov et al. (2009)[12].

Whether the hybrid model is data- or physics-based, the first

Fig. 2 *An example of a data-centric hybridization model.*

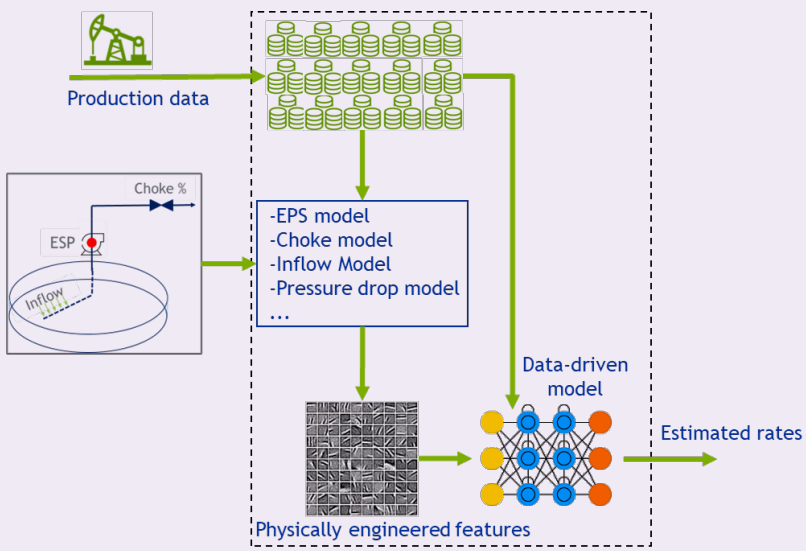


Fig. 3 An open loop physics-based hybrid model.

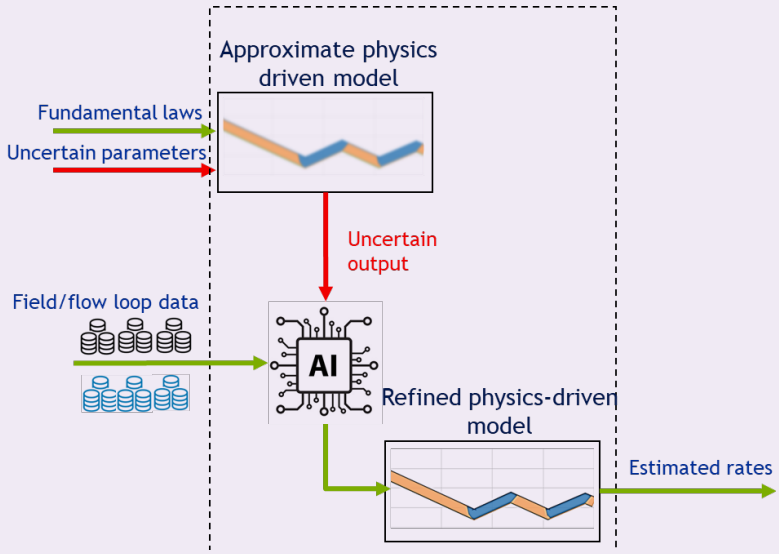
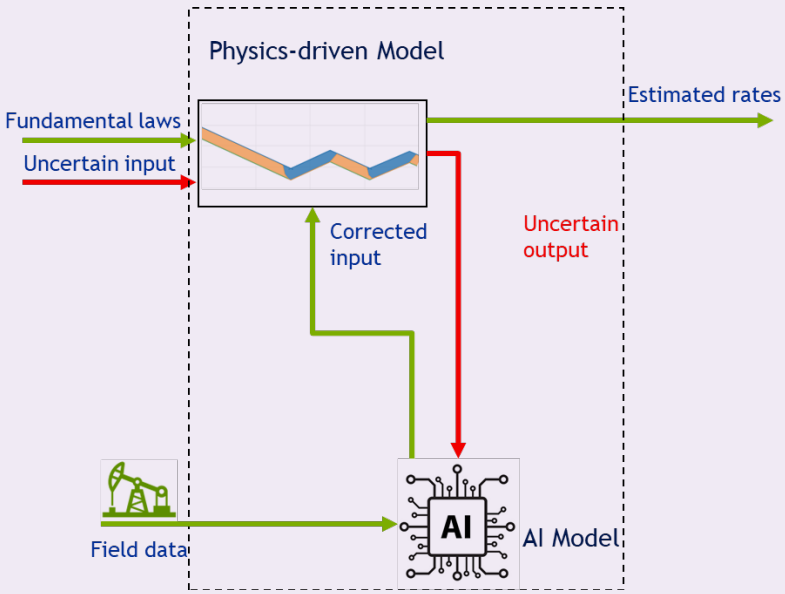


Fig. 4 A closed loop physics-based hybrid model.



principle model is still an essential part of any prediction scheme. Based on the considered scenarios, this model is required to be sufficiently fast to be integrated either in the inversion algorithm or for generating synthetic data for multiple flow scenarios. The model needs to be simple, yet include all the necessary physics to be able to follow the trends in production dynamics and create features for machine learning algorithms.

An additional requirement is that the simulator source code needs to be accessible and easily adjustable.

Wellbore Flow Modeling

The generally recognized approach to describe wellbore flow is to use 1D multiphase flow numerical modeling, which is justified by an enormous length-to-diameter aspect ratio in wells and pipelines. For the fully developed flow and stabilized flow regimes, such 1D formulation is obtained from cross-sectional and temporal averaging of Navier-Stokes equations, supplemented with a flow regime dependent closure term. The diffusion terms in such simplified conservation equations are neglected and the flow is assumed to be advection dominated. The simplified

equations are discretized for the finite number of grid blocks and the governing equations are solved numerically by defining the dynamic parameters for each grid point.

The dynamic variables include an average velocity for each phase, an average pressure for each phase (though the single pressure scenario is depicted in Fig. 5), and a phase fraction that is the geometrical part of each grid block filled with a particular liquid. In most general cases, a solution of eight equations (since $a_g + a_o + a_w = 1$) is needed. The number of equations, and therefore, the complexity of the model used can further be reduced by introducing additional assumption.

Table 1 lists the key available models ranged by the decrease in complexity.

While the commercially available tools for wellbore modeling are based on the multifluid formalism, it is suggested to develop a flow simulator for virtual flow metering application using a simpler drift-flux approach, where the flow is considered as a mixture rather than individual phases. The relative motion between phases is described by an algebraic slip law. Despite an approximate formulation of the drift flux model in a comparison with the multifluid model, the model is of considerable importance as it is applicable to a wide range of two-phase flow problems of practical interest.

From the computational point of view, the drift flux model contains the reduced number of the equations to be numerically solved, which also positively impact the computational efficiency of this simulator.

Mathematical Model

The isothermal compressible three-phase drift-flux model for the simulator is represented by the governing equations written in the following form. Equations 1 to 3 are the mass conservations for each considered phase:

$$\frac{\partial}{\partial t}(\alpha_g \rho_g) + \frac{\partial}{\partial x}(\alpha_g \rho_g v_g) = \frac{q_g}{A}, \quad (1)$$

$$\frac{\partial}{\partial t}(\alpha_w \rho_w) + \frac{\partial}{\partial x}(\alpha_w \rho_w v_w) = \frac{q_w}{A}, \quad (2)$$

$$\frac{\partial}{\partial t}(\alpha_o \rho_o) + \frac{\partial}{\partial x}(\alpha_o \rho_o v_o) = \frac{q_o}{A}. \quad (3)$$

Equation 4 is the mixture momentum conservation equation:

$$\frac{\partial v_m}{\partial t} + v_m \frac{\partial v_m}{\partial x} = -\frac{1}{\rho_m}\frac{\partial p}{\partial x} - g\cos\theta - 2\frac{2f\, v_m |v_m|}{D}, \quad (4)$$

where x denotes the spatial coordinate, t is the time coordinate, α_k is the volume fraction of the k-th phase ($k = g, w, o$). Subscripts

Fig. 5 *An illustration of a 1D approach to wellbore flow modeling.*

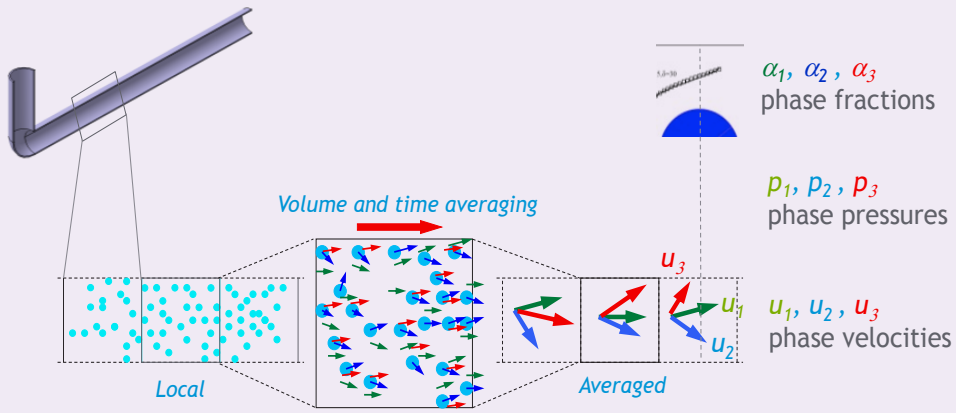


Table 1 *1D models for multiphase wellbore flow simulation.*

Name	Governing Equations	Closures	Complexity
Multifluid[13]	Continuity for each phase Momentum for each phase Continuity for each phase	Friction factor Interfacial forces	1
Drift-Flux[14]	Momentum for mixture Algebraic slip equation Continuity for each phase	Friction factor Drift-flux coefficients	2
No Pressure Wave[15]	Steady momentum for mixture Algebraic slip equation	Friction factor Drift-flux coefficients	3
Homogeneous	Continuity for mixture Momentum for mixture	Friction factor	4

g, w, and o denotes gas, water, and oil phases, respectively. ρ_m is the mixture density, v_k is the velocity of the k-phase, g is the gravitational constant, θ is the wellbore inclination angle with respect to upward vertical, $f(Re_m)$ is the friction coefficient, which is dependent on a mixture of Reynolds numbers, D is the pipe diameter.

The relationship between gas and mixture velocity is given by Eqn. 5:

$$v_g = C_0 v_m + v_{d\theta}, \quad (5)$$

where C_0 is the profile parameter and $v_{d\theta}$ is the drift velocity. Equation 6 relates oil velocity and liquid velocity (defined by Eqn. 7):

$$v_o = C_0' v_l + v_{d\theta}',$$

$$v_l = \frac{\alpha_o v_o + \alpha_w v_w}{\alpha_l}, \quad (6)$$

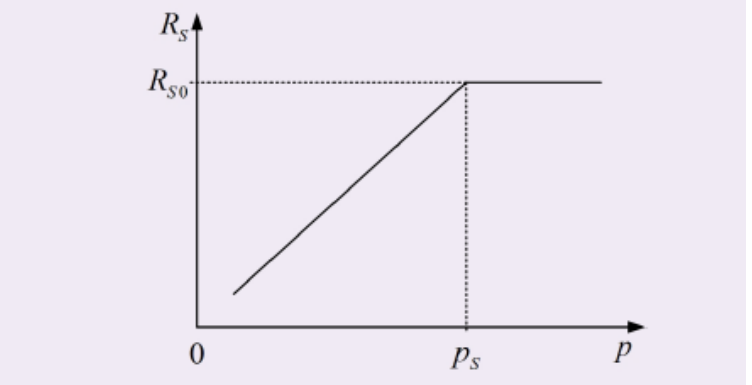
$$v_l = \frac{\alpha_o v_o + \alpha_w v_w}{\alpha_l}, \quad (7)$$

where C_0' and $v_{d\theta}'$ are the profile parameter and the drift velocity for the liquid phase, respectively. In general, the order of velocities or densities determination is the following: at first, the parameters of the liquid phase are computed and after that the parameters of the gas phases are identified. The exact relationships for the pairs C_0, $v_{d\theta}$ and C_0', $v_{d\theta}'$ are chosen following Shi et al. (2005)[16].

The mathematical model described by Eqns. 1 to 5 is formulated for pure fractions of gas, oil, and water; however, a reservoir may also contain live oil that releases gas under decompression. To consider the effect of equilibrium gas release, the volume formation factors for oil and gas, $B_o(p)$, $B_g(p)$, and gas-oil ratio (GOR) $R_S(p)$ are introduced. The volume formation factors describe the ratio of the volume of the phase to the volume at standard conditions. The GOR is the ratio of the volume of gas, that comes out of oil, to the volume of live oil, both measured at standard conditions.

The following relations for density are included in the black-oil model:

Fig. 6 *The typical GOR function.*



$$v_l = \frac{\rho_g^{STD}}{B_g}, \quad v_g = \rho_{o1} + \rho_{o2} = \frac{\rho_o^{STD}}{B_o} + \frac{\rho_g^{STD} R_S}{B_o}, \quad (8)$$

where the superscript *STD* means that the value is taken at the standard conditions. Functions B_o and B_g are set using a pressure-volume-temperature table, while R_S is chosen as a piecewise linear function characterized by bubble point pressure, p_s, and maximum GOR, R_{So}, Fig. 6:

$$\begin{cases} \frac{R_{S0} p}{p_S}; & p < p_S; \\ R_{S0}; & p \geq p_S. \end{cases} \quad (9)$$

The computational algorithm is based on the fully implicit first order time integration scheme, the first order upwind scheme for convective terms, and the direct block-tridiagonal matrix algorithm. The computational domain is a segment of a well length, L, divided into N cells. The grid is uniform, but each grid block can be characterized by an individual inclination angle. The staggered grid approach is used, where all scalar variables — such as pressure and volume fraction — are evaluated at the cell centers, while velocities are evaluated at the cell faces. Eventually, the discretized system of equation is formulated in the form of Eqn. 10 and solved using the Newton method:

$$F(U^{n+1}) = 0, \quad (10)$$

where is the vector of unknown variables related to the new time step $n+1$, which is selected in such a way that it contains all independent variables of the governing system on the entire computational interval. The solution procedure is iterative until the specified convergence criterion is achieved. The numerical efficiency of the simulator is ensured by utilizing an adaptive time step size based on variable change tracking[17].

Brief Overview of the Simulator

The developed tool follows the well-established logic of the numerical simulation software, where the whole process is distinguished in three stages. The first stage is preprocessing, where the simulation model with all relevant parameters is established by a user. The prepared model is then transferred to the solver, where the governing equations are solved numerically, and the corresponding distribution of dynamic variables is stored locally. The final step is a postprocessor, where the obtained results can be visualized in terms of graphs or saved in a suitable format.

Figure 7 shows where both generic naming and the one used in the simulator are given. For a specific flow scenario, all these steps are combined into a single entity called a project.

Figure 8 shows the starting screen of the simulator. To the right there is the list of tutorials, which the user can select to be familiarized with the software. The title of the current active project is given in the upper section. On the left-hand side, three sections are presented: (1) to set up the model, (2) to run the solver, and (3) to visualize the results.

In the initial step of preprocessing, the user must define wellbore geometry, which includes the specification of segments of a certain length. Next, it is needed to specify the boundary and initial conditions and add a sub-model for inflow from the reservoir. For practical purposes, the physical properties of real fluids in hydrocarbon are defined in a tabular way as a result of other numerical simulations or lab experiments. It is also possible to include different pieces of equipment installed

Fig. 7 *The general workflow of the developed simulator.*

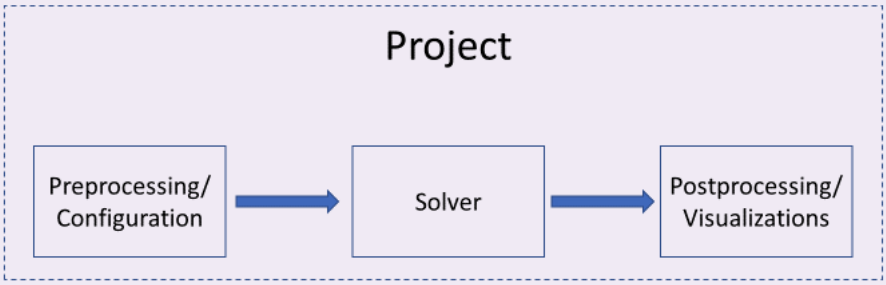
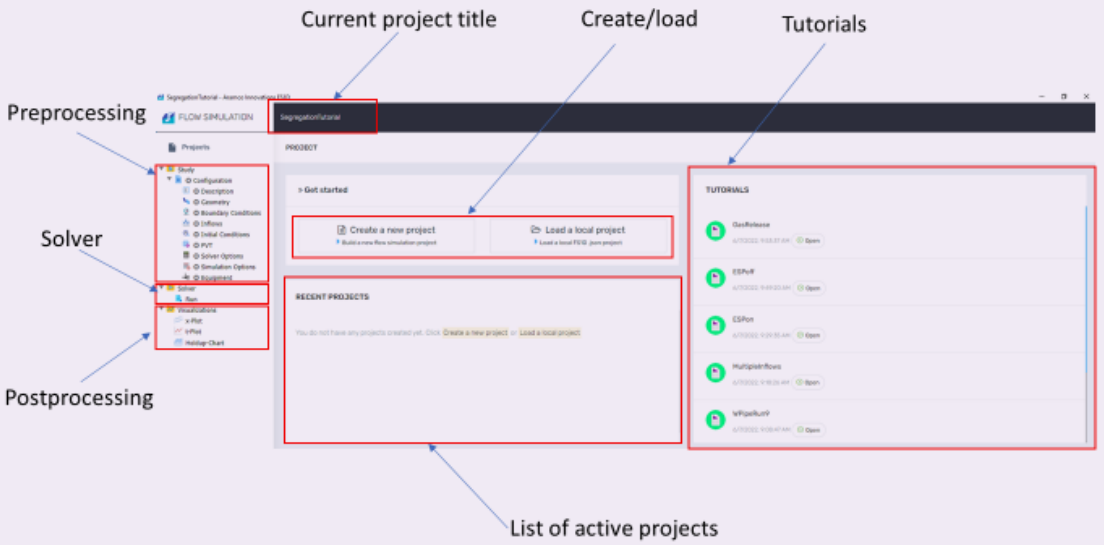


Fig. 8 *The initial screen of the developed simulator.*



in the well, such as an electric submersible pump, or a choke, which are available in the latest software release.

Since the focus of the article is the technical aspects of the developed simulator, no extended discussion on the functionality is given, though it is in a way similar to other commercially available tools. It should be noted that the development of this fast simulator is still in progress and many of the anticipated features are still to be included.

The solver panel includes the option to stop and restart the ongoing simulation. The restart option is needed when simulations are ended or interrupted and there is a need to continue them from either a selected time point with the same or different model setting. This is a particularly handy feature if a user is intended to create an extensive set of synthetic data by varying model parameters of flow conditions.

One of the advanced features of the flow simulator is a holdup chart, where the distribution of volumetric fraction combined with the actual geometry of the well is given, Fig. 9. A user can adjust a time step slider to visualize fluid distribution overlapping a wellbore geometry.

Simulated Test Case I: Three-Phase Segregation

The first demo case considers the three-phase gas-oil-water flow in a closed vertical wellbore. The wellbore is split into three parts: the upper part is initially filled with water, the middle section is filled with oil, and the bottom section is filled with gas. The corresponding initial distribution is physically unstable due to the action of the gravity forces: the light phases start to float up, while the heavy phases start to move to the bottom of the pipe.

The flow considered combines two segregation stages: the gas-liquid segregation, and the oil-water segregation. The first one goes much faster than the second one, which complicates the numerical simulation. The case has a steady-state solution, when the phases change their location: the water phase is on the bottom, the oil phase is in the middle, and the gas phase is on the top of the well.

The evolution of the phase holdup distributions during the simulation are demonstrated in Figs. 10 to 13 for some typical moments in time (computational grid with N = 60 cells). The visualization is performed using a developed postprocessing tool, where blue color indicates water, green is oil, and orange

Fig. 9 *A holdup chart for visualization, where the distribution of volumetric fraction combined with the actual geometry of the well is given.*

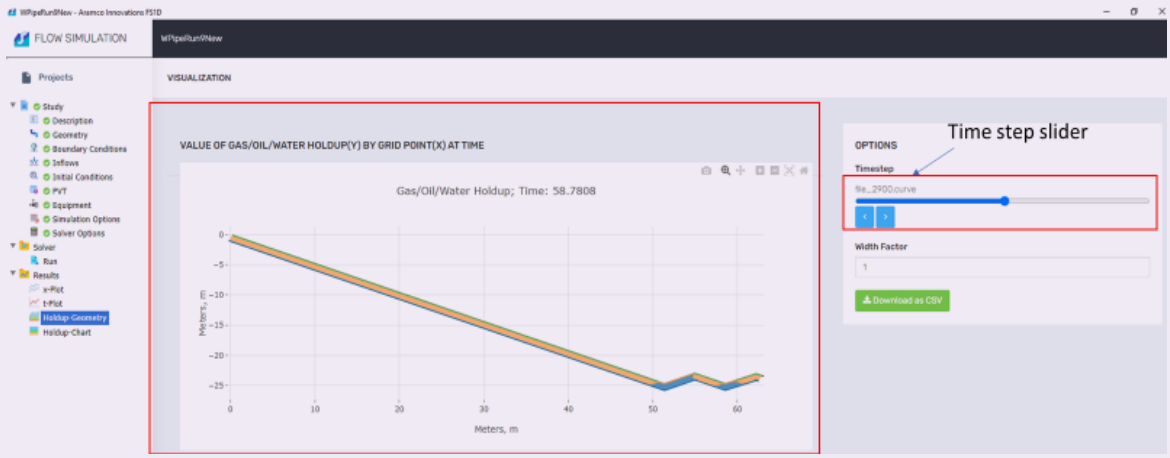


Fig. 10 *The holdup distributions during the three-phase segregation, initial time step.*

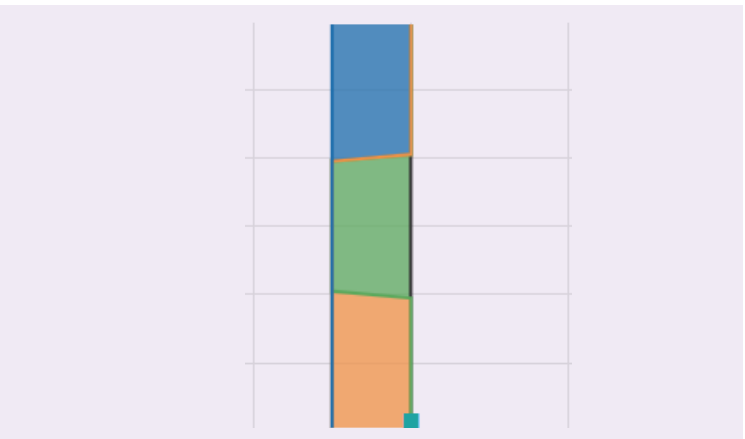
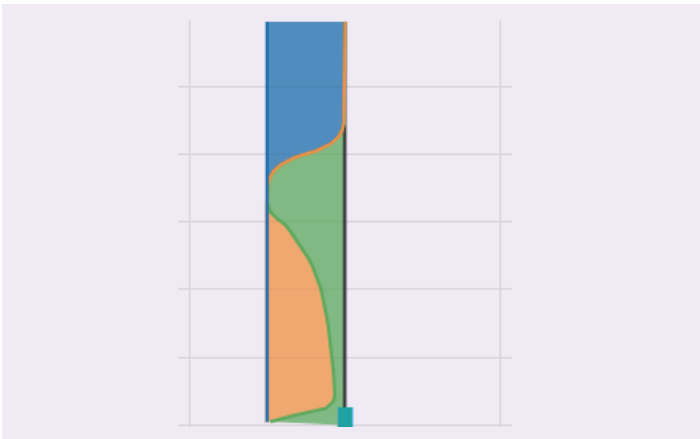


Fig. 11 *The holdup distributions during the three-phase segregation, t = 50 s.*



is gas. The initial holdup distributions, Fig. 10, have sharp interfaces within a single computational cell. Due to gravity forces, the phases start to flow. The next moment in time, t = 50 s, illustrates the start of the segregation process: gas and oil phases are partially mixed, and the water phase is still on the top of the pipe, Fig. 11.

The gas-liquid segregation almost completes at the moment t = 500 s, Fig. 12, while the liquid phases are still of the same order: the heavier water phase is on the top of the oil phase. The full segregation ends at moment t = 2,500 s, Fig. 13. The phases become aligned in accordance with their densities: the heaviest water phase is on the bottom, the lightest gas phase is on top, and the oil phase is in the middle of the pipe. The holdup distributions demonstrate sharp interfaces between the regions within 1 to 2 computational cells, which correlates with the physical problem statement and demonstrates the correctness of the obtained simulation results.

The same simulation was performed with the twice refined

Fig. 12 *The holdup distributions during the three-phase segregation, t = 500 s.*

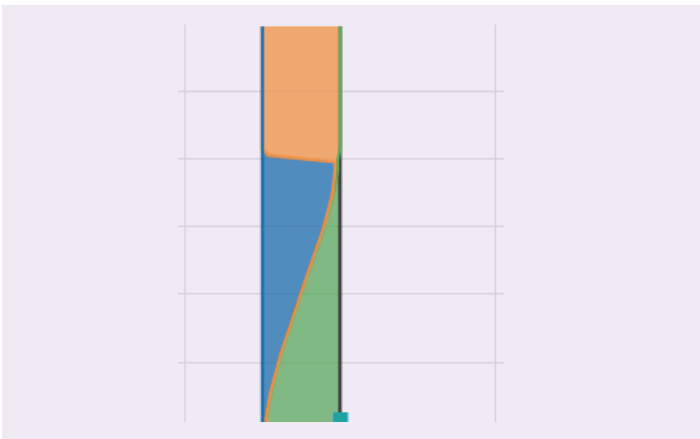
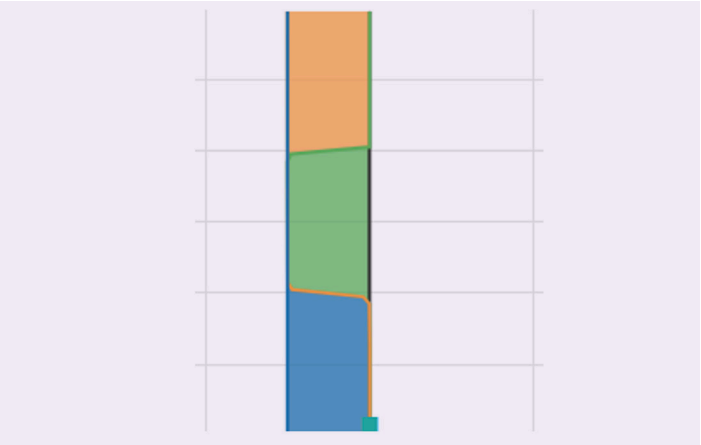


Fig. 13 *The holdup distributions during the three-phase segregation, t = 2,500 s.*



grid, consisting of 120 cells. The corresponding holdup distributions for two simulations with 60 and 120 cells in t = 300 s are compared in Fig. 14. The minor difference in the holdup distributions at the peaks are observed: the more detailed model provides more sharp peak distributions, which also correlates with general expectations. Consequently, both grids reproduce the same solution behavior, and the quantitative difference is not significant.

As previously mentioned, the modeled problem was a superposition of the two processes, the gas-liquid segregation and oil-water segregation. The first one occurs in approximately 500 s, while the second one takes up to 2,500 s. This affects the choice of the optimal time integration step. The adaptive time stepping based on the convergence rate analysis allows us to dynamically adapt the time stepping during the simulation.

Both cases (N = 60, 120) start with Dt = 0.1 s. For the coarse grid the time stepping increases step by step during the gas segregation phase, Fig. 15. The significant time step increase is observed at t ≈450 s, when the gas-liquid segregation was completed. After that, the time step increases up to Δt = 0.5 s (the maximum time step specified in the default configuration file), and the simulation is performed with this time step.

For the fine grid, the time step remains constant at the first simulation stage and increases rapidly when completing the gas-liquid segregation and modeling oil-water segregation stage. These results show the importance of the adaptive time stepping strategy, as the characteristic time integration step may vary significantly during the simulations.

Simulated Test Case II: Terrain Induced Slugging

The next case models the gas-water terrain-induced slug flow. The *w*-pipe configuration similar to the one used in experiments by de Henau and Raithby (1995)[18] is considered. The pipe consists of four segments of different inclinations and an additional 53 m length pipe at the inlet, Fig. 16, which effectively acts as a pressure accumulator. Each pipe section is approximately equal to 4 m, and 1 m section is added at the outlet to simplify the corresponding system behavior and the specification of the boundary condition at the outlet, e.g., avoiding inflow for the fluid from the outlet.

The test considered includes a complex physics process: Due to the irregular pipe configuration, the water is accumulated in the bottom elbows of the pipe, Fig. 17. When closing the cross-section by the water and blocking the gas, the entering gas is accumulated in the reservoir, which leads to a pressure increase. After the limiting point, the pressurized gas displaces the liquid in the elbows and breaks through them to the outlet. Pressure drops after gas depressurizing, which leads to accumulation of the water in the elbows and blocking the gas. Therefore,

Fig. 14 *The holdup distributions during the three-phase segregation, t = 300 s; two computational grids with N = 60 (continuous lines) and N = 120 cells (markers).*

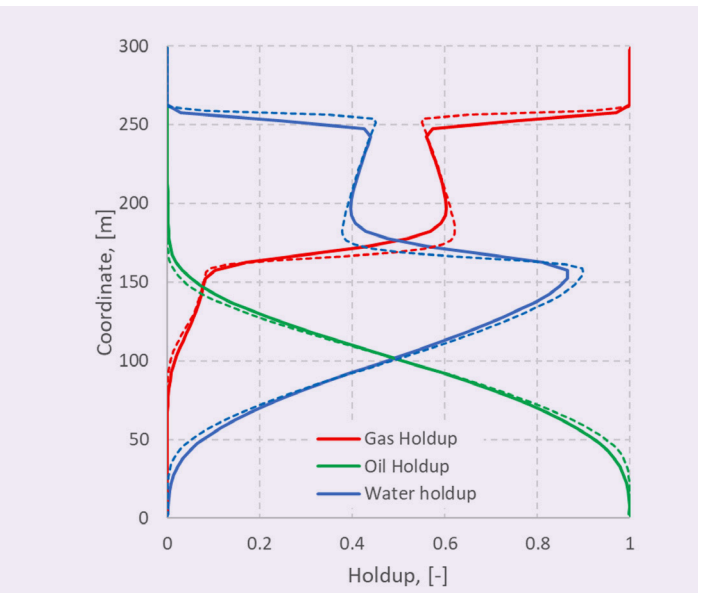


Fig. 15 *Time integration step as a function of a moment in time.*

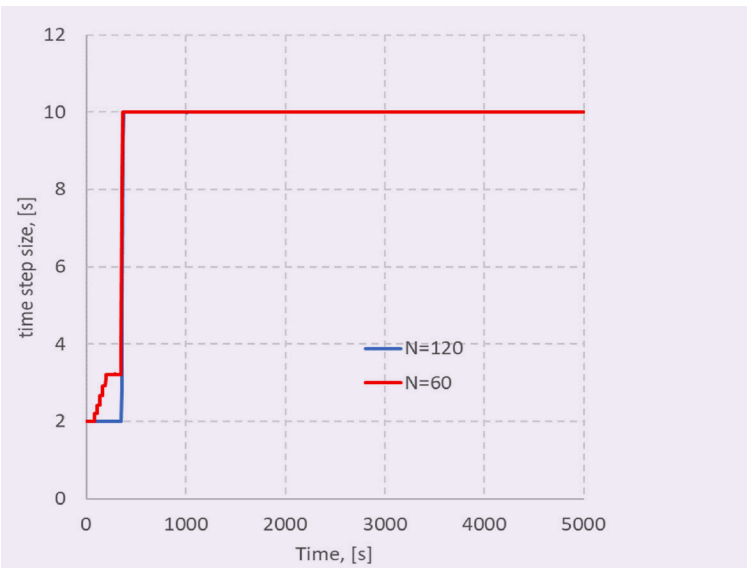


Fig. 16 *A sketch of the w-pipe problem configuration.*

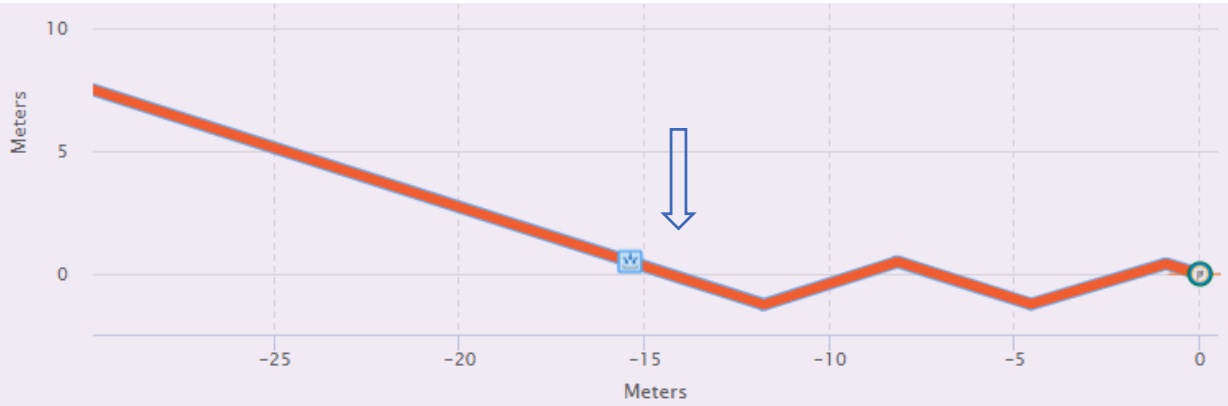
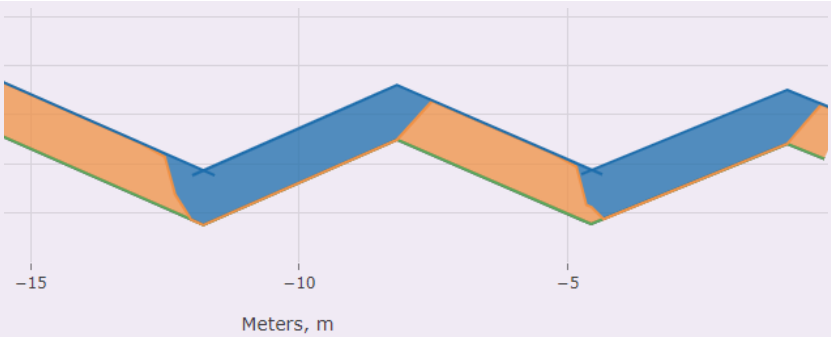


Fig. 17 *The formation of the liquid slugs in the bottom elbows of the pipe.*



this process has periodic behavior with regular water blowouts from the pipe. The *w*-pipe demo case has been modeled with two computational grids of 140 and 280 cells.

The main control parameter, such as the water mass flow rate at the outlet, was monitored and compared with the experimental data presented[18]. Figure 18 shows the corresponding results. The obtained results, while showing some quantitative differences, demonstrate similar behavior of the water mass flow rate as a function in time. The developed wellbore simulator prototype is capable to reproduce the periodic flow regime, and the amplitude and duration of water blowouts are close to the experimental ones. Some difference can be seen in the blowout's frequency (and a number of blowouts in the specified time instant, t = 450 s), which, however, can be decreased by a specific tuning of the drift-flux closure relations[19].

The complex flow behavior during the simulation is reflected in the convergence rate, and as a result, the time integration step, Fig. 19. The water accumulation stage is a more regular flow regime and is calculated with the increased time step. The blowout stage produces a more perturbed flow, which requires more iterations (lower time step) to obtain the solution.

Conclusions and Future Work

In this work, the fast multiphase wellbore simulator is introduced, which is based on a 1D formulation of a drift-flux model. The

Fig. 18 *The water mass flow rate at the outlet of the pipe.*

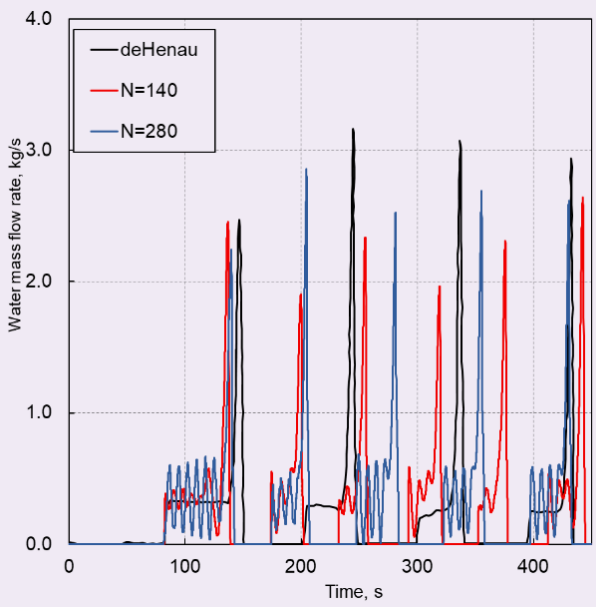
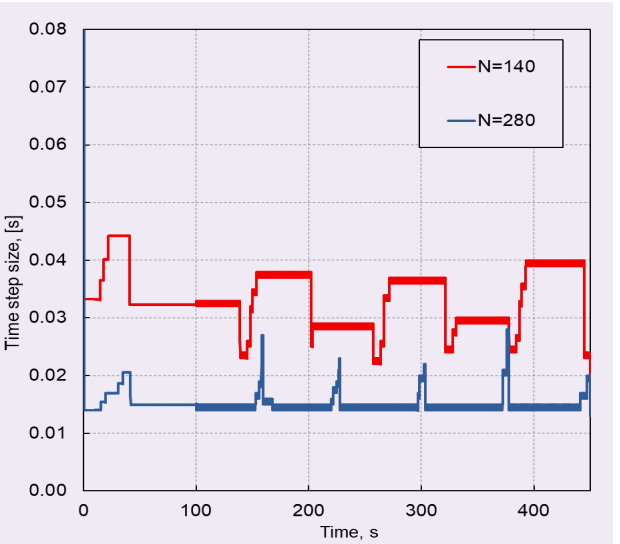


Fig. 19 *The time integration step as a function of time.*



simulator is developed for the application for the hybrid virtual flow metering problem, where a fast and relatively accurate numerical response is needed. Two computational test cases have been presented, which demonstrate and discuss in detail the terrain-induced slugging and multiphase fluid segregation.

The fast numerical solver and advanced graphical user interface demonstrate that the developed tool is very capable to perform multiphase flow simulations and be comparable with other commercial counterparts.

Several approaches for combining the physical model and measurements for the virtual flow metering problem have also been reported in this work. It has been noted that depending on the considered scenario, and the availability of the data, this hybridization can either be data- or physics-based. It is a part of our future work to evaluate the developed simulator with each hybrid approach proposed.

The simulator is still at the development phase where the new functionality is being continuously added. The current effort is directed toward the numerical models for non-isothermal flows and multilateral wells. The future research will also focus on the optimization of a computational engine to improve the performance of the simulator.

Acknowledgments

This article was presented at the Abu Dhabi International Petroleum Exhibition and Conference, Abu Dhabi, UAE, October 2-5, 2023.

References

1. Bendiksen, K.H., Malnes, D., Moe, R. and Nuland, S.: "The Dynamic Two-Fluid Model OLGA: Theory and Application," *SPE Production Engineering*, Vol. 6, Issue 2, May 1991, pp. 171-180.

2. Schlumberger: "Olga Dynamic Multiphase Flow Simulator," 2014, *https://www.software.slb.com/products/olga*.

3. Danielson, T.J., Bansal, K.M., Hansen, R. and Leporcher, E.: "LEDA: The Next Multiphase Flow Performance Simulator," paper presented at the 12th International Conference on Multiphase Production Technology, Barcelona, Spain, May 25-27, 2005.

4. Aarsnes, U.J.F., Ambrus, A., Di Meglio, F., Vajargah, A.K., et al.: "A Simplified Two-Phase Flow Model Using a Quasi-Equilibrium Momentum Balance," *International Journal of Multiphase Flow*, Vol. 83, July 2016, pp. 77-85.

5. Lorentzen, R.J., Naevdal, G. and Lage, A.C.V.M.: "Tuning of Parameters in a Two-Phase Flow Model Using an Ensemble Kalman Filter," *International Journal of Multiphase Flow*, Vol. 29, Issue 8, August 2003, pp. 1283-1309.

6. Aursand, P., Hammer, M., Munkejord, S.T. and Wilhelmsen, Ø.: "Pipeline Transport of CO_2 Mixtures: Models for Transient Simulation," *International Journal of Greenhouse Gas Control*, Vol. 15, July 2013, pp. 174-185.

7. Bikmukhametov, T. and Jäschke, J.: "First Principles and Machine Learning Virtual Flow Metering: A Literature Review," *Journal of Petroleum Science and Engineering*, Vol. 184, January 2020.

8. Gryzlov, A., Safonov, S. and Arsalan, M.: "Intelligent Production Monitoring with Continuous Deep Learning Models," *SPE Journal*, Vol. 27, Issue 2, April 2022, pp. 1304-1320.

9. Bikmukhametov, T. and Jäschke, J.: "Combining Machine Learning and Process Engineering Physics toward Enhanced Accuracy and Explainability of Data-Driven Models," *Computers and Chemical Engineering*, Vol. 138, July 2020.

10. Hotvedt, M., Grimstad, B., Ljungquist, D. and Imsland, L.: "On Gray-Box Modeling for Virtual Flow Metering," *Control Engineering Practice*, Vol. 118, January 2022.

11. Kanin, E.A., Osiptsov, A.A., Vainshtein, A.L. and Burnaev, E.V.: "A Predictive Model for Steady-State Multiphase Pipe Flow: Machine Learning on Lab Data," *Journal of Petroleum Science and Engineering*, Vol. 180, September 2019, pp. 727-746.

12. Gryzlov, A., Leskens, M. and Mudde, R.F.: "Soft Sensing for Two-Phase Flow Using an Ensemble Kalman Filter, *IFAC Proceedings Volumes*, Vol. 42, Issue 11, 2009, pp. 584-589.

13. Stewart, H.B. and Wendroff, B.: "Two-Phase Glow: Models and Methods," *Journal of Computational Physics*, Vol. 56, Issue 3, December 1984, pp. 363-409.

14. Zuber, N. and Findlay, J.A.: "Average Volumetric Concentration in Two-Phase Flow Systems," *ASME Journal of Heat and Mass Transfer*, Vol. 87, Issue 4, November 1965, pp. 453-468.

15. Masella, J.M., Tran, Q.H., Ferre, D. and Pauchon, C.: "Transient Simulation of Two-Phase Flows in Pipes," *International Journal of Multiphase Flow*, Vol. 24, Issue 5, August 1998, pp. 739-755.

16. Shi, H., Holmes, J.A., Diaz, L.R., Durlofsky, L.J., et al.: "Drift-Flux Parameters for Three-Phase Steady-State Flow in Wellbores," *SPE Journal*, Vol. 10, Issue 2, June 2005, pp. 130-137.

17. Pope, M.A. and Mousseau, V.A.: "Accuracy and Efficiency of a Coupled Neutronics and Thermal Hydraulics Model," *Nuclear Engineering and Technology*, Vol. 41, Issue 7, September 2007, pp. 885-892.

18. de Henau, V. and Raithby, G.D.: "A Study of Terrain-Induced Slugging in Two-Phase Flows," *International Journal of Multiphase Flow*, Vol. 21, Issue 3, June 1995, pp. 365-379.

19. Spesivtsev, P., Sinkov, K. and Osiptsov, A.: "Comparison of Drift-Flux and Multifluid Approaches to Modeling of Multiphase Flow in Oil and Gas Wells," *WIT Transactions on Engineering Sciences*, Vol. 79, 2013, pp. 89-99.

About the Authors

Dr. Anton Gryzlov

Ph.D. in Applied Physics,
Delft University of Technology

Dr. Anton Gryzlov is a Petroleum Engineering Specialist working at the Aramco Innovations Global Research Center (GRC) in Moscow, Russia. He is involved in the development of intelligent solutions for multiphase flow metering and optimization and control.

Prior to joining the newly established Moscow GRC in 2019, Anton worked for 14 years in various positions related to different aspects of multiphase flow metering development and commercialization. This includes extensive R&D experience at Roxar and Schlumberger.

He is the author of more than 15 technical publications on fluid flow, including Society of Petroleum Engineering (SPE) proceedings and papers in peer-reviewed journals.

In 2005, Anton received his M.S. degree in Mechanical Engineering from Bauman Moscow State Technical University, Moscow, Russia. In 2010, he received his Ph.D. degree in Applied Physics from Delft University of Technology, Delft, the Netherlands.

Dr. Sergey Safonov

Ph.D. in Quantum Semiconductor Physics,
University of Exeter

Dr. Sergey Safonov is a Research Program Director working at the Aramco Innovations Global Research Center in Moscow, Russia. He is currently leading a new team of research data scientists focusing on developing new digital solutions using novel artificial intelligence, machine learning, and data analytics technologies.

Sergey has 15 years of R&D experience in upstream oil and gas gained from working on various research positions in Schlumberger in Russia and in the U.K. He has extensive experience in multidomain aspects of multiphase fluid flow, advanced core analysis, digital rock modeling, and drilling processes.

Sergey is the author of more than 30 scientific and technical papers, including Society of Petroleum Engineering (SPE) proceedings and papers in peer-reviewed journals.

He received his M.S. degree in Applied Physics from the Moscow Institute of Physics and Technology, Moscow, Russia, and his Ph.D. degree in Quantum Semiconductor Physics from the University of Exeter, Exeter, U.K.

Dr. Boris Krasnopolsky

Ph.D. in Fluid Dynamics,
Lomonosov Moscow State University

Dr. Boris Krasnopolsky is a Leading Researcher in the Institute of Mechanics at Lomonosov Moscow State University. His key research areas are the development of algorithms for modeling turbulent flows on high performance computer systems and the modeling of multiphase flows.

Boris joined the Institute of Mechanics 17 years ago. He has over 15 years of experience in the development of computer codes for modeling various phenomena in fluid dynamics, including multiphase pipe flows. For approximately 10 years, Boris was a Consultant at Schlumberger Moscow Research Center.

He is the author of more than 30 papers in proceedings and several peer-reviewed journals, including the *Journal of Computational Physics*, and *Computer Physics Communications*.

In 2006, Boris received his M.S. degree in Applied Mathematics from the Moscow Engineering Physics Institute, Moscow, Russia. In 2010, Boris received his Ph.D. degree in Fluid Dynamics from Lomonosov Moscow State University, Moscow, Russia.

Dr. Muhammad Arsalan

Ph.D. in Electronics Engineering,
Carleton University

Dr. Muhammad Arsalan joined Saudi Aramco in 2013 as a Senior Research Scientist. He is leading a team of experts in multiphase metering, sensing, intervention, and robotics focus area within the Production Technology Division of Saudi Aramco's Exploration and Petroleum Engineering Center – Advanced Research Center (EXPEC ARC). Muhammad is also leading the global digital transformation team of EXPEC ARC in advanced sensing domain. His team is working on innovative surface and subsurface production monitoring, control, and optimization technologies.

Muhammad is a seasoned professional with over 20 years of experience in academia and various industries, including biomedical, space, chemicals, and oil and gas. He has over 100 international granted patents and publications related to integrated sensors, systems, and tools.

Muhammad is the recipient of several major national and international awards and distinctions for his entrepreneurial skills and his groundbreaking contributions to the innovation, research and technology development.

Muhammad is the co-founder of two North American technology startups.

In 2004, he was an Invited Researcher and Natural Sciences and Engineering Research Council–Japan Society for the Promotion of Science (NSERC–JSPS) Fellow with the Tokyo Institute of Technology. From 2005 to 2008, Muhammad was an NSERC Alexander Graham Bell Graduate Scholar with the Carleton University.

From 2009 to 2010, he was a National Aeronautics and Space Administration (NASA) postdoctoral Fellow. In 2010, Muhammad joined King Abdullah University of Science and Technology (KAUST) in Thuwal, Saudi Arabia, as an NSERC postdoctoral Research Fellow.

From 2011 to 2016 he was an Adjunct Research Professor with Carleton University, Ottawa, Canada.

Muhammad received his B.Eng. degree from the Institute of Industrial Electronic Engineering, NED University of Engineering and Technology, Karachi, Pakistan in 1999, and his M.S. and Ph.D. degrees, both in Electronic Engineering, from Carleton University, Ottawa, Ontario, Canada, in 2004 and 2009, respectively.

Surfactants Structured by Nanoparticles to Stabilize CO_2 Foam at High Temperature

Prasad B. Karadkar, Dr. Shahid Ali, Tamim Alshehri, Dr. Bader G. Alharbi, Mohammed Alsakkaf, Dr. Muhammad Mansha and Dr. Safyan A. Khan

Abstract /

Foamed fracturing fluids offer an attractive alternative over conventional stimulation fluids, particularly in water sensitive formations, to shorten the flow back period and energize the created fracture geometry. The thermal stability of foam at high temperatures is one of the main challenges. The gas-liquid interface of foam tends to collapse with temperature. In this article, carbon dioxide (CO_2) foam stability is enhanced by nanoparticles (NPs) structurally supporting foaming agents at high temperature.

NPs tend to stabilize foam formulations under harsh conditions of temperature and salinity. In this study, different sizes of silica NPs (7 nm, 30 nm) were utilized to enhance the stability of the CO_2 foam. The NPs were characterized by various techniques such as X-ray diffraction (XRD), transmission electron microscopy (TEM), dogleg severity, and Brunauer-Emmett-Teller (BET) surface area (S_{BET}) measurements. The foaming characteristics of various formulations were analyzed by a dynamic foam analyzer (DFA-100), respectively. Rheological properties of CO_2-based foams were measured by a circulating flow loop foam rheometer at high temperature (250 °F) and a shear rate up to 500 1/s.

CO_2 foam stability is enhanced by optimizing the concentrations of cetyltrimethylammonium bromide (CTAB) surfactant and silica NPs at high temperature. According to the XRD findings, commercial silica (CS-7 and CS-30) are amorphous materials with a hexagonal crystal structure. The average diameter of the CS-7 and CS-30 silica NPs, as shown by field emission TEM (FETEM) images, is 12 nm and 25 nm, respectively. CS-7 has a S_{BET} that is 2.27 times more than the CS-30 sample. The CS-7 silica NPs were confirmed to have a more uniform shape, a smaller particle size, and a larger surface area based on these findings.

Both the CS-7 NPs and the CS-7+CTAB formulation have zeta potential values of -36.9 mV and 42.1 mV, respectively, which support the stability of the foamed colloidal suspension and the development of a densely packed particle arrangement at the liquid/gas interface. The foam analysis results demonstrate that adding CS-7 silica NPs (0.005 wt%) to a CO_2-based formulation increases the foam stability by up to 12%, demonstrating the ability of the NPs to stabilize foam formulations. The NPs stabilized CO_2 foamed fluids' rheological characteristics exhibited 12 cP at 100 1/s utilizing water as the external phase at 2,000 pressure and 250 °F.

Maintaining the stability of the CO_2 foam was a challenging task, especially at high temperatures. The stability of the CO_2 foam greatly depends upon the optimum hydrophilic-lipophilic balance (HLB) of surfactants. This was achieved by optimizing various formulations using a suitable CTAB surfactant and silica NPs to overcome water drainage, CO_2 gas diffusion rate, and rupturing of foam at high temperatures.

Introduction

Hydraulic fracturing has emerged as a crucial technique for well stimulation, which permanently changes the geology of tight and shale gas formation by creating new pathways for oil or gas to flow. Subsequently, traditional fracturing fluids, such as water-based or slick water solutions, present formidable obstacles, spanning environmental issues, water consumption, formation damage, and economic drawbacks[1]. Consequently, an exploration of alternative fracturing fluids has unfolded, primarily centered around the stability and effectiveness of carbon dioxide (CO_2) based foam used for fracking technology.

In fracking technology, CO_2 foam is used as a mobility control agent to improve the displacement efficiency of CO_2 flooding. When CO_2 is injected into an oil reservoir, it passes through preferential pathways and leaves some areas of the reservoir unswept. This can result in poor oil recovery and lower efficiency. By adding a foaming agent to the injected CO_2, it is possible to create a foam having the ability to block these preferential

pathways and divert the CO_2 into previously unswept areas. The foam acts as a mobility control barrier, forcing the CO_2 to move more uniformly and sweep a larger volume of oil. This can improve the overall sweep efficiency and increase oil recovery.

CO_2 foam-based fracturing fluids exhibit improved proppant transport, effective solid-free fluid loss control, reduced fluid retention due to the foam's low water content, and compatibility with reservoir fluids[2]. Additionally, their lower hydrostatic pressure accelerates cleanup. Such advantages have been substantiated through laboratory and field studies since the 1970s, notably within the framework of carbonate reservoirs and matrix acidizing[3, 4].

Surfactants play a key role in the formation and stabilization of CO_2 foam. The selection of appropriate surfactants for CO_2 foam depends on several factors, including their ability to reduce interfacial tension (IFT), generate foam stability, and be compatible with harsh reservoir conditions (temperature, pressure, and salinity). Anionic surfactants such as alkyl sulfonates or alkylbenzene sulfonates are frequently used for enhanced oil recovery applications. Fluorosurfactants are also effective in reducing the IFT between CO_2 and oil, due to their unique molecular structure. Moreover, non-ionic surfactants (alcohol ethoxylates) and Gemini surfactants have demonstrated promising results in generating stable CO_2 foam, reducing IFT reduction, and contributing to improved oil recovery. In this research work, we potentially explore the role of a cationic surfactant, i.e., cetyltrimethylammonium bromide (CTAB), to produce a stable CO_2 foam.

Nanoparticles (NPs), in combination with surfactants, are being used more frequently in the field to enhance the stability and performance of CO_2 foam. Studies indicate that incorporating NPs such as silica, augments foam stability by providing a solid framework or reinforcing the foam structure[5]. Silica NPs can act as foam stabilizers by adsorbing at the gas-liquid interface, forming a shell around the gas bubbles, and reducing coalescence and drainage. This leads to increased foam stability and improved resistance to shear forces[6, 7]. Silica NPs can also contribute to reducing the IFT and decreasing CO_2 mobility by increasing the viscosity of the displacing phase. Moreover, silica NPs can bridge and strain through porous media, such as rock formations, assisting in diverting the injected CO_2 to areas with bypassed oil. This mechanism helps improve the distribution and contact of the CO_2 with the oil, resulting in enhanced oil recovery.

This research strives to optimize the concentration of CTAB surfactant and silica NPs to produce a denser CO_2 foam structure, which ensures a longer foam lifespan and superior blocking capacity within the reservoir. For this purpose, silica NPs were well characterized by various techniques such as X-ray diffraction (XRD), TEM, dogleg severity, and Brunauer-Emmett-Teller (BET) surface area (S_{BET}) measurements.

The foaming characteristics of various formulations were analyzed by a dynamic foam analyzer to measure the foam stability and half-life. The rheological properties of CO_2-based foams were measured by a circulating flow loop foam rheometer at high temperature and a shear rate up to 1,000 1/s.

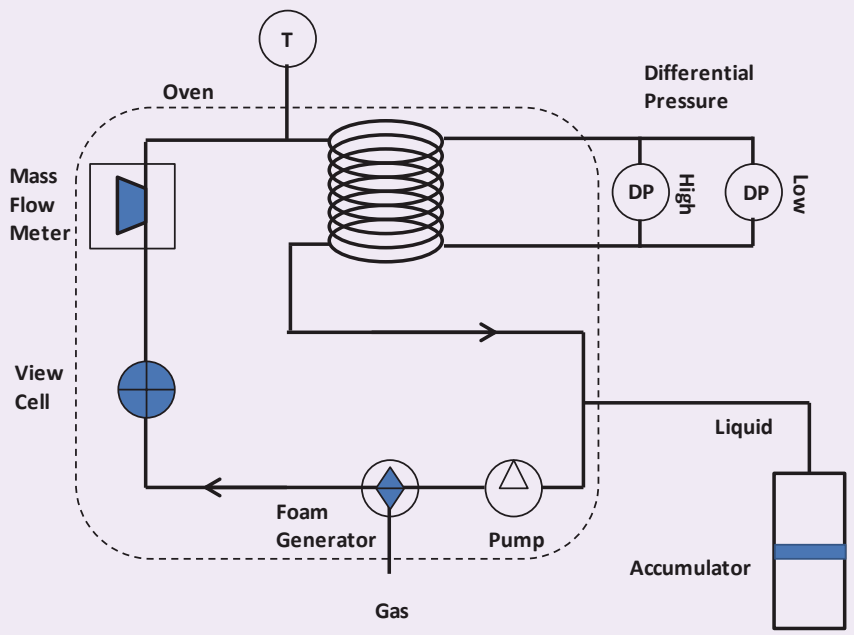
This research highlights the use of cost-effective commercial surfactants and NPs for reservoir fracturing.

Experimental Methods

Materials

Silica (99.5%, 7 nm) was purchased from Sigma-Aldrich, while silica (99.5%, 20-30 nm) was procured from U.S. Research Nanomaterials Inc. CTAB (≥ 98%) was purchased from Sigma-Aldrich and utilized without further purification. CO_2 (99.999%) gas was procured from Abdullah Hashim Industrial Gases &

Fig. 1 *A schematic of a circulating loop foam rheometer.*



Equipment (AHG), KSA. Ultra-pure milli-Q water having a resistivity (18.2 MΩ·cm at 25 °C) was used for the preparation of CO_2 foam formulations.

Characterization Techniques

The crystal structure and phase of silica NPs were investigated using a benchtop X-ray diffractometer (Rigaku MiniFlexII, Japan) having Cu K_{a1} radiation (γ = 0.15416 nm). The powder samples were scanned between 2θ angle (10° to 60°) and a step size of 0.03°. The surface morphology and particle size of silica NPs were examined via a field emission transmission electron microscope (FETEM) (JEM-2100F, JEOL, Japan).

For this purpose, the silica nanopowder was dispersed in ethanol using an ultrasonic probe sonicator to have maximum deagglomeration of particles before imaging. The S_{BET} of both silica NPs was measured by the N_2 adsorption-desorption method using a Micromeritics (ASAP 2010, Micromeritics, USA) analyzer. Silica NPs were degassed under a N_2 environment at 250 °C before the measurements. Zetasizer (ZEN3600, Malvern) was used to investigate the surface charge and zeta potential of silica NPs by dispersing the particles in deionized water.

The optimization of the CO_2 foam formulations was performed at room temperature using a dynamic foam analyzer (DFA-100).

Foam Rheology Testing

The stability of CO_2 foamed water with and without NPs at 250 °F was studied using a circulating loop foam rheometer with a 0.25" internal diameter and 10 ft long tube. All foamed experiments in this study were adjusted to maintain a 70% foam quality. Figure 1 is a schematic of the circulating loop foam rheometer.

To test the stability of the foam, a 500 shear rate was used while maintaining the foam's quality and then it was dropped to 100 1/s to measure foam stability. The proportion of shear stress to shear rate was used to calculate the viscosity of the foam. The shear rate and shear stress are calculated using the rate at which the fluid is pushed through the coil, and using the differential pressure across the coil, respectively.

Results and Discussions

Materials Characterization

The crystal structure, phase, and purity of commercial silica (CS) NPs were examined by XRD analysis. Figure 2 exhibits the diffraction patterns of the powdered silica — CS-7 and CS-30 — having a hexagonal crystal structure. The amorphous nature of silica NPs was confirmed by a broad diffraction peak observed at 2θ position ~22.5° (JCPDS No., 00-001-0649)[8, 9]. Moreover, no further peaks were found in the XRD patterns showing the high purity of the CS NPs.

The surface morphology, particle size, and aggregation behavior of silica NPs were examined via FETEM. Figures 3a and 3b are the low resolution FETEM images of the CS-7 and CS-30 silica NPs. Both types of silica NPs are spherical with some aggregation, due to the presence of attractive forces between the particles. Figures 3c and 3d are the high resolution FETEM images of the CS-7 and CS-30 silica NPs, having an average diameter of ~12 nm and ~25 nm, respectively.

The N_2 adsorption-desorption isotherms for the silica NPs were attained by plotting relative pressure vs. volume adsorbed. Then, the S_{BET} of the CS-7 and CS-30 silica NPs were calculated from the isotherms, Fig. 4, which were found to be 357.43 and 157.54 $m^2 g^{-1}$, respectively. The comparison indicates that the S_{BET} of CS-7 is 2.27 times higher than that of the CS-30 sample.

Based on the results attained from XRD, FETEM, and surface area measurements, it seems that CS-7 silica NPs have more uniform morphology, smaller particle size, and greater surface area. Therefore, the CS-7 silica NPs were selected as a promising material for CO_2 foam stabilization.

The zeta potential can significantly affect the properties of foamed suspensions. Generally, the zeta potential of 30 mV to 40 mV is the range for stable foams. A zeta potential value below 30 mV promotes instability of the foamed colloidal suspension. Having strong interparticle repulsion forces prevent forming of a densely packed particle arrangement at liquid/gas interfaces. The stronger attraction between surfactants and NPs in a foam can limit the number of NPs at the gas-liquid interface and cause the lamella thinning as well as liquid drainage, and gas

Fig. 2 The XRD patterns of the CS-7 and CS-30 powdered silica materials.

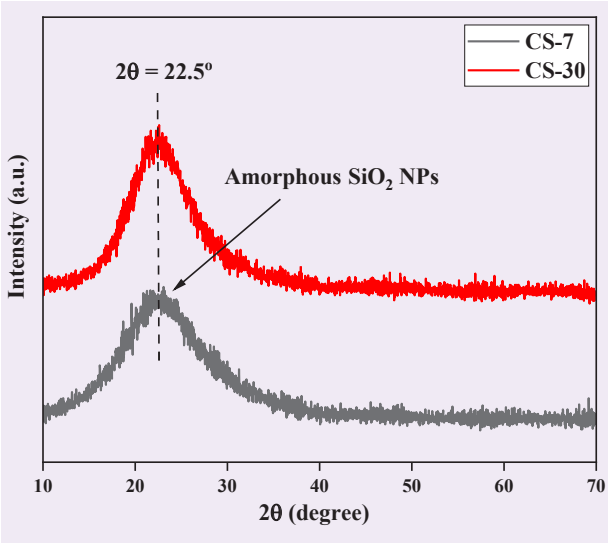


Fig. 3 The low and high resolution FETEM images of CS-7 (a) and (c), and CS-30 (b) and (d) silica NPs, respectively.

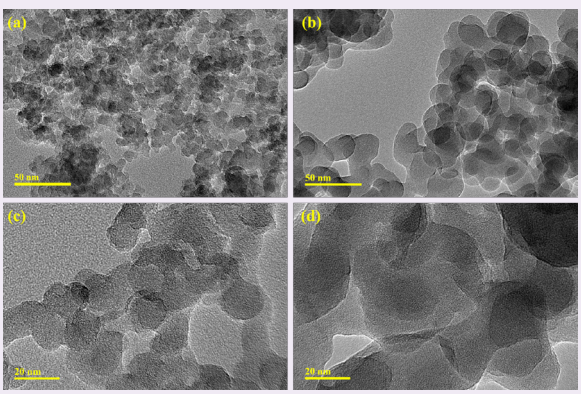
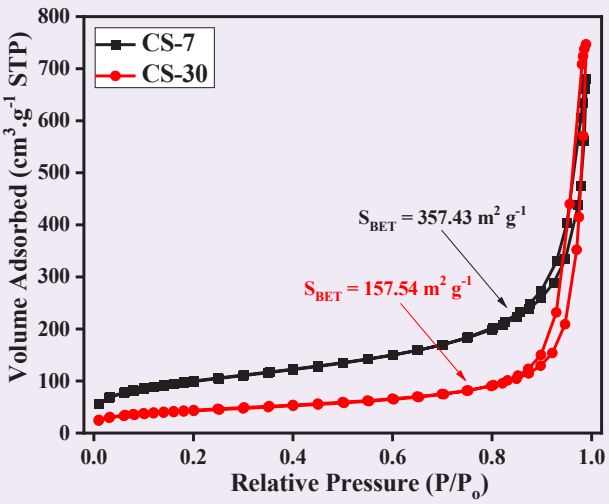


Fig. 4 *The N_2 adsorption-desorption isotherms of the CS-7 and CS-30 silica NPs.*



bubble rupturing.

Therefore, negatively charged NPs can easily interact with cationic surfactants to produce a stable foam. Positioning more NPs at the gas-liquid interface increases the surface tension, and in turn, the bubble strength of produced foam is increased. Keeping in mind the importance of the surface charge of silica NPs and their interaction with a CTAB surfactant, the zeta potential values of the CS-7 NPs and the CS-7+CTAB formulation were recorded, Figs. 5a and 5b, respectively.

The results reveal that the CS-7 silica NPs are negatively charged having a zeta potential value of -36.9 mV. While the CS-7+CTAB formulation shows positively charged micelles having a zeta potential value of 42.1 mV, respectively. The comparison indicates that the CS-7+CTAB formulation further improves the stability of the silica NPs (CS-7) in the aqueous system.

Foam Formulation Studies

The commercially available CTAB surfactant was utilized with cost-effective silica NPs (CS-7) to develop stable CO_2-based foam formulations at an ambient temperature. To optimize the formulations, first, the effect of the flow rate (CO_2 gas) was investigated. For this purpose, various flow rates of CO_2 gas (such as 0.2 L/min, 0.3 L/min, 0.4 L/min, 0.5 L/min, and 0.6 L/min) were tested, and it was observed that the optimum flow is 0.3 L/min, which has better foam stability and half-life. In the preliminary tests, the effect of CTAB concentration has been investigated. For this purpose, a range of concentrations of CTAB (0.02 wt%, 0.03 wt%, 0.04 wt%, 0.05 wt%, and 0.10 wt%) were tested, and the results indicate that the 0.03 wt% CTAB produces the most stable foam in the absence of NPs.

To study the effect of NPs on the foam formulations, the foam stability was investigated using different concentrations (0.0 wt%, 0.001 wt%, 0.005 wt%, 0.010 wt%, and 0.050 wt%) of CS-7 silica NPs by keeping the surfactant concentration (0.3 wt%) and other parameters constant (CO_2 gas = 0.3 L/min, foaming time = 45 s), Fig. 6a. The results indicate that the addition of silica NPs improved the foam stability, and a CO_2-based formulation having CS-7 silica NPs (0.005 wt%) produces the most stable foam. Figure 6b exhibits the foam half-life (242.8, 256.7, 291.1, 274.0, and 271.1) at various concentrations (0.0 wt%, 0.001 wt%, 0.005 wt%, 0.010 wt%, and 0.050 wt%) of CS-7 silica NPs, respectively. The comparison indicates that CO_2-based formulation having CS-7 silica NPs (0.005 wt%) improves the foam stability by up to 12%, which shows the positive impact of silica NPs.

The foam structure of various foam formulations was investigated, and their representative images are displayed in Figs. 7a to 7e. These images were captured after 250 seconds of foam formation. The comparison indicates that the CS-7 silica NPs having a concentration of 0.005 wt% show more compact foam, which improves the foam stability by controlling the bubble size, inter-bubble gas diffusion, and foam's lamellae.

The experimental approach we adopted to use silica NPs is promising. This encourages us to work on different types/sizes of NPs and the functionalization of silica NPs using various silanes to achieve the optimum hydrophilic-lipophilic balance (HLB) value. The optimum HLB value of surfactants and the right concentration of NPs are the key components to further improving foam stability.

Rheological Studies

CO_2 is in a supercritical state during fracturing and flows like gas with liquid-like densities. Pressure and solvent properties improve the solubility of CO_2, which aids in the formation of

Fig. 5 *The zeta potential measurements of the CS-7 silica NPs and CS-7+CTAB formulation.*

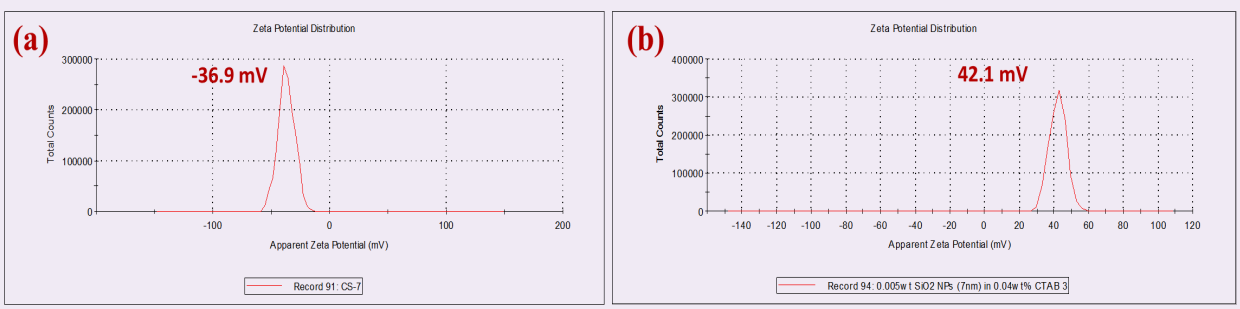


Fig. 6 *(a) The foam stability, and (b) foam half-life results using CTAB surfactant at various concentrations of CS-7 silica NPs (Conditions: CTAB = 0.03 wt%, CO_2 gas = 0.3 L/min, foaming time = 45 s).*

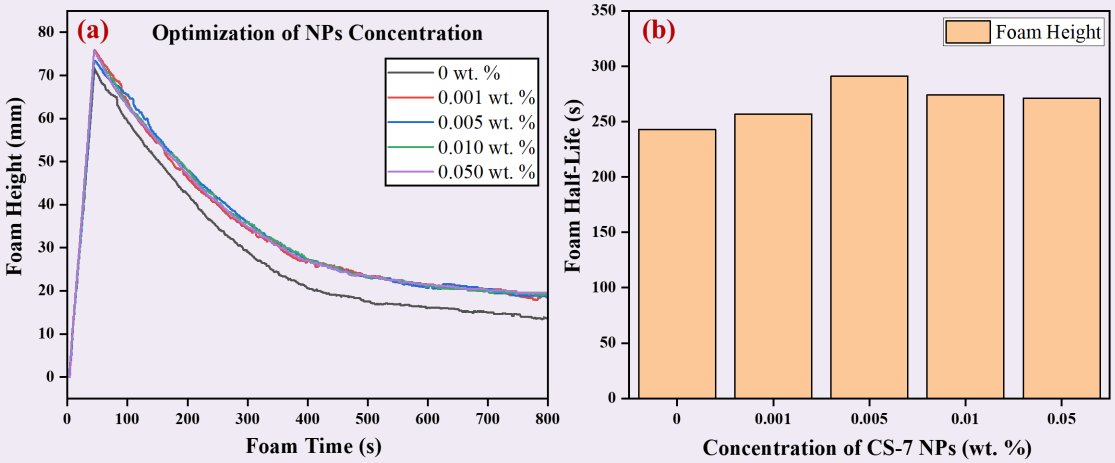
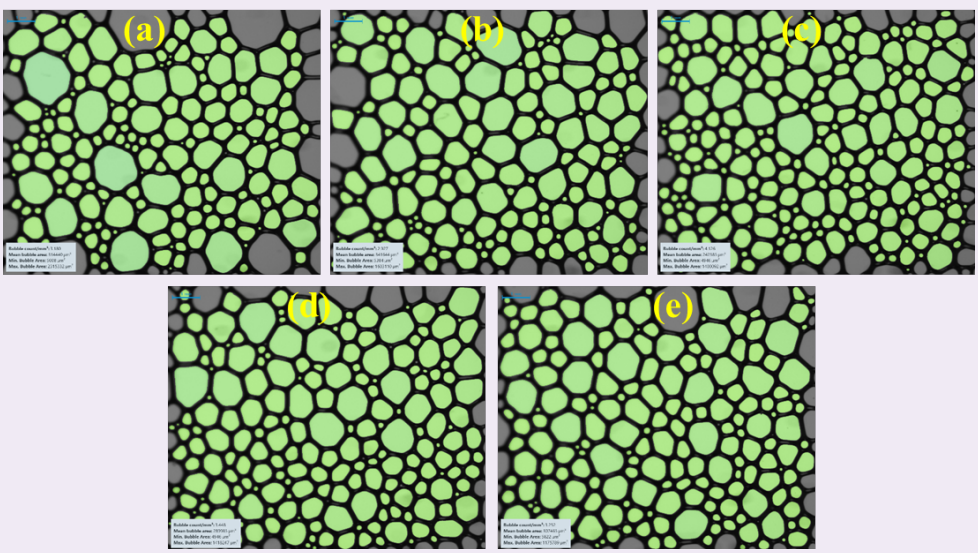


Fig. 7 *Representative images of CO_2 foam structures at various concentrations (0.0 wt%, 0.001 wt%, 0.005 wt%, 0.010 wt%, and 0.050 wt%) of CS-7 silica (Conditions: CTAB = 0.03 wt%, CO_2 gas = 0.3 L/min, foaming time = 45 s). The images were captured after allowing foam formation for 250 seconds.*



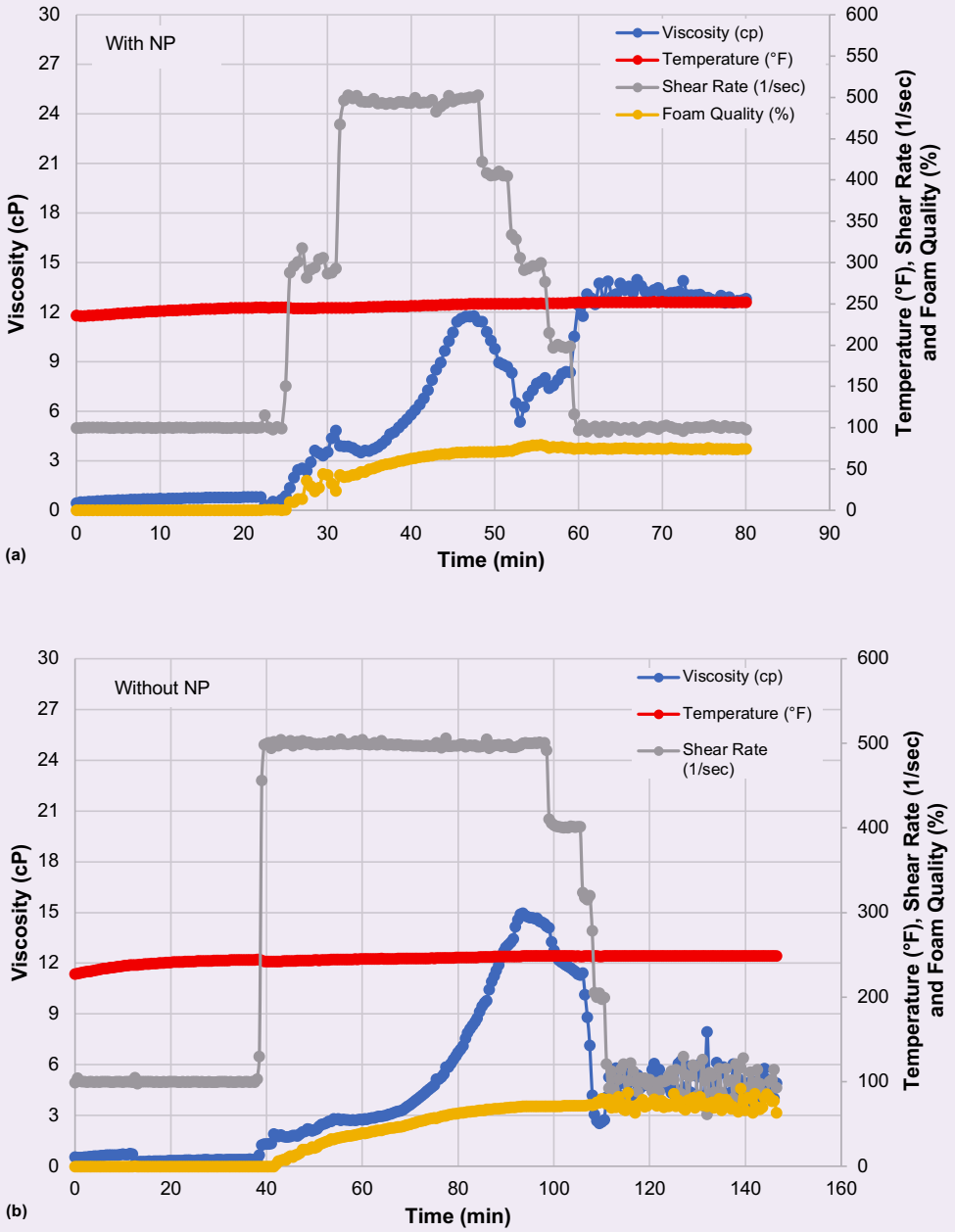
a homogeneous fracturing fluid combination. With standard equipment, liquid CO_2 may be pumped and transported at a liquid, non-cryogenic temperature. It expands to reservoir pressure and vaporizes to become gaseous after being heated to reservoir temperature. The post-fracturing flow back and cleanup can be helped by the gaseous CO_2. The high density of liquid/supercritical CO_2 during injection, which is approximately a specific gravity of 1.014, contributes to an increased hydrostatic pressure. Lowered IFT and clay inhibition are two additional advantages of CO_2[10].

Figure 8 shows the CO_2 foamed viscosity prepared using water with and without NP. The fluid without NPs was prepared using 0.04 wt% CTAB surfactant while fluid with NPs were prepared using 0.04 wt% CTAB and 0.005% NP. A 70% foam quality was achieved with water as a base fluid using CO_2 while shearing fluid at 500 1/s, 2,000 psi, and 250 °F. After foam stabilization, the shear rate was dropped to 100 1/s and kept constant throughout the test. The viscosity of the generated foam was stabilized and measured to be 4 cP at 100 1/s. The test with NPs showed 12 cP after dropping the shear rate to 100 1/s, which showed three times the enhancement in CO_2 foamed viscosity.

Conclusions

In this article, CO_2 foam stability is enhanced by optimizing

Fig. 8 *The CO_2 foamed viscosity was measured at 2,000 psi and 250 °F with NP (a), and without NP (b).*



the concentrations of a CTAB surfactant and silica NPs at high temperature. XRD results reveal that CS-7 and CS-30 are amorphous in nature having hexagonal crystal structure. FETEM images exhibit that CS-7 and CS-30 silica NPs have an average diameter of ~12 nm and ~25 nm, respectively. The surface area of CS-7 is 2.27 times higher than that of the CS-30 sample.

Based on these results, it was affirmed that CS-7 silica NPs have more uniform morphology, smaller particle size, and greater surface area. The zeta potential values of the CS-7 NPs and CS-7+CTAB formulation were found to be -36.9 and 42.1 mV, respectively, which promotes the stability of the foamed colloidal suspension and the formation of a densely packed particle arrangement at the liquid/gas interface.

The physical characteristics of the NPs such as crystalline phase, particle size, shape, porosity, and surface area are important factors to understand foam formulations and stability phenomena. The foam analysis results indicate that the CO_2-based formulation having CS-7 silica NPs (0.005 wt%) improves the foam stability by up to 12%, which shows the NPs tend to stabilize foam formulations. The rheological properties of the NPs stabilized CO_2 foamed fluids showed 12 cP at 100 1/s using water as external phase at 2,000 psi and 250 °F. The utilization of NPs overcomes the factors of foam destabilization, such as the foam's lamellae thinning, water drainage, and inter-bubble

gas diffusion. The optimum HLB value of surfactants and the right concentration of NPs are the key components to improve the foam stability.

Acknowledgments

This article was presented at the SPE/IATMI Asia Pacific Oil and Gas Conference and Exhibition, Jakarta, Indonesia, October 10-12, 2023.

References

1. Yekeen, N., Padmanabhan, E., Idris, A.K. and Chauhan, P.S.: "Nanoparticles Applications for Hydraulic Fracturing of Unconventional Reservoirs: A Comprehensive Review of Recent Advances and Prospects," *Journal of Petroleum Science and Engineering*, Vol. 178, July 2019, pp. 41-73.
2. Slatter, T.D., Rucker, J.R. and Crisp, E.L.: "Natural Gas Stimulation in Tight, Clay-Bearing Sandstone Using Foamed CO_2 as Hydraulic Fracturing Media," SPE paper 15238, presented at the SPE Unconventional Gas Technology Symposium, Louisville, Kentucky, May 18-21, 1986.
3. Briscoe, H.R.: "Stabilized Foamed Acid, a New Stimulation Technique for Carbonate Gas Reservoirs," SPE paper 8141, presented at the SPE Permian Basin Oil and Gas Recovery Conference, Midland, Texas, February 22-23, 1979.
4. Scherubel, G.A. and Crowe, C.W.: "Foamed Acid, a New Concept in Fracture Acidizing," SPE paper 7568, presented at the SPE Annual Fall Technical Conference and Exhibition, Houston, Texas, October 1-3, 1978.
5. Tang, F-Q., Xiao, Z., Tang, J-A. and Jiang, L.: "The Effect of SiO_2 Particles upon Stabilization of Foam," *Journal of Colloid and Interface Science*, Vol. 131, Issue 2, September 1989, pp. 498-502.
6. Yekeen, N., Manan, M.A., Idris, A.K., Padmanabhan, E., et al.: "A Comprehensive Review of Experimental Studies of Nanoparticles Stabilized Foam for Enhanced Oil Recovery," *Journal of Petroleum Science and Engineering*, Vol. 164, May 2018, pp. 43-74.
7. Yu, J., Liu, N., Li, L. and Lee, R.L.: "Generation of Nanoparticle-Stabilized Supercritical CO_2 Foams," CMTC paper 150849, presented at the Carbon Management Technology Conference, Orlando, Florida, February 7-9, 2012.
8. Khan, A.M., Shafiq, F., Khan, S.A., Ali, S., et al.: "Surface Modification of Colloidal Silica Particles Using Cationic Surfactant and the Resulting Adsorption of Dyes," *Journal of Molecular Liquids*, Vol. 274, January 2019, pp. 673-680.
9. Rehman, A.U., Khan, S.A., Ali, S., Nazar, M.F., et al.: "Counterion Engineered Surfactants for the Novel Synthesis of Colloidal Metal and Bimetal Oxide/SiO_2 Materials with Catalytic Applications," *Colloids and Surfaces A: Physicochemical and Engineering Aspects*, Vol. 571, June 2019, pp. 80-85.
10. Karadkar, P.B., Bataweel, M.A., Bulekbay, A. and Alshaikh, A.A.: "Energized Fluids for Upstream Production Enhancement: A Review," SPE paper 192255, presented at the SPE Kingdom of Saudi Arabia Annual Technical Symposium and Exhibition, Dammam, Kingdom of Saudi Arabia, April 23-26, 2018.

About the Authors

Prasad B. Karadkar

M.S. in Chemical Engineering, Nagpur University

Prasad B. Karadkar is a Petroleum Engineer with the Production Technology Team of Saudi Aramco's Exploration and Petroleum Engineering Center – Advanced Research Center (EXPEC ARC). Prior to joining Saudi Aramco in April 2016, he worked as a Senior Technical Professional for Halliburton for 9 years. Prasad's areas of expertise include developing new fluid systems in the area of hydraulic fracturing, acidizing, diversion, and water shutoff.

He has authored and coauthored 16 papers, published one patent, and has several patent applications in process.

In 2003, Prasad received his B.S. degree in Chemical Engineering from Shivaji University, Kolhapur, India, and in 2007, he received his M.S. degree in Chemical Engineering from Nagpur University, Nagpur, India.

Dr. Shahid Ali

Ph.D. in Chemistry, King Fahd University of Petroleum and Minerals

Dr. Shahid Ali is a Research Scientist (Associate Professor) at the Interdisciplinary Research Center for Hydrogen and Energy Storage (IRC-HES), King Fahd University of Petroleum and Minerals (KFUPM). His work concentrates on the development of advanced colloidal nanomaterials, fluorescent sensing materials, energy storage materials, electrolytes and membranes for redox (reduction-oxidation) flow battery systems, and MRI/CT contrast agents for oil reservoir applications.

Shahid has been actively involved in various research projects funded by Saudi Aramco, the National Science, Technology and Innovation Plan (NSTIP), the Deanship of Scientific Research (DSR) at KFUPM, and the IRC-HES.

He has published more than 50 peer-reviewed research articles in reputable international journals and holds several U.S. patents.

In 2017, Shahid received his Ph.D. degree in Chemistry from KFUPM, Dhahran, Saudi Arabia.

Tamim Alshehri

Tamim Alshehri is a Senior Lab Technician with the Production Technology Team of Saudi Aramco's Exploration and Petroleum Engineering Center – Advanced Research Center (EXPEC ARC).

He has been working with the Smart Fluid team for six years, mastering the coreflooding system, and the rheology testing using different types of equipment. Tamim is an expert on many bench test methods, building and designing new setups for various types of experiments.

He has participated on several different programs throughout his time with Saudi Aramco.

Tamim has coauthored more than seven publications and has two patent applications.

Dr. Bader G. Alharbi

Ph.D. in Petroleum Engineering, Heriot-Watt University

Dr. Bader G. Alharbi joined Saudi Aramco in 2006 as a Petroleum Engineer. Bader is currently working in the Production Technology Division of Saudi Aramco's Exploration and Petroleum Engineering Center – Advanced Research Center (EXPEC ARC), where he is a focus area champion of smart fluid. Bader's research interests include well stimulation and scale mitigation.

He has authored and coauthored more than 35 journal and conference papers. Bader has more than 25 granted and submitted invention disclosures.

He received his B.S. degree in Chemical Engineering, and his M.S. degree in Petroleum Engineering, both from King Fahd University of Petroleum and Minerals (KFUPM), Dhahran, Saudi Arabia. Bader received his Ph.D. degree in Petroleum Engineering from Heriot-Watt University, Edinburgh, Scotland, U.K.

Mohammed Alsakkaf

M.S. in Chemical Engineering, King Fahd University of Petroleum and Minerals

Mohammed Alsakkaf is currently a Ph.D. candidate at King Fahd University of Petroleum and Minerals. He is actively engaged in two primary areas of research: Enhanced oil recovery (EOR), and hydraulic fracturing. Mohammed's EOR research, resulting in four published articles, employs biosurfactants in formulating stable crude oil/water nanoemulsions for efficient EOR; however, the formulated nanoemulsion can be quickly separated as needed.

Concurrently, his hydraulic fracturing research explores the use of CO_2 as a fracking agent, striving to reduce water demand and pollution by stabilizing CO_2 foam using functionalized nanoparticles. Both areas of Mohammed's research emphasize environmental considerations in the pursuit of more efficient fossil fuel extraction processes.

He received both his B.S. and M.S. degrees in Chemical Engineering with honors from King Fahd University of Petroleum and Minerals (KFUPM), Dhahran, Saudi Arabia.

Dr. Muhammad Mansha

Ph.D. in Chemistry, King Fahd University of Petroleum and Minerals

Dr. Muhammad Mansha is a Research Scientist at the Interdisciplinary Research Center for Hydrogen and Energy Storage (IRC-HES), King Fahd University of Petroleum and Minerals (KFUPM).

In 2018, he joined KFUPM as a Post-Doctoral Fellow and worked on the development of novel viscoelastic surfactants (VES) and synthesis of water-soluble hyperbranched polymers for oil field applications. Currently, Muhammad's focus areas of research are organic redox (reduction-oxidation) flow batteries, organic-nanohybrids, sensing nanomaterials, and colloidal formulations.

He received his Ph.D. in Chemistry from KFUPM, Dhahran, Saudi Arabia. In Muhammad's work for his Ph.D., he carried out the syntheses of pyrazole-based anticancer drugs, conjugated polymers for chemosensing, water splitting, and water purification.

Dr. Safyan A. Khan

Ph.D. in Colloidal Chemistry, University of Bristol

Dr. Safyan A. Khan is a Research Scientist at the Interdisciplinary Research Center for Hydrogen and Energy Storage (IRC-HES), King Fahd University of Petroleum and Minerals (KFUPM). His research mainly focuses on the field of colloidal formulation, synthesis of nanomaterials, and surface science.

In the past, Safyan has undertaken a number of technology challenges on the synthesis and colloidal aspects of colored poly(methyl methacrylate) for electrophoretic displays, core/shell silica nanoparticles, quantum dot encapsulations in hydrophobic and hydrophilic shells, nano-detergents for lubricants, neutron radiation absorbing coating, superparamagnetic nanoparticles, polymer coated nanoparticles for water purification, complex fluids, rheological properties of phenolic resin, polysulfides for redox flow batteries, colloidal fluids for oil upstream, sand consolidation, foam stabilization and other novel uses of colloidal nanoparticles.

Safyan received his Ph.D. degree in Colloidal Chemistry from the University of Bristol, Bristol, U.K.

Water Hammering Evaluation in Perforation Efficiency for Variable Perforation Designs in Unconventional Horizontal Wells

Abdulrahman M. Alowaid, Tayyar S. AlTayyar and Karim Mechkak

Abstract /

The main scope of this article is to expand the existing efforts exerted in the field of water hammering through the reprocessing of existing post-treatment data in the estimation of perforation efficiency and subsequent fracture geometry. The focus is on special applications when perforation designs were varied across subject wells that underwent stimulation through multistage hydraulic fracturing. The article investigates fluctuating pressure behavior noticed immediately after a single hydraulic fracturing stage is pumped, commonly referred to as water hammering.

The objective of this article is to showcase the results of examining water hammering signatures across different perforation designs and linking these variances to perforation efficiency, by zooming into the variability of the water hammer amplitude magnitude, and its incremental difference from one perforation design to the next, or from one well to the other.

Two application examples are highlighted in the article: The first evaluated a horizontal well with three different perforation designs, while the second compared a stand-alone well to an offset well with identical drilling and completion designs.

In the first application, there was an inverse relationship between the perforation efficiency and the amplitude of the water hammer; where higher perforation efficiency was consistently matched with a lower amplitude magnitude, resulting from lowering the total number of perforations per stage, and vice versa.

In the second application, two offset wells with similar geomechanical, drilling, and completion properties were analyzed. The first well had a lower perforation efficiency compared to the second, which corresponded to a larger water hammer amplitude confirming the repeatability of the inverse relationship between the two parameters. For both examples, estimating the incremental reduction in the water hammer amplitude corresponded to the same percentage of improvement in perforation efficiency.

That variability was the sole focus of this article at which it was investigated in detail and compared to the perforation efficiency estimated using other methodologies such as the step-down test. The novelty of this approach is that it capitalized on existing data that is usually overlooked, in detailing the understanding of perforation performance and efficiency in variable perforation designs implemented, or in performing multiple well comparison.

Introduction

The past few decades have observed a rapid growth in exploration and development activities of unconventional hydrocarbon resources worldwide. This rapid growth is attributed to rising demands in fossil fuels to meet ever growing global energy demands.

The definition of unconventional hydrocarbon resources is continuously disputed, where a large portion of professionals link it to the ultra-low permeability that prevents its natural commerciality, while others link it to large capital investment in drilling and stimulation activities that turn them into profitable ventures. Nonetheless, and especially for low permeable shale formations, there is a unanimous agreement on the need for horizontal drilling and aggressive stimulation operations to unlock the full potential of those targeted layers. Currently, horizontal laterals and multistage hydraulic fracturing became the norm in the development of unconventional hydrocarbon resources.

Compared to its conventional counterpart, those practices are an extreme necessity to tip the scales of commerciality. Consequently, the margin of profit is relatively volatile depending on the completion needs of each well at a specific formation, and how much can it deliver post-stimulation. As a result, development of unconventional hydrocarbon resources is driven by practicality and operational efficiency, and sometimes, those come at the expense of costly and time-consuming well diagnostics.

One of the most common techniques followed in multistage hydraulic fracturing is the plug-and-perf (PnP) technique used for zonal isolation and perforation of new stages, where a bottom-hole assembly comprising of a fracturing plug and perforating guns are used to isolate the previously stimulated stage, and perforate holes into a new section of the lateral, Fig. 1.

The number of perforated holes is extremely important to the diagnostics of each stimulated hydraulic fracturing stage, where often the number of perforations that open and undergo stimulation is less than the total number of holes physically perforated. The ratio of open to total number of perforations is commonly referred to as perforation efficiency. This directly impacts the resulted stimulated geometry of that particular stage, where higher perforation efficiency corresponds to a more uniform fracture geometry and vice versa. Accordingly, efforts in selecting the optimum perforation design that maximizes the ratio of active to total perforations is essential to maximize the return on investment for stimulation operations.

There are many industry practices that focus on the diagnostics of perforation efficiency, one of which is the use of a downhole camera to quantify perforation erosion pre- and post-stimulation, another is the utilization of fiber optics to analyze disturbed acoustic sensing and disturbed temperature sensing in visualizing fluid distribution across perforations. Due to the operational intensity in unconventional hydrocarbon resources and their distinct level of activity, operators are shifting toward cost-effective practical alternatives for decision making. An excellent example to that would be the implementation of the step-down test for the quantification of frictional losses and the number of open perforations.

This article follows a similar approach in the practical principle, but with the competitive advantage of having zero cost, as it capitalizes on readily available raw stimulation data that are usually overlooked, specifically discrepancies in post-treatment water hammering signatures to analyze perforation efficiency and subsequent fracture geometry.

The article focuses on the water hammer amplitude magnitude, and how it varies across multiple perforation designs, or from one well to another. These findings are then translated into variances in perforation efficiency based on the incremental difference from one design to the next.

Background

The primary subjects of this study are wells in an area that targets a shale formation that was deposited at very low energy, resulting in ultra-low permeability that ranges in the nano-darcy scale. The targeted reservoir is considered relatively homogeneous, especially across its horizontal lateral, confirmed by well logging and formation micro-imaging, which streamlines the assessment of stimulation operations through the lateral, and across the close vicinity of the evaluated well.

In multistage hydraulic fracturing, the total frictional losses are comprised of three components: (1) pipe friction due to fluid movement inside the tubing, (2) perforation friction due to the entry of fluids across perforations, and (3) near wellbore friction, commonly referred to as tortuosity. For the subject area, near wellbore frictional losses are negligible, confirmed by multiple step-down tests performed at different perforation designs indicating perforation dominated frictional losses as indicated in Fig. 2, supported by the behavior of water hammering and post-treatment pressure decline.

The studied wells underwent stimulation through multistage hydraulic fracturing utilizing the PnP technique for stage-to-stage zonal isolation and perforation. The primary subject of this study, was a well completed with 38 fracturing stages with consistent fluid and proppant fracturing design pumped through all stimulated stages. Each stage consisted of five perforating clusters, but the number of perforation holes was varied through three different designs utilized across the lateral.

The objective was to investigate the impact that the number of perforations have on the perforation efficiency while maintaining a consistent stimulation design. Consequently, the first perforation design was selected as 45 perforation shots, while the second design had 30 shots, and the third was designed for

Fig. 1 *The lateral section stimulation with hydraulic fracturing utilizing the PnP technique.*

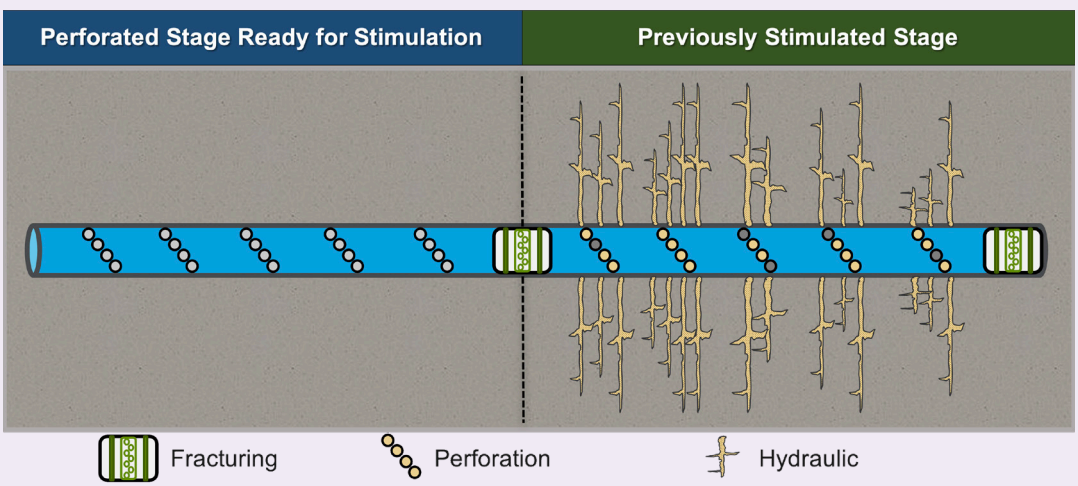
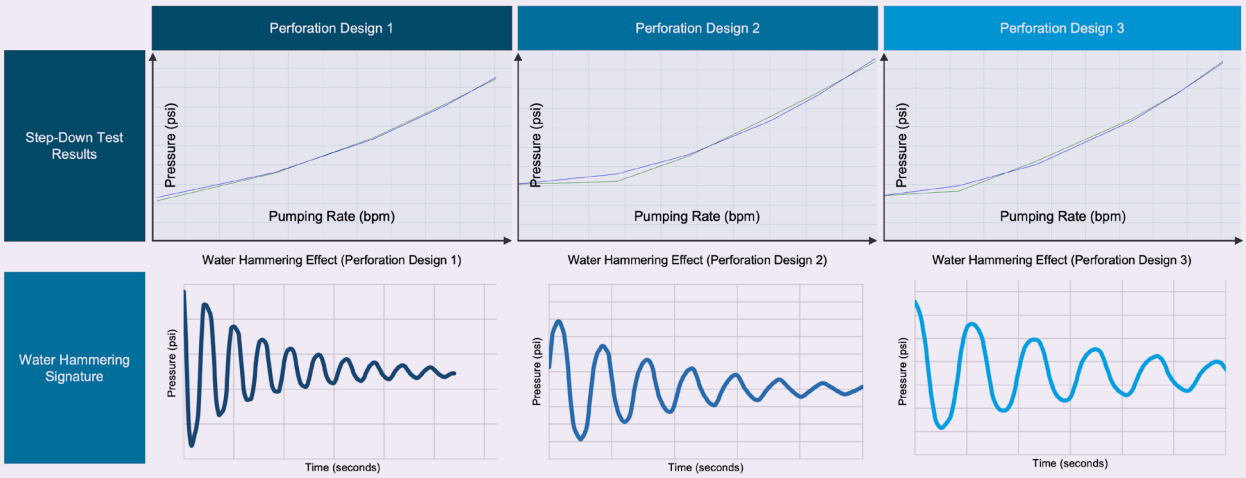


Fig. 2 *The step-down test results and water hammering effect highlighting perforation dominated friction losses.*



22 total perforations. Step-down tests were performed at each perforation design to quantify the ratio of active to the total number of perforations, and ultimately perforation efficiency. During the execution phase, it was observed that the signature of the water hammering effect changed when transitioning from one design to the other. Both the water hammer amplitude and time for that water hammer to stabilize were clearly different for all three perforation designs, which ignited the interest to pursue a closer look on how that translated into perforation efficiency and fracture geometry.

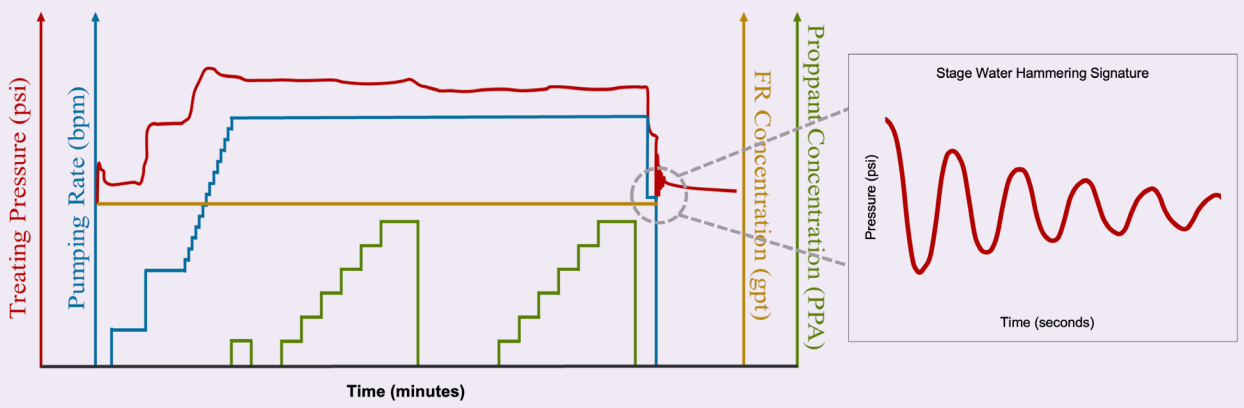
Accordingly, the amplitude of the water hammer became the focus of this study, which was based on a clear observation between the number of perforations and the signature of the water hammer for the same number of perforated clusters. The result indicated that the higher the number of perforations, the larger the magnitude of the water hammer amplitude. That observation became the stepping stone in linking this finding to perforation efficiency and its corresponding fracture geometry. Through the quantification of the magnitude of the water hammer amplitude across the different perforation designs, the variance observed was almost equal to the incremental increase in perforation efficiency quantified through the step-down test of each design.

Since the hydraulic fracturing stages were all pumped through a five cluster design, and the well is relatively homogeneous through its lateral, the variance in water hammering can then be related to fracture geometry generated at each design. Aside from the used methodology having zero cost, it requires only one parameter, an estimation of perforation efficiency at one of the perforation designs to act as a baseline to calculate the variance in reference to this baseline value.

Methodology

The water hammering phase is defined as the period immediately after fluid pumping is stopped and the hydraulic fracturing stage is concluded. This period is characterized by large pressure fluctuations (amplitudes) due to the sudden shut down

Fig. 3 *A generic hydraulic fracturing stage treatment plot with water hammering annotation.*



of pumping operations, that slowly reduce and relax with time until it reaches a point at which it stabilizes and pressure leak-off is monitored, Fig. 3.

The pressure wave generates from the sudden change in fluid movement post-treatment, and dissipates slowly through frictional losses between the wellbore and the stimulated zone. Consequently, the magnitude of that pressure wave is a function of the level of communication with the formation, where the higher the amplitude, the lower the frictional losses to the formation, and therefore, the easier it is for fluid to move freely and vice versa.

In the instance of hydraulic fracturing, that can be related to the uniformity of the generated hydraulic fracture, where a more uniform and intense hydraulic fracture with high perforation efficiency, would create higher frictional losses post-treatment, which restricts fluid movement. That understanding translates into a smaller water hammer signature and a faster pressure wave dissipation. On the other hand, a nonuniform fracture geometry with low perforation efficiency would have low frictional losses post-treatment, which expands the amplitude of the water hammer and the time it takes for the pressure wave to dissipate.

The methodology starts first by filtering out the water hammering phase and excludes any nonrelevant data, allowing for the zonal assessment of water hammering across the evaluated stage without external disturbance generated from the actual pumping of the stage. Next, the water hammering effect is analyzed by quantifying the pressure amplitude magnitude starting from the lowest value of the first amplitude to the highest value of the second amplitude, Fig. 4 and Eqn. 1.

$$P_{amplitude} = P_1 - P_2 \quad (1)$$

The option to pursue these specific intervals was determined to avoid possible lag in pressure data acquisition immediately when pumping is stopped. It was observed that for the same stimulation and cluster design, the lower the number of perforations, the smaller the water hammer and vice versa. Accordingly, the variance in the water hammering amplitude in reference to the baseline perforation design was quantified by simply dividing the difference between the amplitude of both designs over the amplitude of the baseline design as highlighted in Eqn. 2:

$$\%\, Variance_{\,Water\ Hammer} = \frac{P_{amplitude\ (Design\ 1)} - P_{amplitude\ (Design\ 2)}}{P_{amplitude\ (Design\ 1)}}\ x\ 100. \quad (2)$$

Next, the variance or incremental change was compared to the variance in perforation efficiency estimated from the step-down test performed at each design to determine the correlation between water hammering and the perforation efficiency. In the step-down test, the pumping rate is lowered in steps until pumping is stopped, with the corresponding pressure at each pumping rate estimated, and pressure when pumping is stopped referring to pressure with no frictional losses.

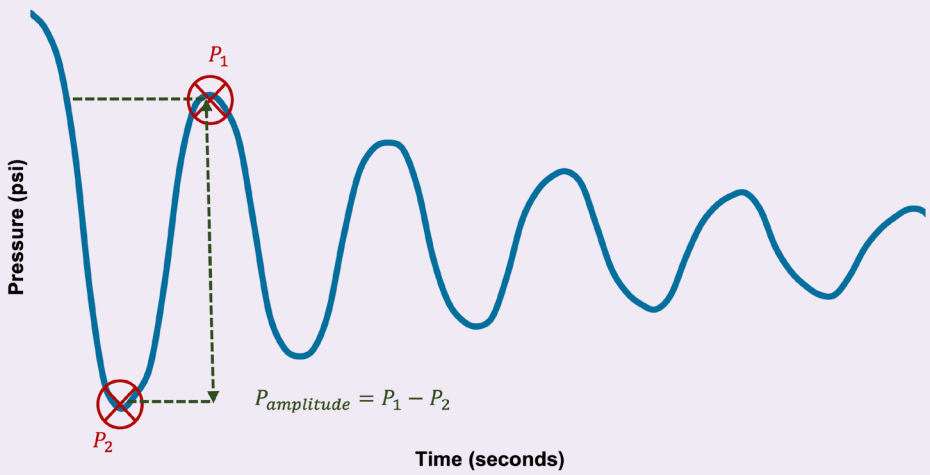
The objective is to acquire a rate and pressure dataset that is then matched by altering the frictional losses and the number of open perforations in the open perf equation derived from the orifice flow meter equation. Since every variable related to stimulation and perforation design was kept constant except for the number of perforations per stage, the methodology was applied to quantify the incremental improvement or reduction in perforation efficiency when transitioning from one design to the next. The results were benchmarked against results from the step-down test to confirm its findings.

Another byproduct of this methodology was an observation similar to the amplitude magnitude. That observation was the time the water hammer required to reach stabilization, and for those pressure fluctuations to dissipate. That yielded similar results where the higher the number of perforations, the longer the time required to reach stabilization. Subsequently, that observation and the incremental difference related to it, yielded qualitative and not quantitative understandings, mainly due to the subjectivity of what classifies a pressure trend to be stable.

Application Example 1 (Variable Perforation Design)

The main application of this methodology was in a horizontal well that was stimulated through multistage hydraulic fracturing utilizing the PnP technique. On the subject well, all stimulation

Fig. 4 *A water hammering signature with methodology selected amplitudes.*



and perforation variables were kept constant aside from the number of perforations per stage. Three different perforation designs were tested: 45 perforations, 30 perforations, and 22 total perforations per stage, respectively, Fig. 5. The perforation clusters were kept constant as five clusters per stage, and therefore, the number of perforations per cluster was the only variable, which was reduced from design 1 to design 2, and finally to design 3. Step-down tests were performed in all three designs to estimate the perforation efficiency at each design.

When transitioning directly from design 1 to design 2, there was a direct and clear observation in the signature of water hammering. That observation was then confirmed when the design was changed again to design 3 with 22 perforations, where both the amplitude magnitude and stabilization time was reduced with a lower number of perforations. That triggered the curiosity for further evaluation to capitalize on that readily available information, and strive at linking it to the perforation efficiency and fracture geometry through quantifying these discrepancies, and then comparing them to the results of the step-down tests performed at each design.

Since the three designs were altered across the lateral, an average water hammering effect was used for each design, where the water hammering signature of all stages pumped using a specific design were averaged to generate a signature that describes all stages pumped at that design, Fig. 6.

It was clearly observed that the water hammering signature tended to shrink in size with the lower number of perforations, in this case, the water hammer amplitude was highest for design 1 with 45 perforations, less for design 2 with 30 perforations, and smallest for design 3 with the lowest number of perforations at 22 holes. Quantifying the amplitude magnitude for each design yielded the results provided in Table 1.

Design 1 with 45 perforations was considered as the baseline design, and therefore, was used as the reference point in computing the incremental variance for designs 2 and 3. Consequently, a 16% reduction in the water hammer amplitude was observed when transitioning from design 1 to design 2. Similarly, a 39% reduction in the amplitude magnitude was estimated when transitioning from design 1 to design 3, and a 28% reduction when transitioning from design 2 to 3.

Integrating the results of the step-down tests performed at each design, design 1 with 45 perforations yielded an average of 24 active perforations with a perforation efficiency of 53%, while design 2 with 30 perforations had 20 active perforations with a 67% perforation efficiency, and design 3 yielded 21 active perforations out of the total 22 perforations with a 95% perforation efficiency.

Interestingly, both the number of active perforations and average treating pressures were almost similar for all three designs, which supported the understanding that through lowering the number of total perforations, a more uniform proppant distribution across perforations was achieved. Comparing the variance in reference to the step-down test, transitioning from design 1 to 2 yielded a 14% improvement in perforation efficiency, changing from design 1 to 3 resulted in 42% increased perforation efficiency, and moving from design 2 to 3 yielded a 28% improvement in perforation efficiency.

Comparing these results with the magnitude of the water hammer amplitude, transitioning from design 1 to 2 yielded a 16% reduction in the amplitude magnitude corresponding to the 14% increase in the perforation efficiency estimated from the step-down test. Similarly, transitioning from design 1 to 3 resulted

Fig. 5 *Application example 1 with three perforation designs.*

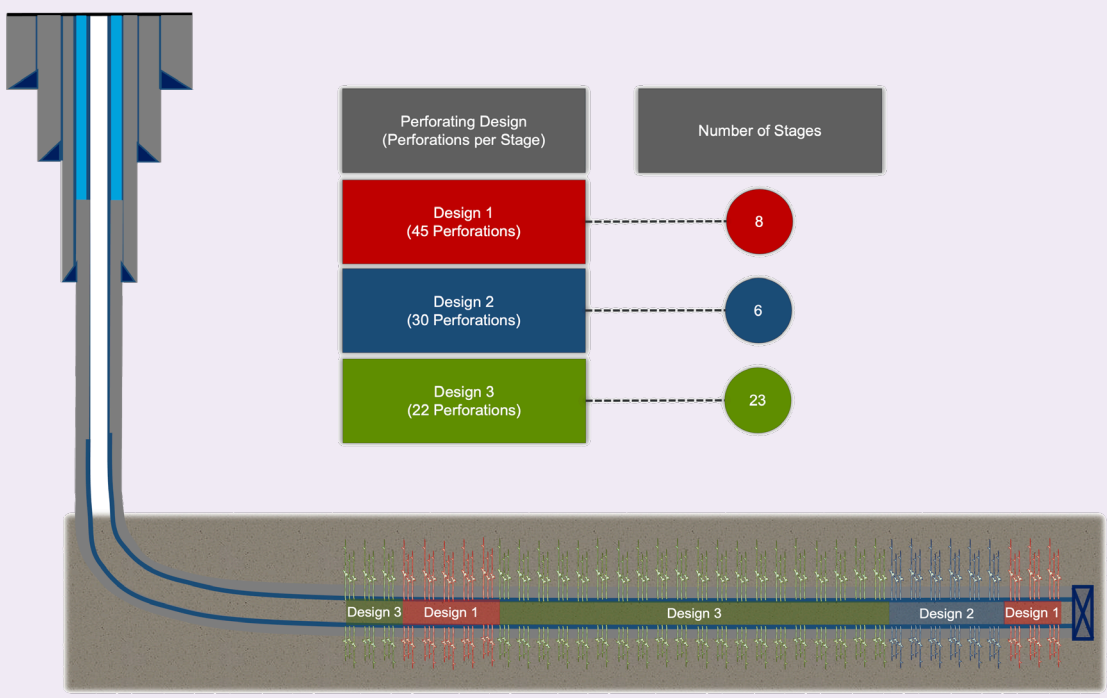


Fig. 6 *The averaged water hammer signatures for each perforation design.*

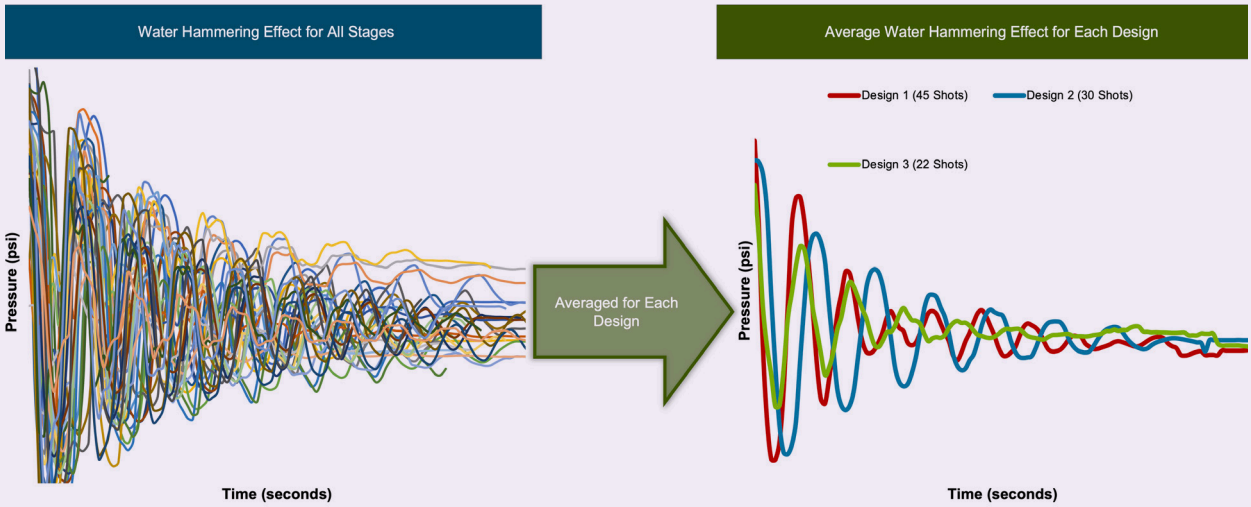


Table 1 *The results summary and comparison of application example 1.*

Parameter	**Design 1**	**Design 2**	**Design 3**
Number of Perforations	45	30	22
Amplitude Magnitude (psi)	1,364	1,150	829
Perforation Efficiency from Step-Down Test (%)	53%	67%	95%
Incremental Improvement	**Design 1 to 2**	**Design 1 to 3**	**Design 2 to 3**
% Improvement (Step-Down Test)	14%	41.5%	27.5%
% Variance (Water Hammer)	15.7%	39.3%	28%
% Difference	1.7%	2.2%	0.5%

in a 39% reduction in water hammer amplitude, very close to the 42% increase in perforation efficiency from the step-down test. Finally, a 28% reduction in amplitude when moving from design 2 to 3 was matched with a 28% perforation efficiency enhancement through the step-down test, Fig. 7.

These observations, and their resemblance in magnitude to the results from the step-down tests, indicated their direct correlation with perforation efficiency, and corresponding fracture geometry, Fig. 8. A higher cluster efficiency indicates a more uniform fracture geometry created through the studied fracturing stage. In other words, a lower water hammer amplitude yields a higher cluster efficiency and a more uniform fracture distribution across the stimulated stage. The incremental increase in cluster efficiency can be estimated through the incremental variance in the magnitude of the water hammer amplitude when transitioning from one perforation design to the next.

Application Example 2 (Two Offset Wells)

The second application was in an area with two independent wells offset to one another with exactly similar geomechanical properties, confirmed by the implementation of a diagnostic fracture injection test on both wells. Drilling and completion practices were mirrored for both wells to ensure a uniform and fair comparison, and to minimize uncertainty around frictional losses or stimulation practices. Well construction, perforation, and stimulation designs were kept constant for both wells. The number of perforations per hydraulic fracturing stage was 45 holes distributed across five clusters, and was mirrored for all stages across both wells. The initial expectations were that both wells should have mirror execution, and assessment of stimulation operations, with identical net pressure and perforation efficiency. On the contrary, the first well had a higher net pressure and a lower perforation efficiency compared to the second well.

The difference in perforation efficiency was estimated as 16% between the two wells, where Well-1 had 61% while Well-2 had a 77% perforation efficiency, both values estimated through utilizing an independent perforation efficiency estimation tool that is beyond the scope of this article. Taking a closer look into water hammering, interestingly, Well-1 yielded a 15.5% increase in the magnitude of the water hammer amplitude compared to

Fig. 7 *A comparison between the results from the step-down test and water hammering.*

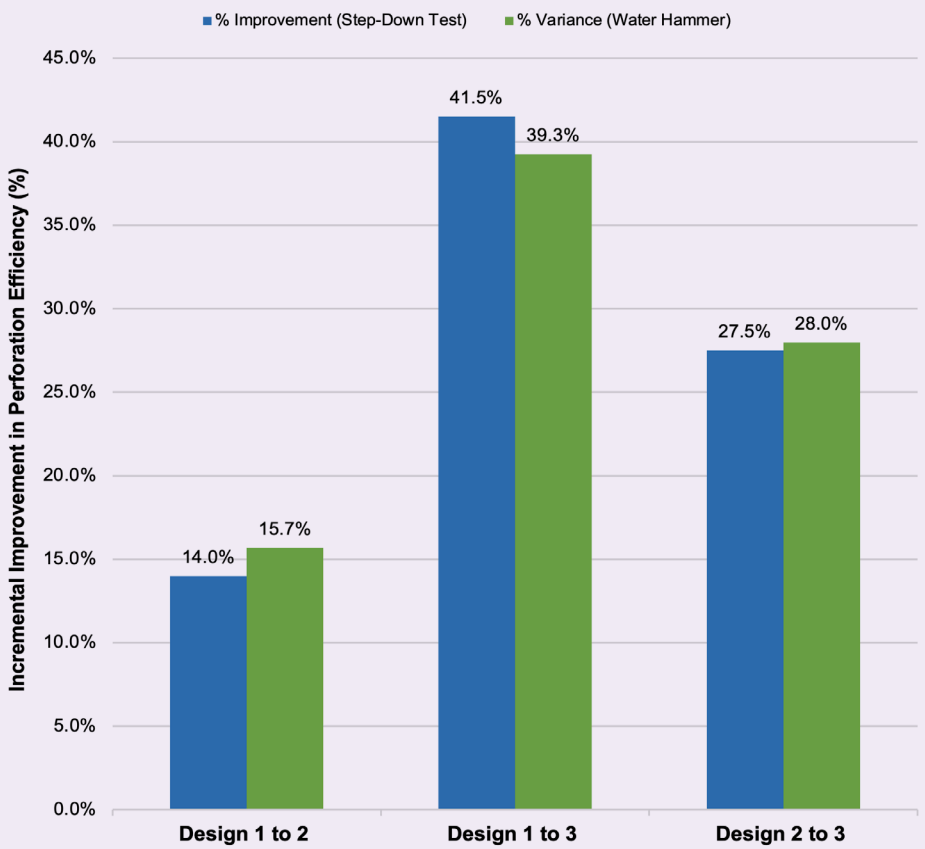
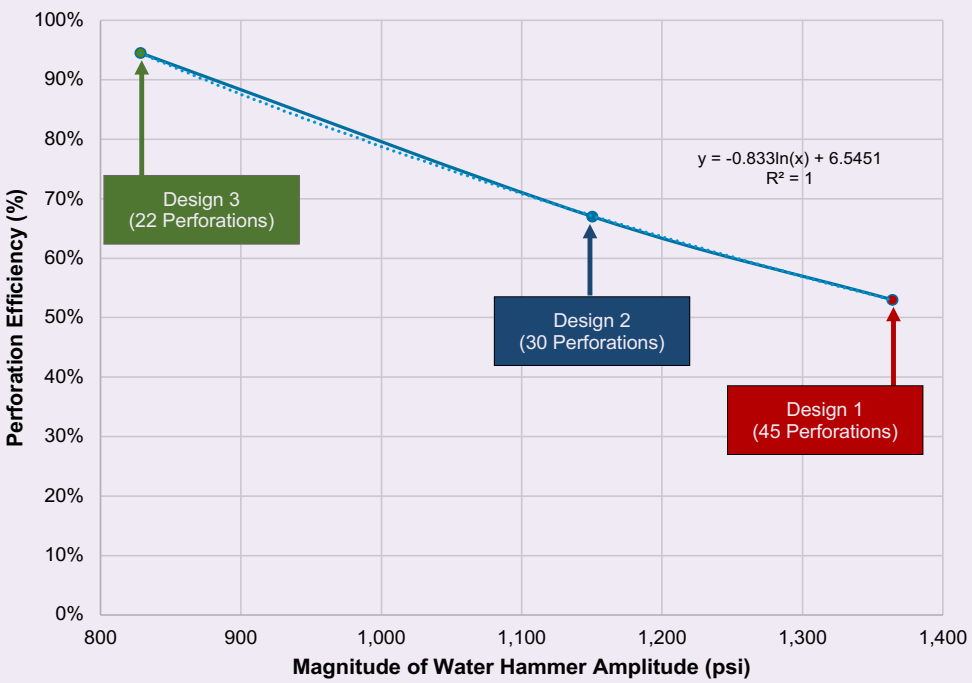


Fig. 8 *The relationship between the perforation efficiency and the magnitude of the water hammer amplitude.*



Well-2, as summarized in Table 2 and Fig. 9. Similar to example 1, this assessment had the same inverse relationship between the magnitude of water hammer and perforation efficiency. Although unlike example 1, this second example expanded the assessment to an aerial scale rather than a single well scale, with results principally aligned for both examples.

Results and Discussion

The first application example highlighted the correlated understanding between water hammering and perforation efficiency in an unconventional horizontal well that underwent multistage hydraulic fracturing. Three different perforation designs were tested on the subject well with the objective of improving the ratio of the active to the total number of perforations, and therefore, perforation efficiency.

The three designs consisted of 45, 30, and 22 total perforations per stage, with improvement in perforation efficiency achieved with a lower number of perforations. The signature of the water hammer was significant for each perforation design, where it tended to shrink in size and magnitude with the reduction of perforations per stage. Through the quantification of the incremental difference in the water hammer amplitude, the percentage directly correlated with the perforation efficiency improvement observed from the step-down test.

In other words, an assessment of the water hammering amplitude magnitude corresponded to the direct estimates of perforation efficiency, where a reduction in the amplitude would yield an increase in perforation efficiency and vice versa. The second application example was in two offset wells with similar drilling, completion, and geomechanical properties. The cluster efficiency was estimated as 61% and 77% for both wells, respectively, even though they had exactly similar perforation and stimulation designs.

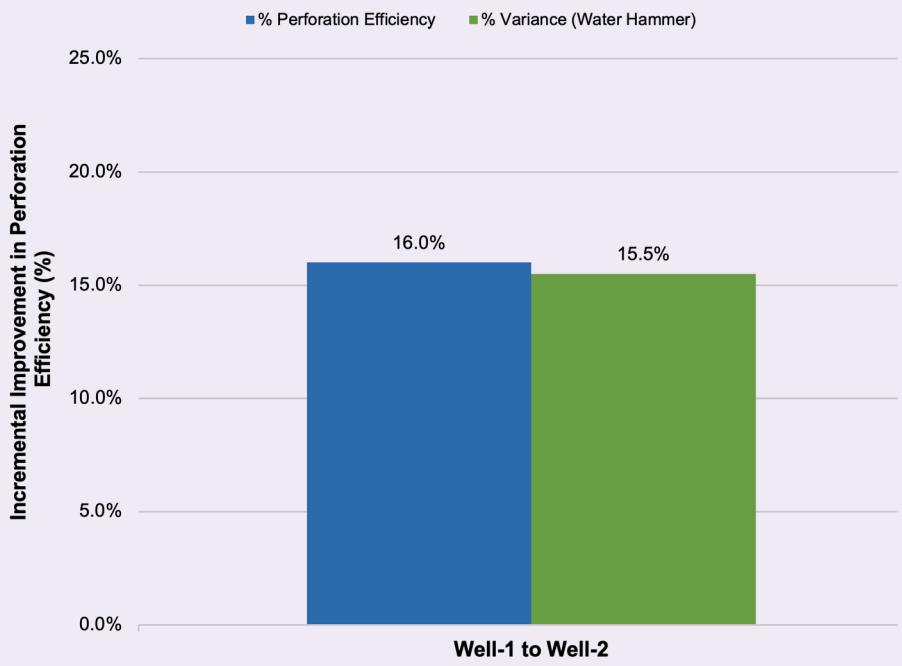
A zoomed look into the water hammering effect yielded interesting findings, where Well-1 had a larger water hammer amplitude magnitude compared to Well-2. The incremental difference in the amplitude magnitude was estimated as 15.5%, almost identical to the difference in the perforation efficiency between the two wells estimated using an independent perforation efficiency estimation tool. The findings and understandings from the adaptation of the implemented methodology were numerous.

The ability to translate observations into quantifiable outcomes referenced to perforation efficiency was the methodology's significance, especially in unconventional hydrocarbon resources where perforation efficiency is a continuous challenge to model,

Table 2 *The results summary and comparison of application example 2.*

Parameter	Well-1	Well-2
Number of Perforations	45	
Amplitude Magnitude (psi)	844	713
Perforation Efficiency (%)	61%	77%
Incremental Improvement	From Well-1 to Well-2	
% Perforation Efficiency	16%	
% Variance (Water Hammer)	15.5%	
% Difference	0.5%	

Fig. 9 *A comparison between the perforation efficiency and water hammering variance.*



quantify, and optimize. Since the methodology utilizes readily available data, which is often overlooked, it is considered as a cost-effective solution, which is the methodology's competitive advantage compared to its peer diagnostic tools.

Another advantage is that since this methodology utilizes the signature of water hammering, it accounts for perforation erosion post-treatment, which corresponds to the actual conditions of perforations after stimulation.

The two examples demonstrated the applicability of utilizing the magnitude of the water hammer amplitude to assess perforation efficiency across designs implemented on the same well, or in performing multiple well comparisons with offset wells with identical completion designs.

Conclusions and Recommendations

Stimulation is one of the key parameters that led to the boom and commercialization of the unconventional business. The most widely used stimulation technique in unconventional hydrocarbon resources is multistage hydraulic fracturing where a large number of fracturing stages are placed along the length of the horizontal lateral to maximize the areal contact with the targeted formation. One of the main challenges facing unconventional hydrocarbon resource operators, especially in PnP operations, is partial perforation efficiency, where a fraction of the total perforations open and contribute to the overall geometry of that stage, while others remain closed and nonactive.

Diagnostics of such phenomena has been engineers' and practitioners' focus of study for many years, with experts introducing analytical tools such as the step-down test, or physical tools such as the use of a downhole camera or fiber optics. Those techniques either require changes in operational procedures or well intervention, which are both not favorable. Alternatively, the introduced methodology capitalizes on readily available data based on observations retrieved from the water hammering signature.

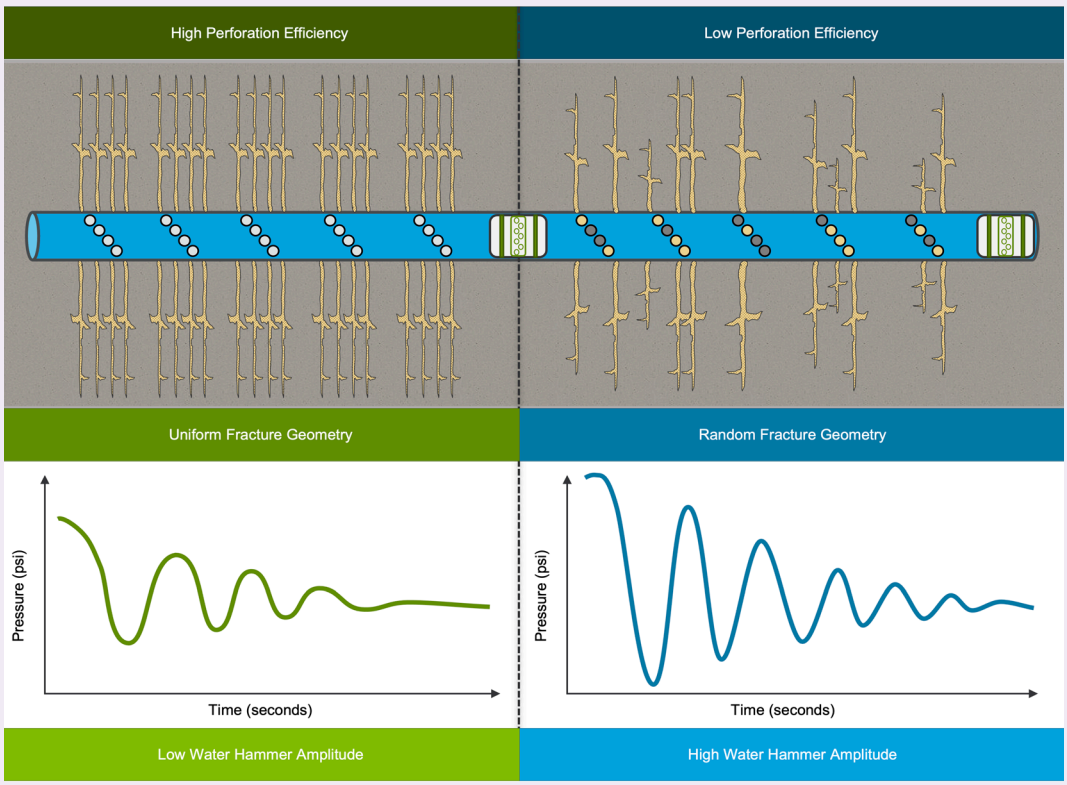
It was observed that for the same stimulation and cluster design, the number of perforations had a direct relationship with the magnitude of the water hammer amplitude, a decrease in the number of perforations, corresponded to a smaller water hammer, and vice versa. Those lessons were then translated into perforation efficiency, where the lower the number of perforations, the smaller the water hammer, and the larger the perforation efficiency, a more uniform fracture geometry is generated.

By quantifying the magnitude of the water hammer amplitude, and computing the incremental difference between one design to the next, the corresponding percentage yielded a value that is almost identical to the percentage of increase or decrease in perforation efficiency estimated from one design to the next.

The first application example highlighted the findings of three perforating designs implemented on the same horizontal well. The applied methodology yielded similar values to the incremental increase achieved through step-down tests performed at all three designs.

The second application example was from a well-to-offset comparison of two wells with identical completion and stimulation

Fig. 10 *An illustration of the impact of high vs. low perforation efficiency on fracture geometry.*



operations. Well-1 had lower cluster efficiency compared to Well-2, which correlated to a larger water hammer. The percentage of difference in the amplitude of water hammer correlated as well to the difference in perforation efficiency between the two wells.

The knowledge and understanding highlighted in this article confirm the ability to utilize the signature of water hammering in the diagnostics of perforation efficiency and resulting fracture geometry, Fig. 10.

The findings confirmed the ability to better understand fracture geometry through recycling readily available data during the water hammering phase. Subsequently, there is always room for development and improvement.

The recommendation that can further refine and fine-tune the application of the described methodology are:

1. Validate the findings with a large pool of perforation designs, and benchmark the findings against step-down tests at each design.
2. Extend the application of the methodology on variable cluster designs, to identify whether similar observations to the number of perforations will be identified.
3. Application example 1 highlighted a logarithmic correlation between the perforation efficiency and the magnitude of the water hammering amplitude, which should be further fine-tuned with additional results from recommendation point 2.
4. Utilize machine learning to propose the ideal number of perforations per stage to maximize perforation efficiency based on the water hammering signature, and the learnings of recommendation point 3.

Acknowledgments

This article was presented at the SPE International Hydraulic Fracturing Technology Conference and Exhibition, Muscat, Sultanate of Oman, September 12-14, 2023.

About the Authors

Abdulrahman M. Alowaid

M.Eng. in Unconventional Hydrocarbon Resources, King Fahd University of Petroleum and Minerals

Abdulrahman M. Alowaid is a Unconventional Production Engineer working in the North Jufurah Production Engineering Unit of Saudi Aramco's Well Completion Operations and Producing Engineering Department. During his career, Abdulrahman has assumed multiple roles within unconventional resources, including a Production Engineer, Wellsite Operations Foreman, and a Reservoir Engineer. His expertise is in the field of unconventional resources completions, stimulation, and production engineering.

Abdulrahman is currently working on the design, planning, execution, and evaluation of multiple stimulation and well intervention operations within unconventional wells.

He received his B.S. degree in Petroleum Engineering and an M.Eng. degree in Unconventional Hydrocarbon Resources, both from King Fahd University of Petroleum and Minerals (KFUPM), Dhahran, Saudi Arabia.

Tayyar S. AlTayyar

M.S. in Petroleum Engineering, Missouri University of Science and Technology

Tayyar S. AlTayyar is a Senior Petroleum Engineer working in the South Ghawar and North Arabia Technical Support Unit of Saudi Aramco's Well Completion Operations and Producing Engineering Department. He has 7 years of experience as a Production Engineer within Unconventional Resources, and a wide range of experience in reservoir-related evaluation and assessment.

Tayyar's expertise is focused on the design, modeling, execution, and evaluation of well stimulation operations, primarily hydraulic fracturing.

He received his B.S. degree in Petroleum Engineering from King Saud University, Riyadh, Saudi Arabia, and his M.S. degree in Petroleum Engineering from Missouri University of Science and Technology, Rolla, MO. Tayyar's M.S. degree focused on Reservoir Engineering.

Karim Mechkak

B.S. in Petroleum Production Engineering, University of Boumerdes

Karim Mechkak is a Supervisor of the Production Engineering Unit in Saudi Aramco's Well Completion Operations and Producing Engineering Department. He has 19 years of experience in the oil and gas industry.

Karim started his career with Schlumberger working as a Stimulation Engineer in the North Africa Geomarket, where he spent 4 years supporting all SLB clients. Karim then moved to the North Sea as a DESC Engineer for ConocoPhillips, supporting all Schlumberger stimulation and completion operations in the Ekofisk offshore oil field.

In 2011, he joined Statoil as a Completion and Intervention Lead Engineer, supporting all operations in the Statfjord giant oil field.

In 2013, Karim joined Saudi Aramco, working as an Unconventional Resources Production Engineer where he has been involved in many projects related to unconventional play stimulation.

In 2022, he won the Saudi Aramco Excellence Award for the implementation of TSE for use in hydraulic fracturing operations.

Karim received his B.S. degree in Petroleum Production Engineering from the University of Boumerdes, Boumerdes, Algeria.

Ultra-High Speed High Gas Volume Fraction Pump Development

Dr. Chidirim E. Ejim, Dr. Jinjiang Xiao, Dr. Anton Shakirov, Yaroslav Alexeev and Anton Shkolnyi

Abstract /

Wellbore conditions below bubble point pressure in high gas-oil ratio (GOR) wells result in a very high amount of free gas at the inlet of electric submersible pumps (ESPs). Conventional multiphase pumps have limitations handling free gas, which exceeds 75% of the intake gas volume fraction (GVF). The objective of this work is to develop and field-test a new ultra-high speed high GVF (UHS HGVF) pump system. The ultimate goal is to facilitate sustained production from wells experiencing HGVF production challenges.

The UHS HGVF pump is a new type of submersible pump with an architecture being investigated to boost hydrocarbon production from high GOR oil wells. The principle of operation is based on turbulent friction, in which a spatial vortex flow is formed, rotating together with the rotor and moving along its axis. The pump housing diameter is 4" and operates at a shaft rotational speed in excess of 3.5 times those of conventional pump systems. Hydraulic design, computational fluid dynamics analysis, prototyping, and physical testing were performed to optimize the performance of the UHS HGVF pump.

The results show that the new pump architecture is capable of handling gas-liquid mixtures with the intake GVF well beyond the 75% GVF limitation of conventional multiphase pumps. This was mainly attributed to the pump features, which impart the required amount of energy and turbulence to the gas-liquid mixture, but simultaneously minimizes separation of the gas and liquid phases. These combined effects facilitated thorough mixing of the gas-liquid streams, ensuring the pump provided sufficient pressure boost for the downhole setting depths, for which the system was designed. The system was also observed to have a high capability of sand tolerance and thrust handling. The ruggedized system has the required attributes to withstand operation in gassy field conditions.

This work presents a conceptually new approach to pump development with the goal of overcoming hydrocarbon production challenges in wells with very high free gas at the pump's intake. The UHS HGVF pump widens the operating envelope to produce a high GOR well, thereby achieving production gains in gassy conditions, where conventional systems are limited. The system therefore serves as an essential artificial lift tool to handle production in increasing numbers of extremely gassy wells.

Introduction

Electric submersible pumps (ESPs) are commonly used in the oil and gas industry for producing or transferring hydrocarbons, water, and gas from a source to a delivery terminal. Typically, weak wells require the use of ESPs to artificially lift or pressurize the fluids. Moreover, in some instances, ESPs may be used to boost production from naturally flowing wells. ESPs contain rotor (impeller) and stator (diffuser) pairs, which form a stage.

The rotary impellers impart kinetic energy to the fluid and the static diffusers convert the kinetic energy to pressure energy. The typical operating speeds for conventional ESPs is up to 4,200 revolutions per minute (rpm). High speed systems (> 4,200 rpm) have also seen increasing applications in recent years[1, 2]. For satisfactory operation, ESPs handle pure liquids or liquids with a very minimal amount of free gas.

When high amounts of free gas exist in a well with an ESP, its pumping capability decreases. The magnitude of free gas can be quantified by the gas volume fraction (GVF). It is defined as the ratio of the volume of free gas to the total volume of fluids at a given pressure and temperature. At high GVFs, depending on the type of ESP, the pressure generation capacity of the pump can decrease to zero, a condition known as gas lock[3]. This results in fluids not reaching the surface in field applications.

These gas challenges may be managed by using gas separators, gas handlers, or multiphase pumps. Subsequently, conventional multiphase pumps that operate up to 4,200 rpm have a GVF handling capability of up to 75%[4]. These limitations have led to studies on high speed (> 4,200 rpm) gas handling pumps to widen the performance envelope beyond the 75% limitation of conventional systems[5].

Ultra-high speed pumping (>= 10,000 rpm) has been demonstrated by Zamanuri et al. (2019)[6]. A benefit is the utilization of a smaller diameter pump to produce higher liquid flow rates and boost pressures over conventional pumps of the same size. The additional benefit of such a system is also in gas handling since the much higher rotational speeds facilitate much higher kinetic energy to be imparted to the fluid to boost the gas and liquid pressures. The authors are not aware of literature presenting the performance of an ultra-high speed pumping system capable of handling high volume intake GVFs up to 90%. This is the major motivation of the current work. The applications are beneficial in slim, deep gassy wells commonly drilled for oil and gas production applications.

This study presents the performance of an ultra-high speed high GVF (UHS HGVF) pump. The goal of this work was to develop an optimized version of the pump with gas handling features incorporated in the design for eventual field installation.

UHS HGVF Pump Architecture

The main pumping components of the UHS HGVF pump are the rotor and stator. The blades on the rotor's outer diameter and stator's internal diameter are helically shaped. The minimum clearance between the rotor and stator clearance are larger than in conventional pumps. As the rotors rotate during operation, gas and liquid in the flow passages are thoroughly mixed, thereby preventing gas-liquid separation that leads to gas lock in pumps. This, along with axial flow through the pump components, contributes to the significantly higher gas handling capability of the UHS HGVF pump. The rotor and stator clearance is attributed to the high tolerance to sand (up to 10 g/l) compared to conventional pumps.

The UHS HGVF pump includes an optimized rotor and stator thread shape to increase hydraulic efficiency. A thrust unloading module, along with associated features are incorporated in each rotor to handle the large pump thrust loads, which would have been a challenge to handle alone by the protector or seal section of the pump. The modular construction of each pumping section comprises a shaft per pumping section. This configuration increases the critical speed of the rotating system and prevents high vibration amplitudes that occur when rotating systems operate at speeds close to their natural frequencies.

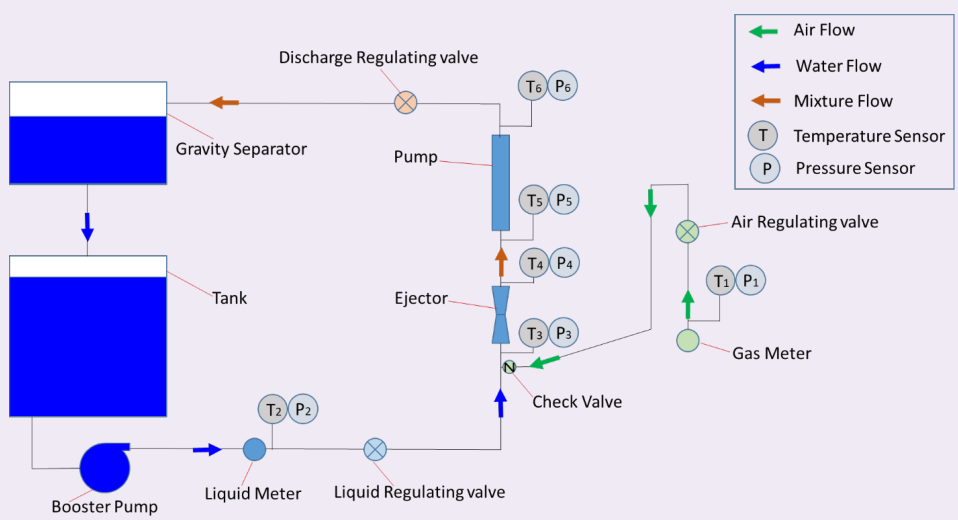
The motor section of the UHS HGVF pump includes a heat exchanger system[7,8]. The system incorporates a forced convection heat transfer mechanism for effective cooling of the downhole motor. The motor has high speed permanent magnet motor technology to enable energy efficient lifting of fluids. Combined with the high speed operation yields, it is a system of relatively compact size to economically produce hydrocarbons from the subsurface. The UHS HGVF pump in this study has a 4.00" housing diameter, consists of 10 rotor and stator pairs, is capable of rotating up to 12,000 rpm, can handle up to a 90% GVF gas-liquid mixture at its intake, and the subsurface system has a total length of less than 60 ft.

Test Layout and Procedure

A verification pump, which handles up to 75% of the intake GVF, was tested using air and water mixed with surfactants. This finely dispersed mixture was used since it better simulates reservoir conditions as oil contains natural surfactants. Subsequently, computational fluid dynamics was applied to the test data of the verification pump to obtain a simulation model used to optimize the design of the UHS HGVF pump and obtain its head-flow performance.

Figure 1 shows the test setup for the verification pump. The pump was operated using a variable frequency drive with operating speeds from 3,000 rpm to 12,000 rpm. The water-surfactant mixture is supplied from the holding tank to the ejector. Due to the fluid velocity in the nozzle section of the ejector, the local pressure is reduced, which in turn creates a suction effect that draws in ambient air through the air line. A check valve on the airline prevents liquid from entering the air line. The air and liquid are thoroughly mixed in the mixing chamber of the ejector located downstream of the nozzle. This results in a finely dispersed mixture, which is fed into the inlet of the pump. The air-liquid mixture is pressurized by the pump and exits into the discharge line and onto a gravity separator, where the air

Fig. 1 *A schematic layout of the test setup for the verification pump.*



and liquid are separated. The separated liquid flows into the holding tank and the entire flow process is repeated.

For pump testing, the water-surfactant mixture is circulated through the system. Pump operating speeds varied up to 12,000 rpm, and liquid flow rates were up to 2,770 barrels per day (bpd) (440 m^3/d). The amount of liquid and air in the system were controlled using the respective regulating valves shown in Fig. 1. The corresponding liquid and gas flow rates were measured using the liquid and gas flow meters, respectively. The temperature and pressure sensors measured the corresponding readings and facilitated conversion to the respective volume flow rates of air in the system. Based on the measurements, the corresponding pump differential pressures or corresponding head (based on water density) were computed.

After receiving the test data for the verification pump, a simulation model was obtained to match the test data. A volume model was not used in the simulation since it requires very large computational resources and time. Instead, a homogeneous approach was used, which gave results within 5% of the test data. This facilitated use of the homogeneous model throughout the simulation analysis. The validated simulation model was used to optimize the design of the UHS HGVF pump at different rotational speeds and intake GVFs.

Results

Figure 2 shows the head variation with flow rate for the verification pump. For brevity only, the result for the highest rotational speed is presented here. The head decreases with increasing liquid flow rate similar to centrifugal pumps, but not necessarily the same performance shape as the latter. At 12,000 rpm, the shut-in head is about 2,461 ft (750 m), which is reduced to approximately 28 ft (8.5 m) at a flow rate of 2,770 bpd. The simulation data is plotted on the same axes to compare with the test data. The simulation results and test data are reasonably close to each other for the flow conditions tested. With the test and simulation data matching well, the gas-liquid results were compared.

Figure 3 shows the head variation with a liquid flow rate at 65% intake GVF for the verification pump operating at 8,000 rpm. Similar to Fig. 2, the same trend of decreasing head with an increasing volume flow rate, is observed. The head varies

Fig. 2 *The verification pump results at 12,000 rpm (liquid tests).*

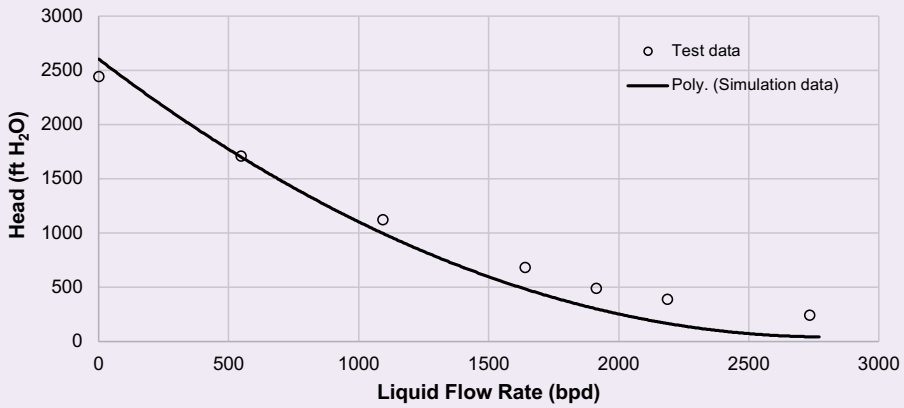


Fig. 3 *The verification pump results at 8,000 rpm.*

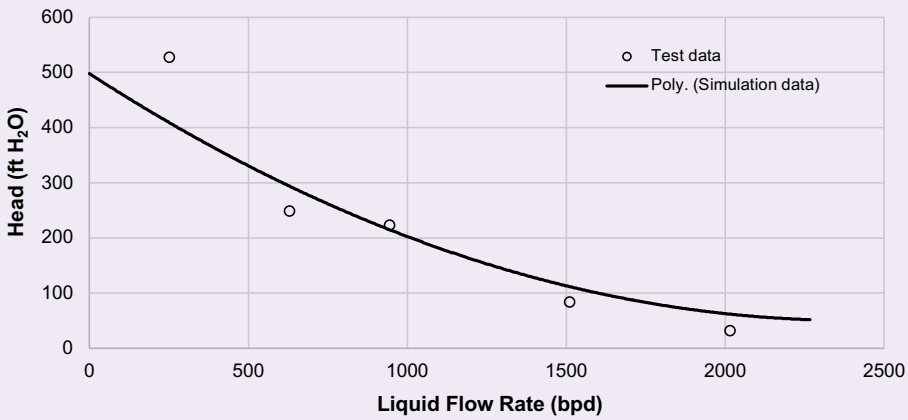
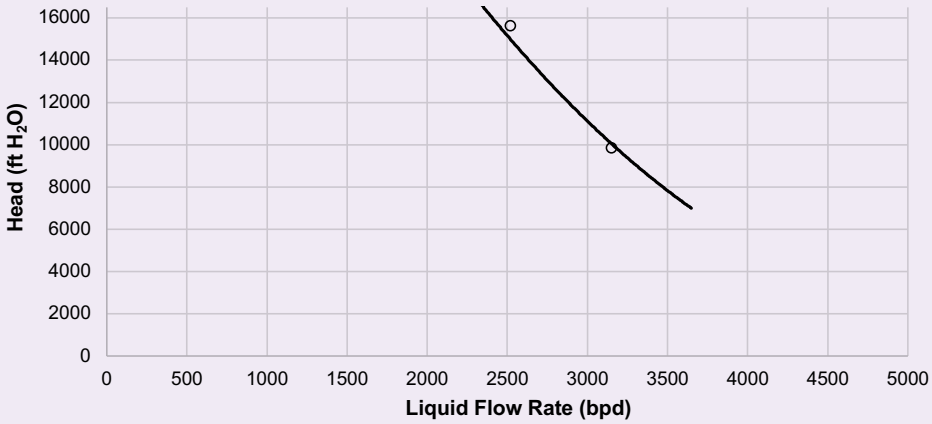


Fig. 4 *The simulation results for a 10-rotor design pump at 90% GVF intake and 10,000 rpm.*



from 490 ft (150 m) at shut-in to approximately 52 ft (16 m) at a liquid flow rate of approximately 2,300 bpd. The generally observed result during the test is that the head developed by the pump is reduced due to the presence of gas in the flow. This trend is commonly observed in literature as well as in the field. Comparing the simulation model with the test data again shows that both data are reasonably close to each other over a wide flow range. Given the fairly close results between the model and test data for the verification pump gave confidence in utilizing the simulation model to optimize the final architecture of the main UHS HGVF pump design.

Figure 4 shows the head flow performance of a 10 rotor and stator pair in the UHS HGVF pump operating at 10,000 rpm and at 90% intake GVF. Multiple rotor and stator pairs were used, which is common in oil and gas artificial lift applications. The higher number of rotor and stator pairs ensures the gas-liquid mixture is compressed to higher pressures. The plot shows that the UHS HGVF pump can deliver approximately 2,520 bpd of liquid at a head of about 16,000 ft (4,877 m).

At the upper end of the flow rates, the UHS HGVF pump develops a head of approximately 4,000 ft (1,219 m) while delivering approximately 4,400 bpd of liquid. At a 90% intake GVF, this corresponds to a total intake flow rate of approximately 44,000 bpd. The wide range of possible head and flow rates from the UHS HGVF pump operating at 10,000 rpm and a 90% intake GVF makes it applicable to a broad range of artificial lift field applications. Widening the operating envelope is further achieved using the variable frequency drive for operational flexibility in the field to handle different conditions in gassy wells.

Summary and Conclusions

The current study presents the performance of a 4.00" housing UHS HGVF pump designed to handle gas-liquid mixtures up to a 90% intake GVF. The pump consists of 10 rotor and stator pairs and can operate at rotational speeds up to 12,000 rpm.

The results showed that the UHS HGVF pump can deliver approximately 16,000 ft (4,877 m) of head at 2,520 bpd of liquid, and up to approximately 4,000 ft (1,219 m) of head at 4,400 bpd of liquid. The flow conditions cover a wide range of operating conditions observed in many wells with high gas content. These capabilities of the pump highlight its suitability for artificial lift field applications in gassy wells.

The UHS HGVF pump results presented in this study show that the system broadens field application in wells with very high gas content, and also in slim, deep wells. This is attributed to the pump rotor and stator architecture, internal features for gas handling, and a systematic development program using a combination of physical tests and a rigorously validated simulation model. Overall, the capability of the pump to handle intake GVFs up to 90% unlocks the potential from wells that could not have been produced due to challenges associated with very high gas content. This in turn significantly increases the economic bottom-line of the field operator.

Acknowledgments

This article was presented at the SPE Gulf Coast Section – Electric Submersible Pump Symposium, The Woodlands, Texas, October 2-6, 2023.

References

1. Amsidom, A.A., Ghonim, E.O., Alexander, E., Kuswanto, K., et al.: "Truly Rigless: A World First through 3½" Tubing Cable Deployed Electrical Submersible Pump on a Live Well," SPE paper 192100, presented at the SPE Asia Pacific Oil and Gas Conference and Exhibition, Brisbane, Australia, October 23-25, 2018.

2. Lastra, R., Xiao, J., Lee, W. and Radcliffe, A.: "High Speed High Rate Slim ESP Development and Qualification Testing," SPE paper 194399, presented at the SPE Gulf Coast Section Electric Submersible Pumps Symposium, The Woodlands, Texas, May 13-17, 2019.

3. Hua, G., Falcone, G., Teodoriu, C. and Morrison, G.L.: "Comparison of Multiphase Pumping Technologies for Subsea and Downhole Applications," *Oil and Gas Facilities,* February 2012, pp. 36-46.

4. Bagci, A.S., Kece, M. and Nava, J.: "Challenges of Using Electrical Submersible Pump (ESP) in High Free Gas Applications," SPE paper 131760, presented at the International Oil and Gas Conference and Exhibition in China, Beijing, China, June 8-10, 2010.

5. Ejim, C.E., Xiao, J., Lee, W. and Zabala, W.: "Physical Testing of a High Speed Helicoaxial Pump for High Gas Volume Fraction Operation," *SPE Production & Operations*, Vol. 37, Issue 4, November 2022, pp. 721-733.

6. Zamanuri, K., Yip, P.M., Radzuan, N.A., Salleh, N.I., et al.: "Accelerating the Shift to a Next-Generation ESP Deployment: Cable Deployed through Tubing Electrical Submersible Pump TTESP Application," SPE paper 194390, presented at the SPE Gulf Coast Section Electric Submersible Pumps Symposium, The Woodlands, Texas, May 13-17, 2019.

7. Shakirov, A., Alexeev, Y. and Gorlov, A.: "World's First Mass Implementation of Ultra-High-Speed ESP Systems in Salym Group of Fields," SPE paper 194416, presented at the SPE Gulf Coast Section Electric Submersible Pumps Symposium, The Woodlands, Texas, May 13-17, 2019.

8. Takacs, G.: *Electrical Submersible Pumps Manual*, 2nd edition, Elsevier Inc., 2018, pp. 109-111.

About the Authors

Dr. Chidirim E. Ejim

Ph.D. in Mechanical Engineering, University of Alberta

Dr. Chidirim E. Ejim is a Petroleum Engineering Specialist working in the artificial lift focus area within the Production Technology Division of Saudi Aramco's Exploration and Petroleum Engineering Center – Advanced Research Center (EXPEC ARC). Prior to joining Saudi Aramco in 2014, Chidirim spent over 7 years with Schlumberger's Artificial Lift Segment, working on surface horizontal pumping systems; downhole pump design, development and testing; multiphase production systems; as well as downhole gas separator/gas handler testing and analysis.

He received his B.Eng. degree (Honors) from the University of Malta, Msida, Malta; his M.S. degree from the University of Waterloo, Ontario, Canada; and his Ph.D. degree from the University of Alberta, Edmonton, Canada, all in Mechanical Engineering.

Chidirim is a Registered Professional Engineer in Alberta, Canada.

Dr. Jinjiang Xiao

Ph.D. in Petroleum Engineering, University of Tulsa

Dr. Jinjiang Xiao was a Senior Petroleum Engineering Consultant working in Saudi Aramco's Exploration and Petroleum Engineering Center – Advanced Research Center (EXPEC ARC). His main focus was artificial lift research and development. Jinjiang retired from Saudi Aramco in July 2023.

Prior to joining Saudi Aramco in 2003, he spent 10 years with Amoco and later BP-Amoco, working on multiphase flow, flow assurance and deep-water production engineering.

Jinjiang received both his M.S. and Ph.D. degrees in Petroleum Engineering from the University of Tulsa, Tulsa, OK.

Dr. Anton Shakirov

Ph.D. in Production Technology Projects, Gubkin Russian State University of Oil and Gas

Dr. Anton Shakirov is the CEO and co-founder of Lex and works at the company headquarters in Cyprus. He has over 18 years of international onshore and offshore experience with artificial lift systems. He has worked mainly in the Middle East, Southeast Asia, East Europe, and Africa, focusing on submersible production equipment applications, design, and reliability.

Anton received his B.S. degree in Engineering from the National University of Oil and Gas, Moscow, Russia, and received his Ph.D. degree in Production Technology Projects from the Gubkin Russian State University of Oil and Gas, Moscow, Russia.

One of his remarkable studies was the development of an empirical formula for natural separation efficiency in radial pump intakes in collaboration with Professor Mischenko. The formula has been adopted by the electric submersible pump (ESP) industry and included in the ESP sizing software package, SubPump, under the name Shakirov-Mischenko.

Yaroslav Alexeev

M.S. in Artificial Lift Production, Gubkin Russian State University of Oil and Gas

Yaroslav Alexeev is a professional in the field of artificial lift production. In 2016, he joined Lex, a renowned player in the artificial lift industry. Over the years, Yaroslav held various engineering roles, and is currently an Engineering Team Leader at the company headquarters in Cyprus, where he oversees product development, technical studies, equipment supervision, and worldwide service support.

Yaroslav's professional journey began at a scientific laboratory while attending university. There, he played a pivotal role in developing and upgrading product lines of artificial lift equipment, creating unique testing facilities and software for equipment selection and operational analysis. Yaroslav furthered his professional journey working in several leading oil companies, where he honed his practical engineering skills and continued pioneering research and development initiatives.

With a career spanning over 13 years, Yaroslav's contributions to the international artificial lift industry has taken a global trajectory covering 50+ countries.

He is the author of over 20 publications, and numerous scientific reports and patents.

Yaroslav is an active member of the Society of Petroleum Engineers (SPE) and American Petroleum Institute (API) subcommittees (API 11S9 and API 11S2).

He received his B.S. degree in Petroleum Engineering, and his M.S. degree in Artificial Lift Production in Harsh Environment, both from Gubkin Russian State University of Oil and Gas, Moscow, Russia.

Anton Shkolnyi

M.S. in Software Engineering, Aerospace Engineering University

Anton Shkolnyi joined the Lex team in 2020 as a Project Manager, and is based at the company headquarters in Cyprus, where he currently oversees innovative company projects.

Anton started his journey in the oil and gas industry in 2013 by developing variable speed drives and automation processes for oil production, and continues to merge his aerospace knowledge with his expertise in the oil industry. Anton innovatively integrates space technologies into oil extraction, bridging two seemingly distinct realms.

In 2010, he received his B.S. degree in Rocket and Spacecraft Engineering, and in 2012, Anton received his M.S. degree in Software Engineering, both from the Aerospace Engineering University, Moscow, Russia.

Chemical Treatment for Sustainable Acid Fracture Conductivity of Weak Carbonates

Mahmoud Desouky, Dr. Murtada S. Al Jawad, Dr. Abduljamiu Amao, Dr. Dhafer A. Al-Shehri, Dr. Murtadha J. AlTammar and Dr. Khalid M. Alruwaili

Abstract /

Acid fracturing is an essential stimulation technology to increase the production of carbonate reservoirs. Consequently, acid usually softens the rock, and the stability of the fracture hydraulic conductivity is hardly maintained. Therefore, rock strength after an acid treatment is crucial in controlling the emerging hydraulic conductivity. Consolidation agents, like diammonium phosphate (DAP), could enhance the mechanical properties of damaged or weak carbonate rocks.

This study investigates the DAP consolidation effect on weak carbonate fracture hydraulic conductivity. Weak Austin chalk samples were soaked in 1 M DAP for 72 hours under high pressure and high temperature. The surface hardness of weak Austin chalk samples was evaluated nondestructively using impulse hammering. The sample's surface hardness was greatly improved upon the DAP treatment.

The treated samples' hydraulic fracture conductivity and compaction were measured and compared with similar untreated samples. The treated samples also exhibited higher and sustained hydraulic conductivity and less compaction under higher stress. The proposed solution could be particularly useful in soft carbonate formations, where induced acid softening is a common problem. Boosting the fracture surface hardness with DAP can improve the efficiency of the acid stimulation process and increase the amount of hydrocarbons that can be extracted.

Introduction

While acid fracturing manifests itself as one of the most deployed stimulation methods in carbonate reservoirs, its success is limited by the carbonate strength after the operation. The asperities that keep the fracture open are more vulnerable to failure because acidizing decreases the compressive strength of the carbonate[1]. Likewise, Nierode and Kruk (1973)[2] in Eqns. 1 and 2, related the hydraulic conductivity ($k_f w_i$) of the fracture to the rock embedment strength (S_{RE}), e.g., the lower the embedment strength, the lower the hydraulic conductivity.

$$k_f w_i = C_1 e^{-C_2 \sigma_C} \quad (1)$$

$$C_2 \times 10^3 = 13.9 - 1.3\, ln(S_{RE}) \quad (2)$$

Moreover, the rock embedment strength determines the rate at which the conductivity falls under stress (σ_C)[3]. Also, soft carbonates like chalk exhibit more time-dependent deformation (creep) than harder carbonates like dolomite[4].

In post-acid fracturing jobs of carbonate gas wells, a severe production loss of more than 60% within 6 months was reported[5]. The reasons behind the sharp decline should be understood before considering re-stimulation jobs, which are not usually successful[4]. Consequently, the best scenario would be to have a sustainable acid fracture at the first trial.

Acid dissolution weakens carbonate rocks, resulting in a reduced ability to maintain hydraulic conductivity. For example, Zhang et al. (2020)[6] found that acid reduced the carbonate compression strength when evaluated with triaxial rock mechanics testing. Also, according to Melendez et al. (2007)[7], the carbonate post-acid etching conductivity was lower when rock embedment strength decreased at the high points that keep the fracture open. In addition, Mustafa et al. (2022)[8] investigated the impact of acid treatment on the mechanical properties of three different carbonate rocks — chalk, limestone, and dolomite — after a wormhole breakthrough. The study found that the acid treatment significantly reduces the rock surface hardness and Young's modulus, with chalk samples being the most impacted. Similarly, an experimental investigation showed that samples containing wormholes have lower pore collapse stress than intact samples[9].

Therefore, different approaches were suggested to enhance the stimulation efficiency and durability. One approach is to preserve the rock strength by controlling the acid leak-off rate into the formation[10]. As a result, the rock integrity was maintained, and the etched fracture length also increased[5]. On the other hand, another

approach employs the proppant to keep the fracture open for hydrocarbon flow post-acid fracturing[11]. Finally, a more comprehensive hybrid approach combines proppant with cross-linked or gelled acid to overcome the challenges of previous methods[12, 13].

This work proposed a less complicated approach to sustain fracture conductivity in soft carbonates by hardening the carbonate surface through a chemical reaction. The chemical reaction is intended to transform the soft surface mineral with a harder one[14]. Mineralogy alteration was proposed in our previous publication to replace calcite, the main mineral in carbonate rocks, with another harder mineral[15]. Al-Jawad et al. (2021)[16] adopted the idea from the art preservation field, where consolidants are used to repair deteriorating carbonate monuments. For instance, Sassoni et al. (2011)[17] observed up to 90% increase in the dynamic Young's modulus of damaged Indiana limestone after immersing it in a diammonium phosphate (DAP) solution.

Moreover, Al-Jawad et al. (2020)[18] showed that by using consolidants, Young's modulus could be enhanced by 10% to 38%. Their modeling research indicated that the well productivity represented in the fold of increase could double with the rock strengthening.

Materials and Methods

In this study, four flat Austin chalk slabs (17.8 cm × 3.4 cm × 7.6 cm) were selected as they resemble a weak carbonate and are more amenable to hardening. In addition, the chalk contains mainly calcite (+99%), as demonstrated by the X-ray diffraction analysis (XRD), Table 1. Therefore, substituting calcite in the samples with harder minerals will result in stiffer ones capable of supporting more loads.

First, the slabs were checked to avoid any features, such as cracks or vugs, within them. Next, the slabs were divided into the control group (S1 and S2) and the treatment group (S3 and S4). The control group's compaction and hydraulic conductivity would be the benchmark to which those of the treatment group would be compared.

A typical substitution reaction happens either by replacing calcite ($CaCO_3$) anion or cation, according to Eqn. 3, and the newly formed mineral should be stable and harder than calcite.

$$XY + CaCO_3 \xrightarrow{H_2O} XCO_3 \downarrow + CaY \downarrow \quad (3)$$

The DAP solution was found more efficient in enhancing the carbonate's mechanical properties than other consolidants when tested with various techniques[19]. Therefore, DAP would be employed as the mineralogy alteration agent for the weak carbonate by forming hydroxyapatite. A DAP solution with unit molarity was prepared by dissolving 132.06 g of DAP salt in 1 L of deionized water.

The treatment group was vacuumed for 24 hours before the chemical treatment. Then, the vacuumed samples were saturated with the prepared DAP solution for 72 hours at a pressure and temperature of 1,000 psi and 75 °C, respectively. According to Sassoni et al. (2011)[17], these are the recommended conditions. Moreover, it is worth mentioning that the treatment conditions were set to values comparable to those encountered in the reservoirs. Afterward, the impact of the chemicals on the surface hardness was assessed nondestructively using AutoScan on a grid covering the surface evenly. The nondestructive evaluation is mandatory for two reasons. First, other mechanical properties' machines cannot accommodate such slabs. Second, the same slabs will be used for further experiments and should have the same original state.

Analysis of variance (ANOVA) was employed to evaluate the variance among surface hardness means of the chalk samples. ANOVA statistically ascertained whether the differences in these means come with the DAP treatment or the chalk heterogeneity. When ANOVA showed statistical significance, the Tukey honestly significant difference (HSD) was used to determine which samples' means differed. All the statistical analyses were performed using the RStudio environment (version: 2022.12.0.353) in the R programming language (version: 4.2.2).

Later, the control group pair (S1 and S2) were attached, where

Table 1 *The XRD mineral quantification of the treated and untreated chalk samples.*

Group	HAP (%)	Calcite (%)
Untreated Chalk	0.6	99.4
Treated Chalk	20.6	79.4

Table 2 *The descriptive statistics of the surface hardness measurements in GPa.*

Group Sample	Control		Treatment			
	S1	S2	S3		S4	
			Before	After	Before	After
Mean	3.4	3.4	3.4	7.4	3.4	9.5
STD	0.5	0.5	1.4	1.8	1.1	1.9
Minimum	2.4	2.3	1.6	3.8	1.8	5.8
Maximum	4.2	4.5	8.2	10.6	6.2	13.9
Range	1.8	2.1	6.6	6.8	4.4	8.2

the aperture between them mimics a fractured carbonate system. Next, the samples were sealed by pouring liquid silicon around them in a mold and letting it thicken. The samples from the S3 and S4 groups were also prepared similarly. Then, hydraulic conductivity was measured at incrementally increasing stresses up to 1,500 psi in the ACM-3000 acid fracture conductivity system by flowing nitrogen gas between them (200 cc/min to 350 cc/min). Simultaneously, a set of four linear variable differential transformers (LVDTs) measures the compaction of the specimen at each stress level.

Meanwhile, 1 cm side-length cubes were cut for scanning electron microscopy (SEM) imaging. Half of the cubes were treated with DAP under the same conditions. The differing behavior of treated slabs might be explained by visualizing the changes that DAP caused in the grain scale and comparing it to benchmark samples that weren't treated. Finally, XRD analysis was performed on the powder of the near-edge pieces extracted from treated and untreated chalk samples.

Results and Discussion

The Austin chalk slabs used in the experiments are naturally heterogeneous. To assess the slabs mechanically, the surface hardness was evaluated by AutoScan at 30 different locations on the slab's surface. The statistical summary of the measurements is tabulated in Table 2. Variation of the measurements from one location to another is attributed to the rooted heterogeneity of the chalk. Selected sister chalk samples have an initial average surface hardness of roughly 3.4 MPa.

After the treatment with DAP, the average surface hardness of S3 and S4 increased to 7.4 GPa and 9.5 GPa, respectively. Also, it can be observed that the spread of the surface hardness measurement after the treatment is wider, Fig. 1. The wide surface hardness variation means the chalk reaction with DAP is also affected by the chalk heterogeneity. Nevertheless, the minimum hardness value measured after the treatment is higher than the average value for the corresponding slab before the treatment.

The ANOVA (formula: hardness ~ sample) suggests that the main effect of the sample is statistically significant and large ($F(5, 174) = 121.74$, $p < .001$; Eta2 = 0.78, 95% CI [0.73, 1.00]). Therefore, the difference in hardness with the DAP treatment could be inferred. After showing a statistical significance of hardness from one sample to another with the DAP treatment, a pairwise comparison between the sample factor means was made utilizing the Tukey post-hoc test. Confidence intervals for the difference in the means for all 15 pairs of samples are represented graphically in Fig. 2.

Any confidence intervals not intersecting with 0 show differences between the groups. Therefore, the S1, S2, S3 (Before), and S4 (Before) pairs are considered equal as they do not show mean differences. Other sample comparisons appear significantly different from each other; however, the pairs could be grouped when having similar confidence intervals. A comprehensive interpretation of how much improvement could be obtained when all other pairwise tests were combined can be determined. For example, the 95% confidence intervals of S3 (After)-S3 (Before) go from 3 GPa to 4 GPa, providing proof that the hardness improvement is some value between 3 GPa and 4 GPa.

The measurement of the fracture hydraulic conductivity for the treated and untreated samples was obtained utilizing an ACM-3000. The hydraulic conductivity values were normalized by dividing them by the first measurable hydraulic conductivity value at 300 psi. Before this stress, the pressure drop along the fracture was too small to be detected by the pressure sensors. Figure 3 shows that the treated samples' normalized hydraulic

Fig. 1 *The surface hardness distribution of all samples.*

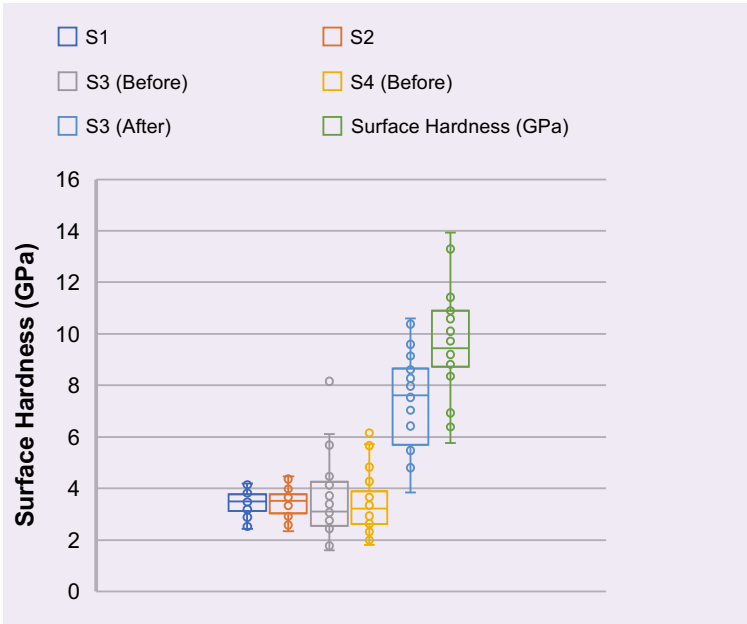


Fig. 2 *The graphical pairwise comparisons from Tukey's HSD for different samples.*

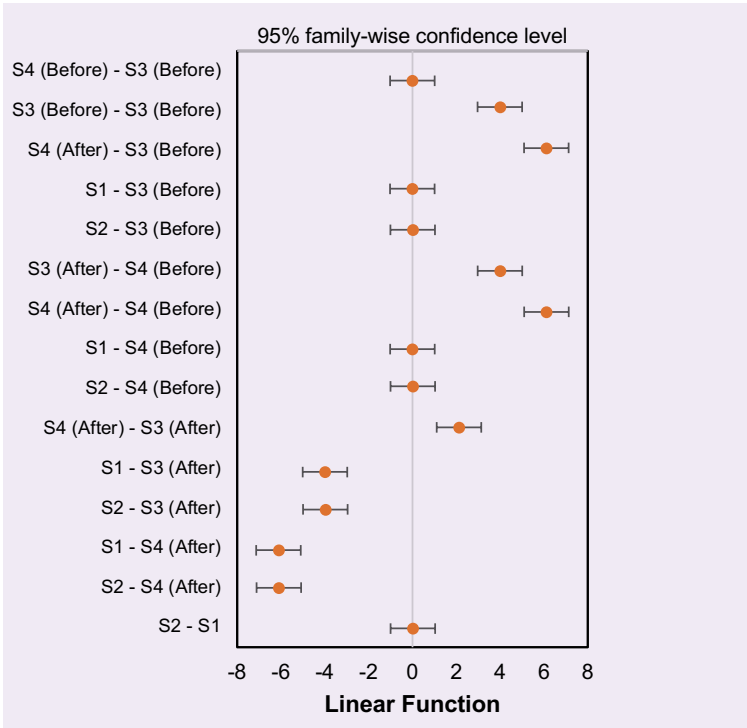
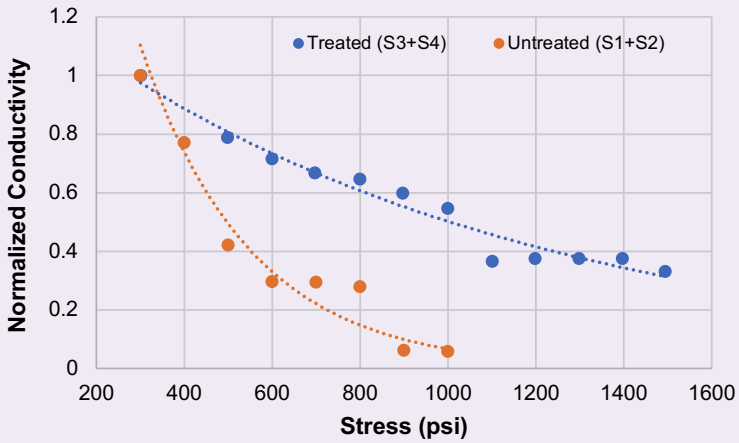


Fig. 3 *The normalized hydraulic conductivity comparison of the treated and untreated samples.*



conductivity is higher over applied stress. Also, the rate at which the normalized hydraulic conductivity of the treated samples dropping is less sharp than that of the untreated samples.

Moreover, the hydraulic conductivity of the treated samples plateaued beyond 1,000 psi at 0.37 compared to 0.06 beyond 800 psi for the untreated samples. The hydraulic conductivity findings agree with a preliminary study on acid damaged chalk samples[20]. Their initial conductivity tests with acidized/untreated and acidized/treated samples revealed that an increase in the hardness of chalk samples led to a less drastic conductivity drop for the treated fracture surface and better conductivity at high stress.

In addition, the compaction of the treated samples is less in the elastic region and upon failure, Fig. 4. Each point in the figure represents the average value of the four LVDT measurements. The LVDT measurement trend line break beyond 800 psi and 1,000 psi for the untreated and treated samples, respectively, implies when the samples failed. This observation is coherent with the hydraulic conductivity trend lines, which show similar breaks at the same stresses.

The SEM imaging of the intact chalk samples shows the separate calcite grains with smooth faces, Fig. 5.

In comparison, the treated samples demonstrate changes in the calcite morphology and the formation of new minerals, Fig. 6. Roy and Linnehan (1974)[21] explained how hydroxyapatite (known shortly as HAP ($Ca_{10}(PO_4)_6(OH)_2$)) is forming when DAP ($6(NH_4)_2HPO_4$) reacts with calcite:

$$10CaCO_3 + 6(NH_4)_2HPO_4 + 2H_2O \rightarrow Ca_{10}(PO_4)_6(OH)_2 + 6(NH_4)_2CO_3 + 4H_2CO_3 \quad (4)$$

The XRD analysis also confirmed the changes observed in the SEM images. Figure 7 displays the XRD response of the powder made from treated chalk, plotted on the same figure with the

Fig. 4 *The axial deformation comparison of the treated and untreated samples.*

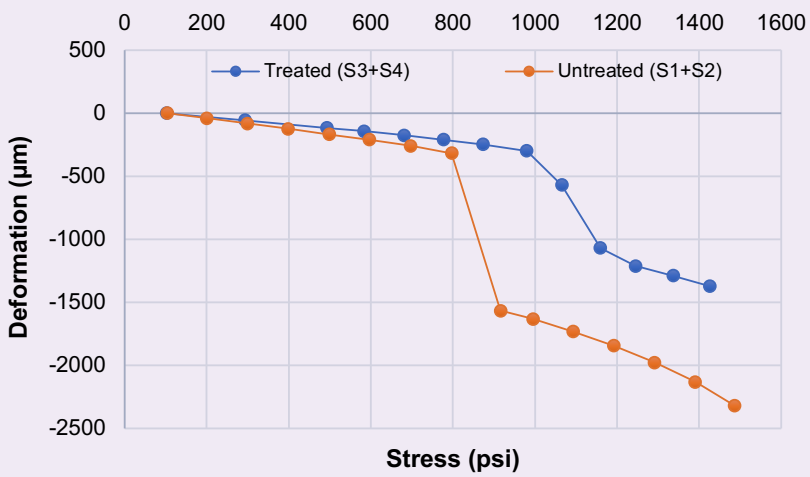


Fig. 5 *The SEM image of the untreated samples showing the calcite grains.*

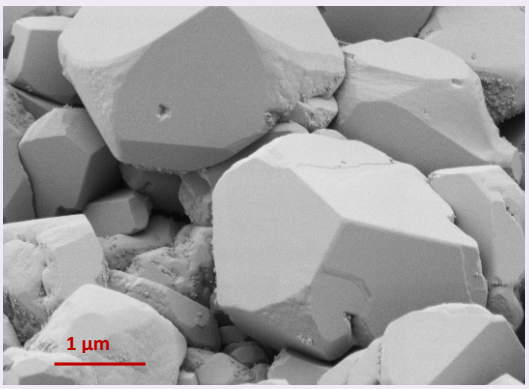
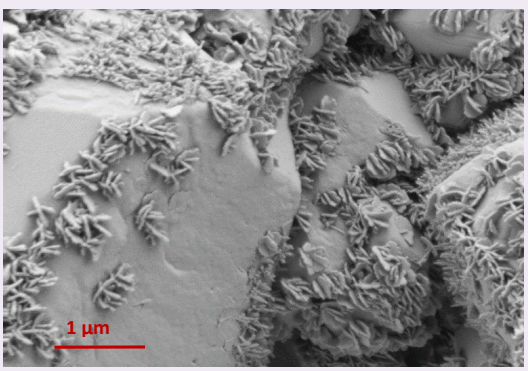


Fig. 6 *A SEM image of treated samples showing the calcite grains covered with HAP formed after the DAP treatment.*



untreated chalk baseline response. The blue line corresponds to the treated chalk, which clearly emphasizes the presence of new peaks. For example, new peaks related to the synthesized HAP can be seen at 2θ° values of 25.9, 31.7, and 34. These HAP characteristic peaks align with those found in the literature[22].

Additionally, as previously shown in Table 1, the XRD qualitatively measured the proportions of HAP and calcite in the treated and untreated chalk powder samples. Therefore, there is no doubt that the treatment caused the HAP to form because of the significant increase in its concentration in the treated sample compared to the untreated one.

The HAP's precipitation is found on the host calcite mineral and at the grain-to-grain contact points. The formed HAP covers the surface of the treated samples and glues the grains where they contact, i.e., enhances the cementation. According to what is observed from the SEM pictures, HAP formation is responsible for the rise in the slabs' stiffness following treatment with DAP. Therefore, the compaction of the slabs, including the short surface asperities, is less than that of the untreated samples. As a result, the fracture aperture that allows gas flow in the treated samples remained open with the application of the stress.

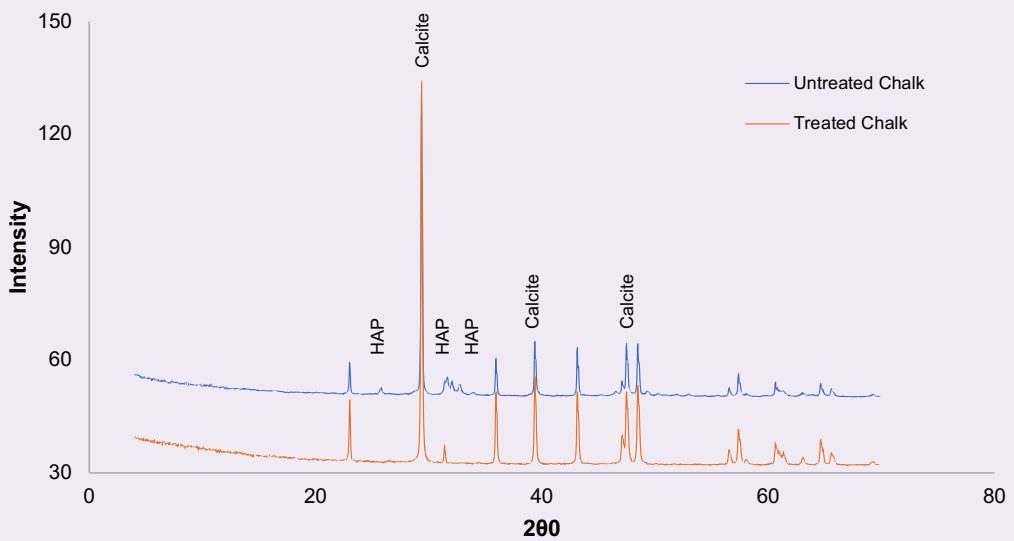
Conclusions

Reacting soft Austin chalk with DAP resulted in HAP precipitation. The formation of HAP significantly improved the surface hardness of the soft chalk. ANOVA provided statistical evidence that the surface hardness improved due to the DAP treatment rather than the inherent heterogeneity of the chalk.

The improved surface hardness was reflected in the chalk's hydraulic conductivity. The normalized hydraulic conductivity of the treated samples was higher than that of untreated samples. Also, the rate at which the treated samples' hydraulic conductivity declined was less than that of the treated samples.

Moreover, the deformation of samples while loading the samples was less in the treated samples, which collapsed at higher

Fig. 7 *The XRD of treated samples showing new peaks corresponding to HAP formed after the DAP treatment.*



stress than the untreated samples. Overall, the DAP treatment, investigated at high pressure and high temperature, is promising in preserving the acid fracture conductivity.

Acknowledgments

This article was presented at the 57th U.S. Rock Mechanics/Geomechanics Symposium, Atlanta, Georgia, June 25-28, 2023.

References

1. Gong, M., Lacote, S. and Hill, A.D.: "New Model of Acid-Fracture Conductivity Based on Deformation of Surface Asperities," *SPE Journal*, Vol. 4, Issue 3, September 1999, pp. 206-214.

2. Nierode, D.E. and Kruk, K.F.: "An Evaluation of Acid Fluid Loss Additives Retarded Acids, and Acidized Fracture Conductivity," SPE paper 4549, presented at the Fall Meeting of the Society of Petroleum Engineers of AIME, Las Vegas, Nevada, September 30-October 3, 1973.

3. Gomaa, A.M. and Nasr-El-Din, H.A.: "Acid Fracturing: The Effect of Formation Strength on Fracture Conductivity," SPE paper 119623, presented at the SPE Hydraulic Fracturing Technology Conference, The Woodlands, Texas, January 19-21, 2009.

4. Abass, H.H., Al-Mulhem, A.A., Alqam, M.S. and Mirajuddin, K.R.: "Acid Fracturing or Proppant Fracturing in Carbonate Formation? A Rock Mechanic's View," SPE paper 102590, presented at the SPE Annual Technical Conference and Exhibition, San Antonio, Texas, September 24-27, 2006.

5. Bartko, K.M., Conway, M.W., Krawietz, T.E., Marquez, R.B., et al.: "Field and Laboratory Experience in Closed Fracture Acidizing the Lisburne Field, Prudhoe Bay, Alaska," SPE paper 24855, presented at the SPE Annual Technical Conference and Exhibition, Washington, D.C., October 4-7, 1992.

6. Zhang, R., Hou, B., Zhou, B., Liu, Y., et al.: "Effect of Acid Fracturing on Carbonate Formation in Southwest China Based on Experimental Investigations," *Journal of Natural Gas Science and Engineering*, Vol. 73, January 2020.

7. Melendez, M.G., Pournik, M., Zhu, D. and Hill, A.D.: "The Effects of Acid Contact Time and the Resulting Weakening of the Rock Surfaces on Acid Fracture Conductivity," SPE paper 107772, presented at the European Formation Damage Conference, Scheveningen, the Netherlands, May 30-June 1, 2007.

8. Mustafa, A., Alzaki, T., Aljawad, M.S., Sølling, T., et al.: "Impact of Acid Wormhole on the Mechanical Properties of Chalk, Limestone, and Dolomite: Experimental and Modeling Studies," *Energy Reports*, Vol. 8, November 2022, pp. 605-616.

9. Bauer, A., Walle, L.E., Stenebråten, J. and Papamichos, E.: "Impact of Acidizing-Induced Wormholes in Chalk on Rock Strength," paper presented at the 47th U.S. Rock Mechanics/Geomechanics Symposium, San Francisco, California, June 23-26, 2013.

10. Nasr-El-Din, H.A., Al-Driweesh, S.M., Metcalf, A.S. and Chesson, J.B.: "Fracture Acidizing: What Role Does Formation Softening Play in Production Response?" *SPE Production & Operations*, Vol. 23, Issue 2, May 2008, pp. 184-191.

11. Bale, A., Smith, M.B. and Klein, H.H.: "Stimulation of Carbonates Combining Acid Fracturing with Proppant (CAPF): A Revolutionary Approach for Enhancement of Sustained Fracture Conductivity and Effective Fracture Half-Length," SPE paper 134307, presented at the SPE Annual Technical Conference and Exhibition, Florence, Italy, September 19-22, 2010.

12. Ding, Y., Li, Y., Xu, Y., Cheng, X., et al.: "Propped Fracturing with a Novel Surface Cross-Linked Acid in High Temperature Deep Carbonate Formation," SPE paper 127312, presented at the North Africa Technical Conference and Exhibition, Cairo, Egypt, February 14-17, 2010.

13. Zhang, L., Zhou, F., Mou, J., Xu, G., et al.: "A New Method to Improve Long-Term Fracture Conductivity in Acid Fracturing under High Closure Stress," *Journal of Petroleum Science and Engineering*, Vol. 171, December 2018, pp. 760-770.

14. Desouky, M., Aljawad, M.S. and Sølling, T.: "Rock Hardness for Hydraulic Fracturing and Art Preservation," U.S. Patent No. 11,492,494, 2022.

15. Desouky, M., Aljawad, M.S., Sølling, T., Abduljamiu, A., et al.: "Improving Long-Term Hydraulic Fracture Conductivity by Alteration of Rock Minerals," *Journal of Petroleum Science and Engineering*, Vol. 196, January 2021.

16. Aljawad, M.S., Desouky, M., Sølling, T., Alramadan, K., et al.: "Method of Improving Rock Hardness in Carbonate Formations," U.S. Patent No. 11,365,345, 2022.

17. Sassoni, E., Naidu, S. and Scherer, G.W.: "The Use of Hydroxyapatite as a New Inorganic Consolidant for Damaged Carbonate Stones," *Journal of Cultural Heritage*, Vol. 12, Issue 4, October-December 2011, pp. 346-355.

18. Aljawad, M.S., Desouky, M., Sølling, T.I., Amao, A.O., et al.: "Improving Carbonate Rock Hardness by Consolidating Additives to Sustain Long-Term Fracture Conductivity," *Journal of Petroleum Science and Engineering*, Vol. 195, December 2020.

19. Samarkin, Y., Aljawad, M., Amao, A., Sølling, T., et al.: "Hydraulic Fracture Conductivity Sustenance in Carbonate Formations through Rock Strengthening by DAP Solution," IPTC paper 22496, presented at the International Petroleum Technology Conference, Riyadh, Kingdom of Saudi Arabia, February 21-23, 2022.

20. Samarkin, Y., Amao, A., Aljawad, M.S., Sølling, T., et al.: "Conductivity Enhancement of Fractured Carbonates through High Temperature Diammonium Hydrogen Phosphate Consolidation: A Preliminary Study," *SPE Journal*, Vol. 28, Issue 4, August 2023, pp. 1-17.

21. Roy, D.M. and Linnehan, S.K.: "Hydroxyapatite Formed from Coral Skeletal Carbonate by Hydrothermal Exchange," *Nature*, Vol. 247, 1974, pp. 220-222.

22. Chen, K-Y. and Arai, Y.: "X-ray Diffraction and X-ray Absorption Near-Edge Structure Spectroscopic Investigation of Hydroxyapatite Formation under Slightly Acidic and Neutral pH Conditions," *ACS Earth and Space Chemistry*, Vol. 3, Issue 10, August 2019, pp. 2266-2275.

About the Authors

Mahmoud Desouky

M.S. in Petroleum Engineering, King Fahd University of Petroleum and Minerals

Mahmoud Desouky is a Ph.D. candidate at the College of Petroleum Engineering & Geosciences at King Fahd University of Petroleum and Minerals (KFUPM), Dhahran, Saudi Arabia. His focus is on enhancing hydraulic fracture conductivity through chemical methods.

Mahmoud is also a certified Data Scientist, augmenting his expertise in data-driven approaches. His notable achievements include securing First Place in the prestigious ARMA Research Contest in 2023, showcasing his exceptional research capabilities and contributions to the field.

In 2013, Mahmoud received his B.S. degree in Petroleum Engineering from Suez University, Suez, Egypt, and in 2019, he received his M.S. degree in Petroleum Engineering from KFUPM.

Dr. Murtada S. Al Jawad

Ph.D. in Petroleum Engineering, Texas A&M University

Dr. Murtada S. Al Jawad is an Associate Professor in the Petroleum Engineering Department at King Fahd University of Petroleum and Minerals (KFUPM), Dhahran, Saudi Arabia. He has actively participated in research projects on reactive transport, geomechanics, and sustainability. Murtada's research interests include reactive transport, geomechanics, sustainability, and productivity enhancement.

Since joining KFUPM in 2018, Murtada has been a member of several internally and externally funded projects. He led the development of a concentration in unconventional hydrocarbon resources. Also, Murtada established a fully equipped, state-of-the-art lab to study and evaluate hydraulic fractures.

He is an active member of the Society of Petroleum Engineers (SPE), and has served as a Committee Member and/or Session Chair in the Middle East Oil and Gas Show (MEOS), the International Petroleum Technology Conference (IPTC), the International Hydraulic Fracturing Technology Conference (IHFTC), and other related workshops and symposiums.

In 2011, Murtada received his B.S. degree in Chemical Engineering from KFUPM; in 2014, he received his M.S. degree in Petroleum Engineering from Texas A&M University, College Station, TX; and in 2018, Murtada received his Ph.D. degree in Petroleum Engineering from Texas A&M University, College Station, TX.

Dr. Abduljamiu Amao

Ph.D. in Geology,
King Fahd University of Petroleum and Minerals

Dr. Abduljamiu Amao is a Research Scientist at the College of Petroleum Engineering & Geosciences at King Fahd University of Petroleum and Minerals (KFUPM), Dhahran, Saudi Arabia. His work is the study of modern benthic foraminifera in the Arabian Gulf, focusing on sampling whole communities along environmental gradients to understand ecological structures and environmental change.

Abduljamiu's research interests include micropaleontology and biostratigraphy, statistics and applied mineralogy, and applied marine geology.

He received his B.S. degree in Biology from Ahmadu Bello University, Zaria, Nigeria, and his M.S. degree in Environmental Sciences from KFUPM. Abduljamiu received his Ph.D. degree in Geology from KFUPM.

Dr. Dhafer A. Al-Shehri

Ph.D. in Petroleum Engineering,
Texas A&M University

Dr. Dhafer A. Al-Shehri is the Chairman of the Petroleum Engineering Department and an Associate Professor within the College of Petroleum Engineering & Geosciences at King Fahd University of Petroleum and Minerals (KFUPM), Dhahran, Saudi Arabia.

He has over 30 years of experience in the oil and gas industry and academia. Dhafer worked at Saudi Aramco for 18 years (1996-2014), during which time he assumed leading technical and management positions within upstream operations, engineering, and field development. Dhafer's research interests include petroleum reservoir engineering and management, reservoir characterization, enhanced oil recovery, and petroleum economics.

He has been an active Society of Petroleum Engineers (SPE) member throughout his career, and has served on many technical and organizing committees for SPE and other technical events. Dhafer was also a keynote speaker at several SPE workshops. He has authored more than 100 papers in peer-reviewed technical journals, along with regional and international conferences.

Dhafer is a recipient of the 2019 International SPE Distinguished Membership Award, and was appointed as a member of the SPE Middle East Advisory Council, He is also an Advisory Board Member of the Petroleum Engineering Department, Khalifa University, UAE; and was named an Executive Board Member of the Petroleum Engineering Department Heads (PEDHA).

Dhafer received B.S. degree and M.S. degree in Petroleum Engineering from KFUPM, and his Ph.D. degree from Texas A&M University, College Station, TX. Dhafer also received an EMBA degree from KFUPM.

Dr. Murtadha J. AlTammar

Ph.D. in Petroleum Engineering,
University of Texas at Austin

Dr. Murtadha J. AlTammar is a Lead Petroleum Engineer working with the Production Technology Team of Saudi Aramco's Exploration and Petroleum Engineering Center – Advanced Research Center (EXPEC ARC).

Previously, Murtadha worked in the field for 18 months as a Completion and Production Engineer with the Southern Area Gas Production Engineering Division.

He received the 2011 SAPED Significant Achievement Award for leading a well intervention campaign, and also the 2017 EXPEC ARC Best-in-Class Young Researcher Award. Murtadha was an invited speaker at the 2017 American Rock Mechanics Association (ARMA) Hydraulic Fracturing Workshop in San Francisco, CA.

He has been a technical reviewer for many journals. Murtadha has also been a member of organizing several technical committees for the Society of Petroleum Engineers (SPE) and ARMA conferences.

He received his B.S. degree in Petroleum Engineering from the Colorado School of Mines, Golden, CO. Murtadha received his M.S. degree and Ph.D. degree in Petroleum Engineering, specializing in hydraulic fracturing mechanics, from the University of Texas at Austin, Austin, TX.

Dr. Khalid M. Alruwaili

Ph.D. in Petroleum Engineering (Geomechanics),
Heriot-Watt University

Dr. Khalid M. Alruwaili is a Petroleum Engineering Specialist leading and supporting several research programs in the Production Technology Division of Saudi Aramco's Exploration and Petroleum Engineering Center – Advanced Research Center (EXPEC ARC).

He joined Saudi Aramco in 2006 as a Petroleum Engineer working in various technical positions for the Northern Area Reservoir Management at Berri field. After this assignment, Khalid worked on the ultimate development plan of the Upper Fadhili reservoir, a tight carbonate reservoir. His area of research is borehole mechanics, wellbore stimulation, hydraulic fracturing, and reservoir geomechanics.

He is an active member of the Society of Petroleum Engineers (SPE) and a technical contributor to the American Rock Mechanics Association. He is a committee member at the International Geomechanics symposium. Khalid has authored and coauthored several technical papers.

He received his B.S. degree in Petroleum and Natural Gas Engineering from King Saud University, Riyadh, Saudi Arabia, an M.S. degree in Petroleum Engineering (Geomechanics) from the University of Calgary, Calgary, Alberta, Canada, and a Ph.D. degree in Petroleum Engineering (Geomechanics) from Heriot-Watt University, Edinburgh, Scotland, U.K.

Multilateral Completion Technology to Improve Reservoir Management

Yousef W. Ameen, Abdulrakeeb Almasri, Abdullah Alsaleh and Mortada A. Alkadem

Abstract /

An effective well completion design is crucial to optimize well and field performance, with many operators utilizing different techniques to achieve this important objective. Although, the conventional means of designating wells for reservoir monitoring and stand-alone wells for production presents challenges to cost-effective reservoir management.

Vertical observation wells are usually drilled in different locations to monitor the reservoir and assist with planning and intervention decisions by running periodic logs to obtain subsurface information. Subsequently, these wells can be costly and occupy valuable space that could be utilized for production. An alternate technique is to drill a pilot hole, perform all the necessary logging, and obtain the required reservoir information. The pilot hole is then plugged and sidetracked to a producer well. Nevertheless, the collected data only remains valid for a limited period due to potential changes to the reservoir.

The demand for cost-effective, optimized drilling of production and observation wells has led to a paradigm shift in multilateral well technology that achieves both production and monitoring objectives for both laterals at the same time. Using this enhanced technology, wells can be completed with a pilot hole (vertical) drilled for reservoir evaluation throughout the life of the well, with permanent downhole gauges (PDHGs) installed for pressure and temperature monitoring, while the horizontal lateral functions as an oil and gas producer. Combining the observation and producer wells into one well results in cost savings and enhanced reservoir production and surveillance programs. In addition, the capability to access the lateral allows for intervention in both the motherbore and lateral at any time.

Well intervention operations for a well completed with this multilateral technology involve slick line runs to gain access to the horizontal lateral, retrieve an isolation sleeve, and install a tubing exit whipstock for lateral reentry. Later, coiled tubing (CT) or a wireline tractor can be run through the window into the lateral to perform the logging and intervention necessary. Upon completion, the tubing exit whipstock is retrieved from the window, the isolation sleeve is reinstalled, and the well is returned to production. Well intervention through such multilateral completion demonstrates the ease and efficiency of accessing both the vertical and horizontal lateral, without requiring a rig or completion retrieval.

This article will highlight the multilateral completion technology for accessing both laterals, which includes real-time monitoring capabilities that provide more reliable data for optimum well and field performance.

Introduction

The ultimate objective in the oil and gas industry is to maximize recovery while minimizing cost. Success relies on reservoir management decision making. As such, reservoir monitoring has become crucial to reservoir management, understanding of a field's dynamic behavior, and supporting base business.

Sound reservoir management can only be founded on regular monitoring and surveillance of the reservoir's overall performance. It is, therefore, common practice to collect surveillance data to implement optimal reservoir management methods, which are designed to be performed periodically to meet three key goals: (1) Address reservoir uncertainty, (2) Monitor reservoir and well performance, and (3) Conform with regulatory standards.

Reservoir data that aids in decision making are acquired during pilot hole drilling and comprehensive logging. Consequently, the opportunity is limited to a single use; in most cases, the pilot hole is abandoned once the logging procedure is completed, and therefore, cannot be used to evaluate reservoir changes after a specific period. As a result, observation wells that can be accessed and logged regularly are being used and are strategically placed to ensure that the data acquired are representative of the entire field. These methods are costly, and as more wells are drilled, it becomes difficult to devote them solely to monitoring. Therefore, other methods are necessary to provide better solutions to these difficulties. One such option is multilateral

technology, which combines the producer and the observer into one well.

Well Completion Effect on Performance

Proper well completion design is key to successful production throughout the life of the well. Many technologies are under development worldwide to enhance well completions and simplify future well intervention. In particular, multilateral technology, which is the ability to drill multiple laterals from a single location and allows access to each lateral, provides a proven strategy to increase well production and reduce capital expenditure.

Moreover, because each field is different, multilateral completion strategies should be tailored to address the particular field requirement. The ability to maintain well integrity during construction and provide full access to the well throughout its life cycle can be difficult. Lateral access is necessary for production optimization, reservoir management, and well treatment to enhance production. In addition, logging and well treatment is required occasionally to maintain well health and provide maximum sweep of the reservoir.

Production Logging Overview

The geology and geophysical wellbore data and formation fluid parameters, such as porosity, permeability, saturation, resistivity, and shale volume, are determined via a traditional well log. All of these parameters are monitored while drilling a well. Production logging is crucial to develop reservoir production modeling and processes, and to identify production and completion anomalies and problems. A production log usually helps measure the zonal contribution of water or hydrocarbons to evaluate the flow performance model and stimulation effectiveness.

Various production logging instruments are utilized to determine the flow behavior of formation fluids. A spinner flow meter is used to estimate the formation fluid velocity while a gradiomanometer is used to determine the fluid density. Individual sensors are also used during production logging for the evaluation of various attributes.

Main Challenges

Stand-alone observation wells can increase the overall cost of development due to the costly drilling process. Additionally, the number of observation wells required increases, as more wells are drilled in the region. Therefore, field progress necessitates an alternate option.

Addressing the Challenges

The cooperation of reservoir and completion engineers introduced an innovative solution for a new multilateral strategy to address the challenges and provide value.

The solution incorporates the following approaches:

- Well construction methods to help maintain the well's integrity throughout the well's life.
- A completion process that allows for lateral access, pressure, and temperature monitoring, as well as straightforward installation and retrieval.
- An intervention plan for the wells completed with multilateral technology to maintain the objectives.

Type of Completions

Wells are usually drilled and completed as vertical or horizontal with open hole or cased hole completions. In general, the wells that are completed as horizontal producers or injectors are either a single lateral with a single packer completion or multilateral.

Multilateral drilling can greatly impact production and overall well costs. Therefore, to achieve maximum benefits and address challenges, an optimum well construction and completion strategy should be sufficient to comply with the approaches previously mentioned.

Well Construction Method

The Technology Advancement of Multilaterals (TAML) system categorizes multilateral wells according to junction functionality and complexity, designated TAML Levels 1 through 6. This ranking system is used to determine the appropriate lateral design.

The TAML levels are defined as:

1. TAML Level 1: A lateral hole is drilled from an open hole main wellbore, Fig. 1. Level 1 multilaterals are drilled in stable formations, although flow control and lateral reentry are not possible.
2. TAML Level 2: The main wellbore is cemented and cased, whereas the lateral is an open hole or drop liner with no connection at the junction, Fig. 2. When an isolation packer is installed below each window, flow control for each lateral is possible. Lateral access, however, is not feasible until the entire completion is pulled out of the well.
3. TAML Level 3: The main wellbore is cased and cemented but the lateral wellbore is not. Although the lateral wellbore is mechanically connected to the main wellbore, the connection is not hydraulically sealed, Fig. 3. In the oil industry, Level 3 construction is uncommon.
4. TAML Level 4: Both the main wellbore and lateral are cased and cemented, and the hydraulic integrity depends on the cement quality, Fig. 4.
5. TAML Level 5: The junction integrity is accomplished by the completion, and the junction can be cemented or

Fig. 1 *TAML Level 1.*

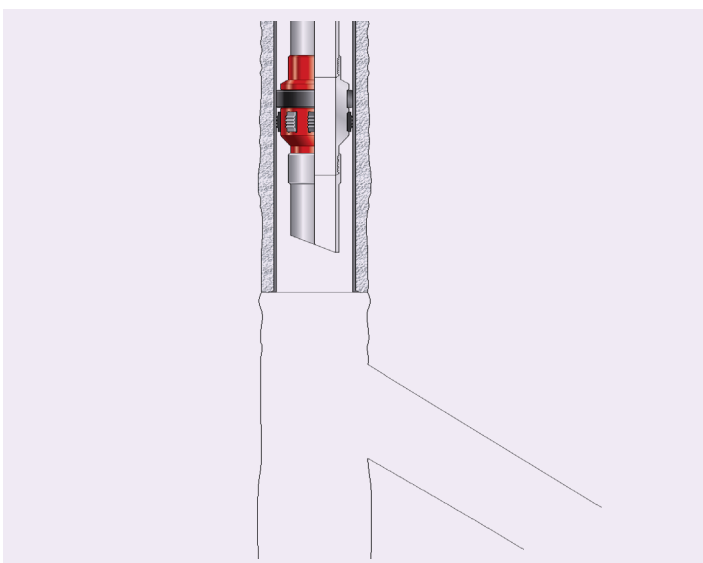


Fig. 2 *TAML Level 2.*

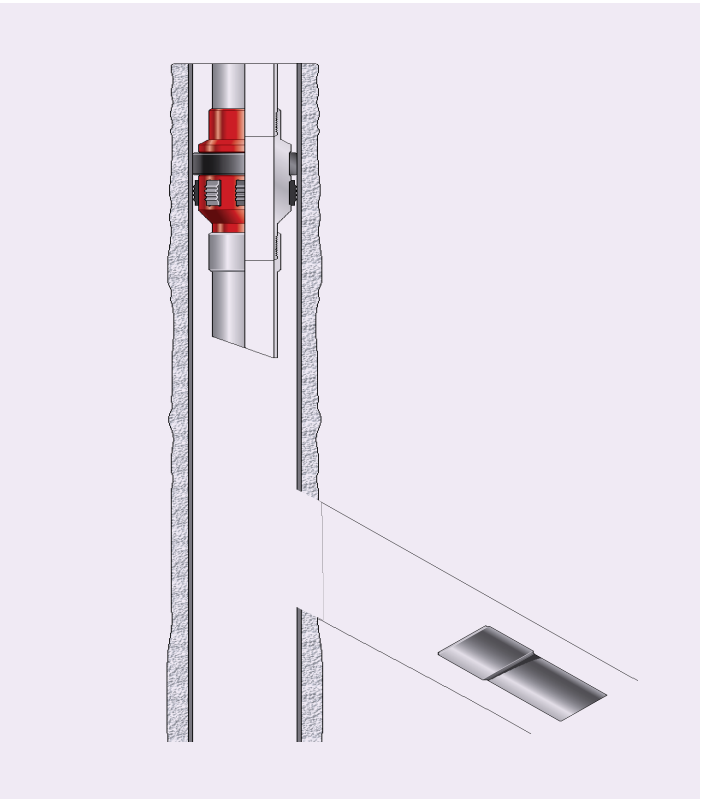


Fig. 3 *TAML Level 3.*

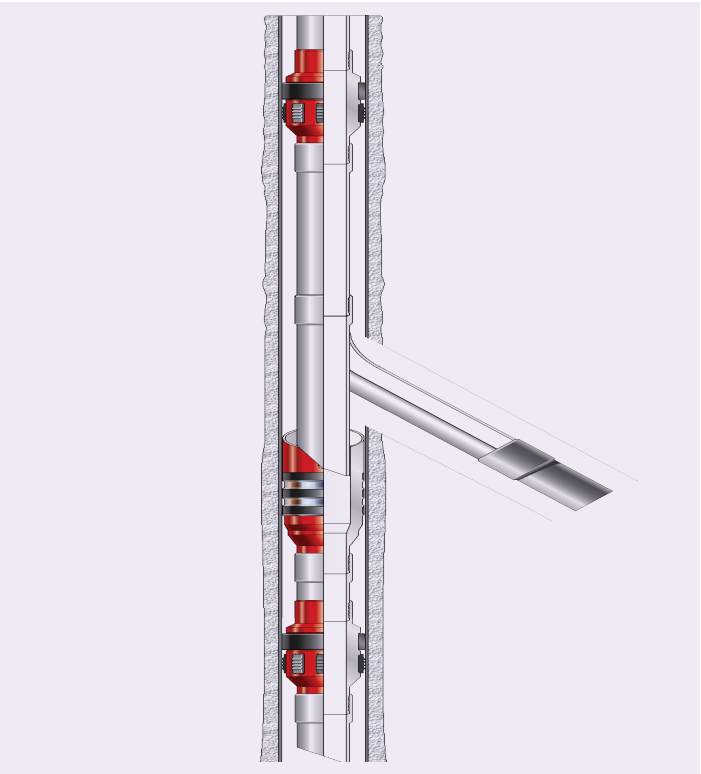


Fig. 4 *TAML Level 4.*

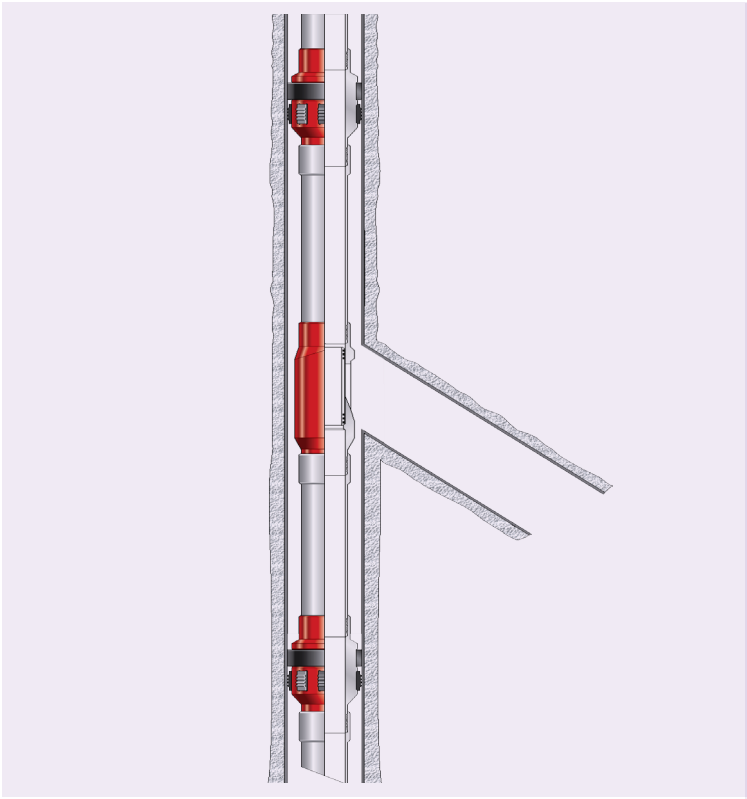


Fig. 5 *TAML Level 5.*

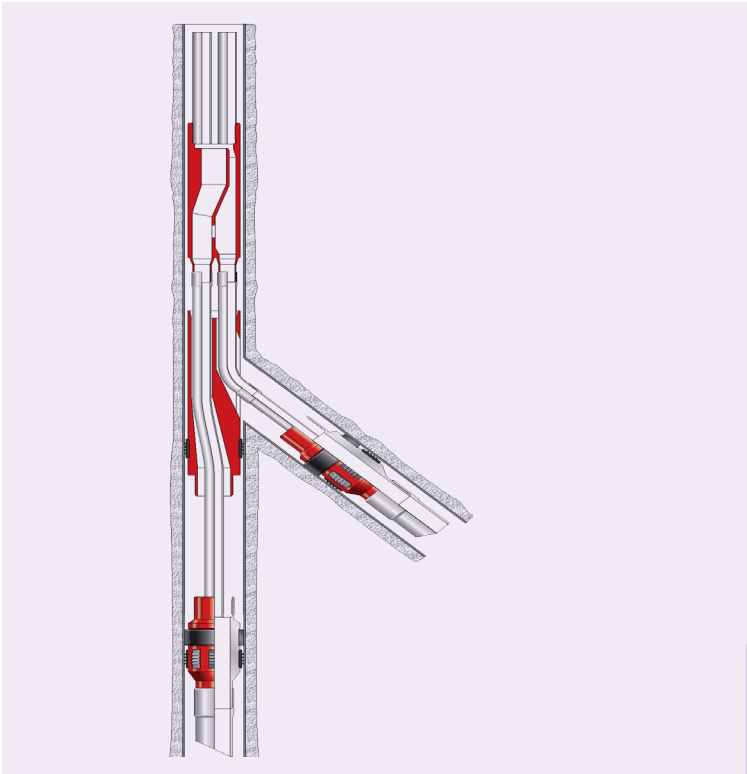
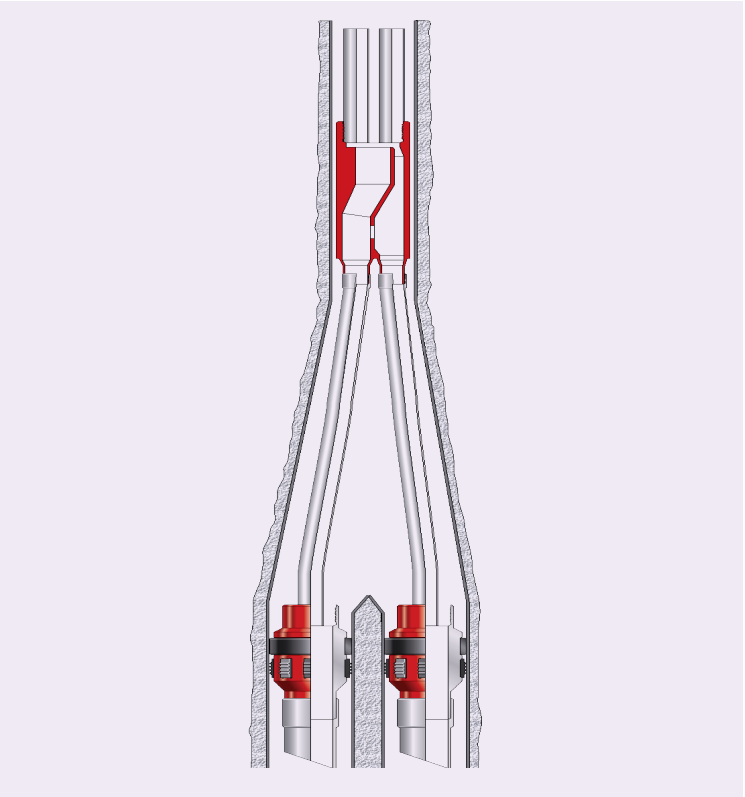


Fig. 6 TAML Level 6.



uncemented, Fig. 5. Level 5 systems are common in fields where gas migration at the junction is detected.

6. TAML Level 6: Two branches are drilled from the original wellbore, and both mechanical and pressure integrity are achieved using the casing to seal the junction, Fig. 6.

The reservoir and completion engineers thoroughly assessed the available options to determine the optimal deployment method to increase output while maintaining access to both laterals. It was agreed that wells would be constructed as a Level 4 multilateral to help ensure junction integrity based on the formation features and well designs. Junction integrity is maintained using a liner in the lateral that extends to the main wellbore, and cement pumped between the lateral and the formation provides the required support and prevents undesirable fluid migration into the main wellbore[1].

Once the lateral liner is cemented, a washover assembly removes the cement residue from within the well and leaves the well with a casing drift size lateral window. Level 4 multilateral construction is common in the oil industry when the window is cut in the build section and a cemented section is required. Level 4 systems are effective in providing well integrity.

Generally, longer laterals help increase production, and operators drill horizontal wells despite the increase in cost and additional challenges; however, as well depths increase, more challenges arise. Therefore, multilateral drilling has become necessary to achieve higher production because multiple laterals can be drilled without going too deep into the reservoir[2].

Multilateral Completion Method

Selection of Multilateral Completion Equipment: The well required a multilateral completion system installed in a cost-effective manner that enabled access to the well during the production phase, without rig intervention and without retrieving the completion equipment[3].

For Well-A, the system selected utilized a completion window designed as an integral part of the production string and equipped with landing profiles and sealbores to enable the setting of deflectors for lateral access or isolation sleeves for lateral flow control and isolation. These profiles are designed such that a special tool can be set inside the window for a specific objective.

Completion Window: The completion window is connected to the tubing and equipped with internal profiles for the service tool to achieve reentry access either to the main wellbore or the lateral, Fig. 7. The inner diameter of the window should be sufficient to allow the entire bottom-hole assembly (BHA) to run into the well and pass through to the main wellbore or the lateral. A latch coupling run as part of the casing helps ensure the window is installed at the optimum depth, with the opening oriented to the lateral, Fig. 8.

Pressure Isolation Sleeve: The completion window has a profile to set the pressure isolation sleeve, Fig. 9, which isolates the lateral and helps ensure the BHA is directed to the main wellbore and logging can be performed. This sleeve is run and retrieved by a special running and retrieving tool.

Tubing Exit Whipstock: The reentry window has another profile to set the tubing exit whipstock when lateral intervention is necessary, Fig. 10. With the tubing exit whipstock tool set inside the window, any BHA run in the hole will be redirected to the lateral. The tubing exit whipstock is run and retrieved by a special running and retrieving tool.

Well Completion Equipment and Accessories

The wells with this technology are designed to include the following completion accessories, Fig. 11:

1. Lower production packer to isolate the main wellbore below the window.
2. Two permanent downhole gauges (PDHGs) above the completion reentry window for pressure and temperature monitoring.

Fig. 7 The reentry window.



Fig. 8 *The reentry window oriented to the lateral.*

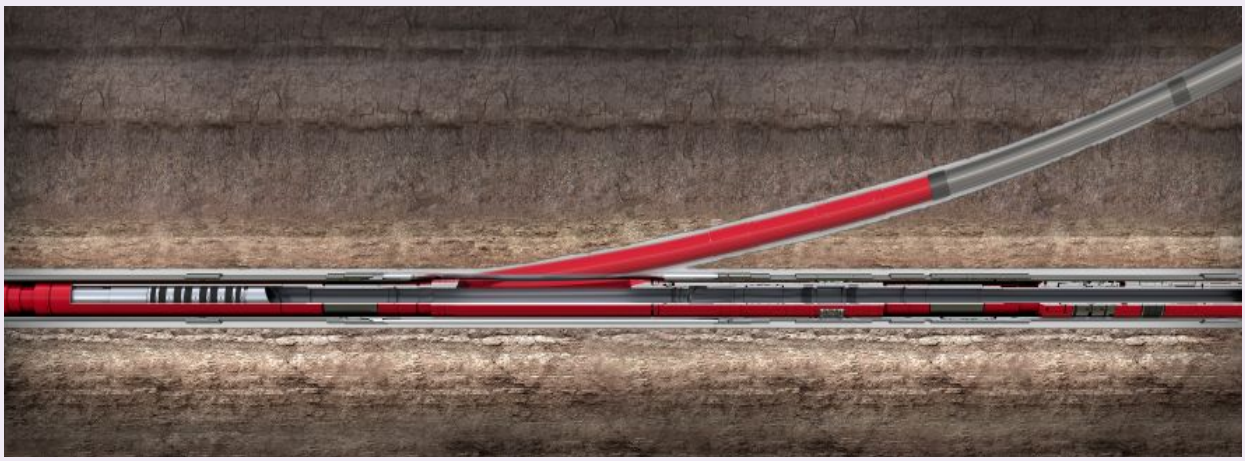
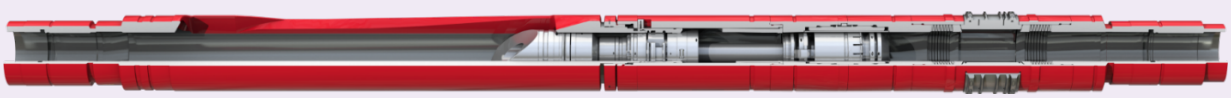


Fig. 9 *The reentry window with a pressure isolation sleeve installed.*



Fig. 10 *The reentry window with a tubing exit whipstock installed.*



The lower gauge sensor measures tubing pressure from the main wellbore; the upper gauge sensor measures annulus pressure from the lateral. The real-time readings allow the production team to detect changes as they occur.

3. Two sliding side-door (SSD) devices that open and close using a slick line. One SSD located below the upper packer flows through the well. A second SSD located above the upper packer displaces the well for lifting before moving the rig.
4. An upper feed-through production packer to isolate the lateral flow and direct it into the SSD below the packer.
5. One landing nipple positioned between the PDHGs. The landing nipple includes a plug to isolate the two PDHGs, which helps prevent interference between the main wellbore and the lateral.
6. One landing nipple positioned below the lower packer to isolate the main wellbore, if necessary, during lateral operations.

Well Logging and Cleanup Application Example

To achieve distinct goals, some intervention has been undertaken for several wells that have been completed and equipped with a TAML Level 4 system and reentry window.

Candidate Well-A Description

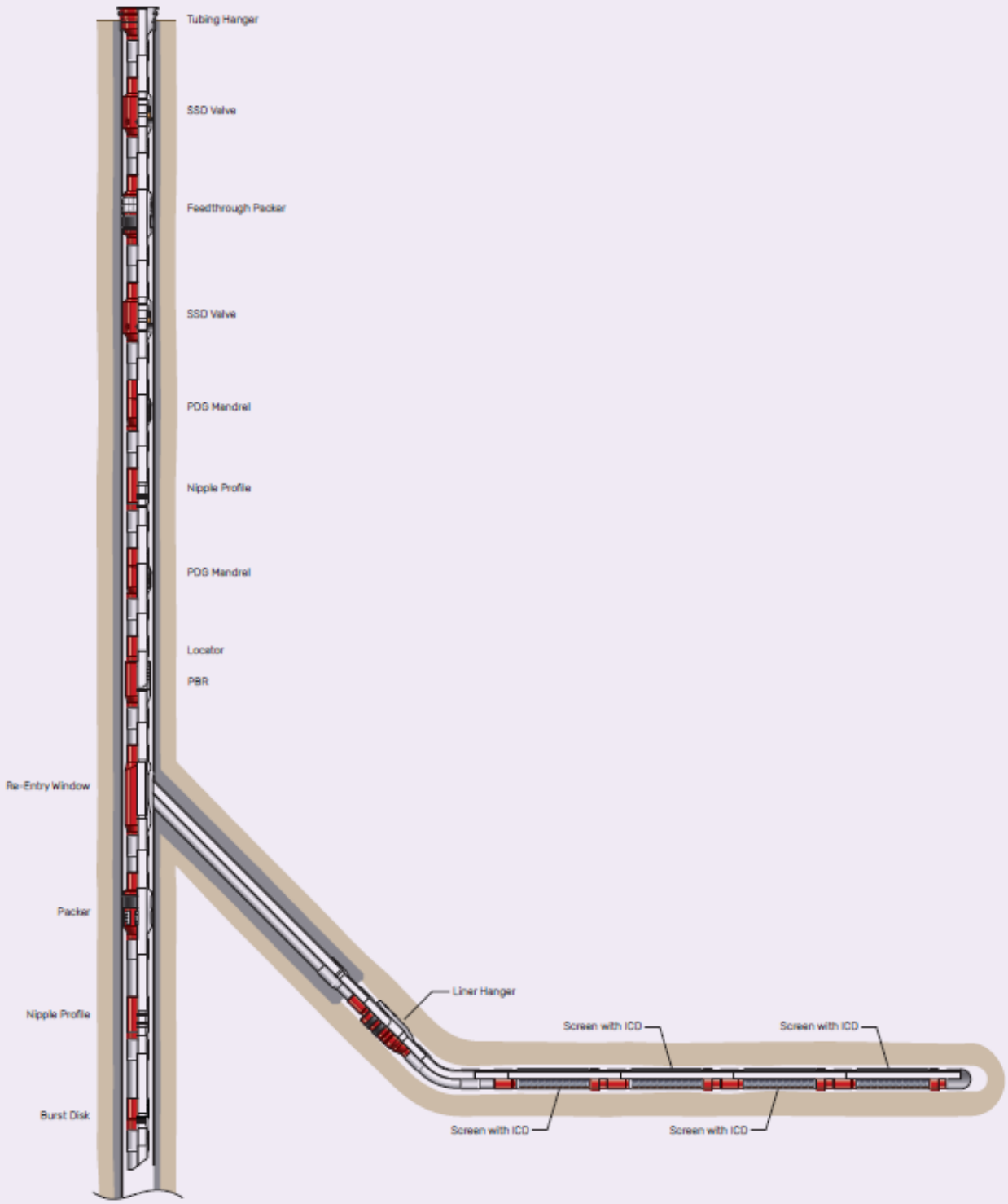
The candidate well, Well-A, was drilled open hole and completed with the multilateral reentry window system and active inflow control devices (ICDs) separated by open hole packers in the lower completion. Then, when put on production, Well-A was underperforming.

Nodal analysis was used to evaluate well performance, which indicated that the well could generate reservoir fluid easily to the surface under the present reservoir conditions. Sensitizing the well parameters for extremes, such as high water cut and moderate reservoir reduction, verified the expected performance of the well.

Operational Summary for Well-A

Well-A was underperforming after drilling and completing the well using the reentry window system, as indicated. To establish

Fig. 11 *A well schematic showing the completion equipment and accessories.*



well readiness, many studies were conducted, including opening the bottom sliding sleeve so that the tubing could be connected to the reservoir. Subsequent examination revealed that the well was drilled using 72-lbm/ft^3 polymer mud without cleaning out after drilling.

The well was sidetracked and completed as a horizontal producer with an equalization completion of nine active/active ICDs (with sliding sleeve) separated by three open hole packers.

To address reservoir challenges and clean out the well, lateral access was necessary for treatment.

Initial Operation: Using a slick line, the following operations were performed:

- A brush was run to confirm the tubing was clean. A proper brush run was performed before running the retrieving or running tool because debris could have accumulated inside the tubing, particularly in the profile area, which could jeopardize the next operation.
- The PX plug was retrieved from the nipple profile. This step was performed in three slick line trips to retrieve the junk basket, retrieve the prong, and retrieve the plug.
- The pressure isolation sleeve retrieved from the reentry window using the retrieving tool, Figs. 12 and 13. Jarring was required to remove the seal from the profile.
- A slick line brush to clean the profile area inside the reentry window.
- Tubing exit whipstock with running tool attached to a slick line and installed in the reentry window, Figs. 14 and Fig. 15. After the tubing exit whipstock was installed, the slick line with the running tool was pulled out of the hole.
- Treatment BHA with coiled tubing (CT) was run in the hole past the window and into the lateral, Fig. 16.
- Cleaning of the wellbore was performed.
- After the treatment was complete, the CT was pulled out of the hole.
- The retrieving tool was run on a slick line and the tubing exit whipstock was retrieved.
- The pressure isolation sleeve was run with a slick line and installed inside the reentry window.
- The PX plug was installed in the landing nipple below the upper production packer.
- The well was delivered and later put on production.

Production Performance: The successful treatment in the wellbore using CT helped clean out the well with very encouraging results. In fact, the well began to flow as expected after the reentry window operations, including wellbore treatment.

Conclusions

The following conclusions are based on the operations performed on Well-A:

- The new multilateral completion technology allows lateral access for improvements in the production optimization approach and the ICD operation.
- Multilateral completions can address many challenges that occur over the well's life.

Fig. 12 *The pressure isolation sleeve retrieved by a slick line.*

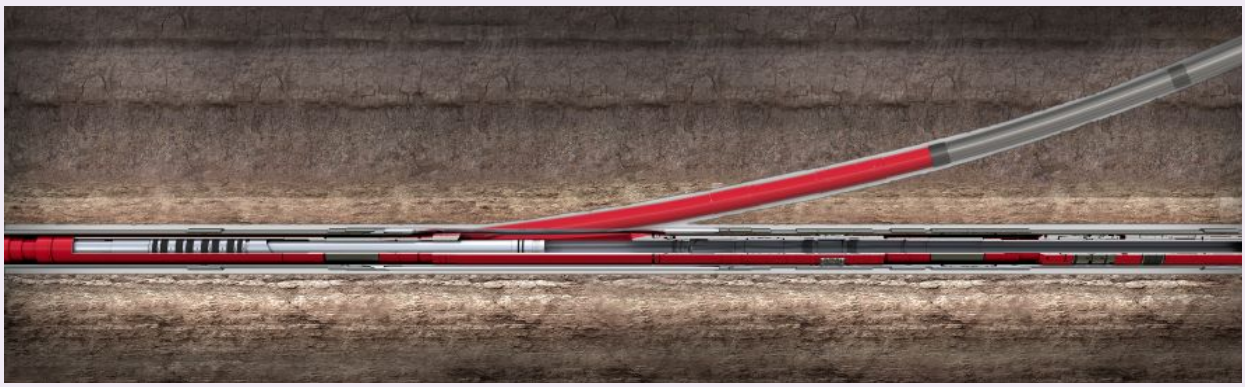


Fig. 13 *The pressure isolation sleeve outside the window.*

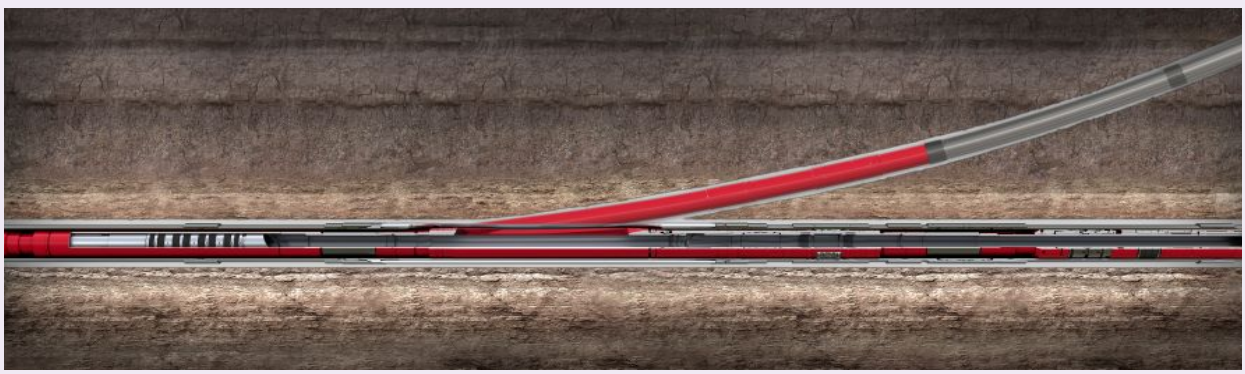


Fig. 14 *The tubing exit whipstock run on a slick line and installed in the window.*

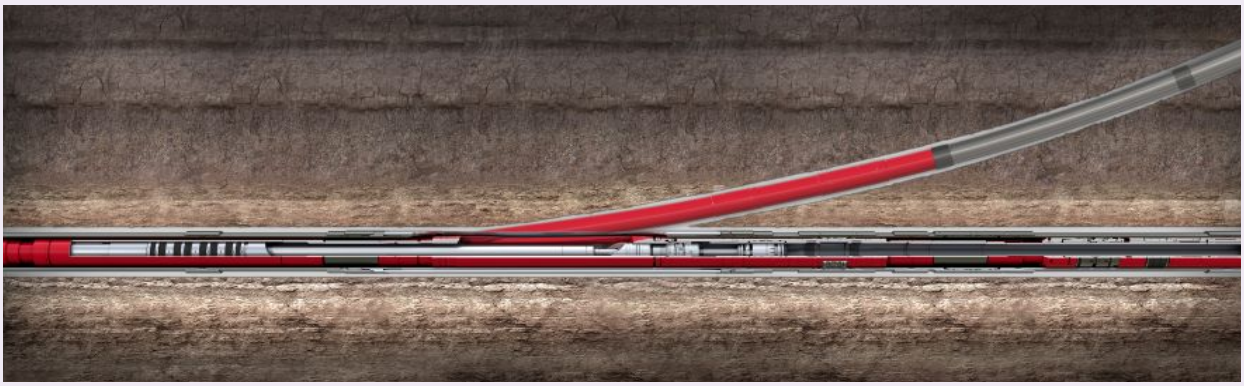


Fig. 15 *The tubing exit whipstock installed inside the reentry window.*

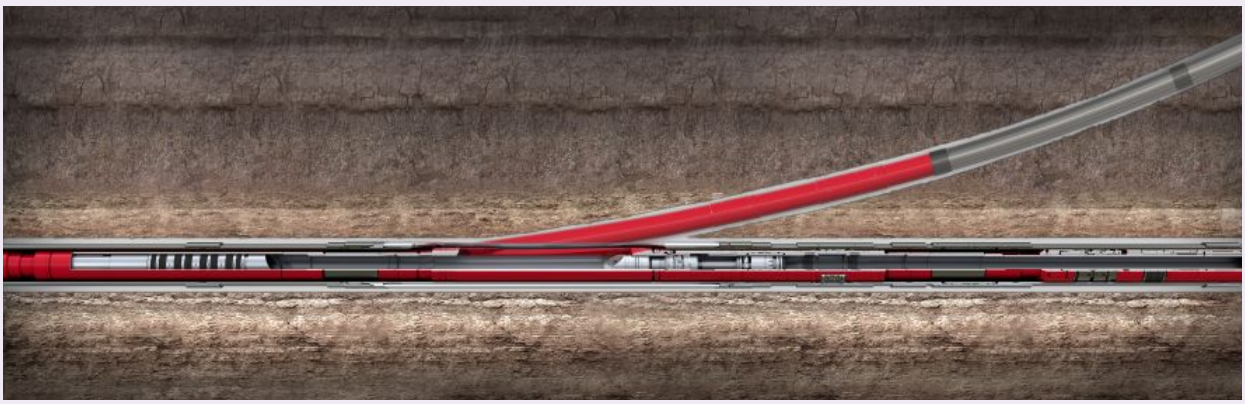


Fig. 16 *The wellbore treatment run inside the lateral.*



- Technology has opened various other techniques for improving water shutoff tactics, which might become more difficult over time.
- Ease of access to the main wellbore helps simplify and reduce the cost of performing the surveillance strategy.
- Multilateral completion technology allows access to the vertical wellbore to monitor sweep efficiency through running periodic logging.
- Multilateral completion technology allows access to monitor reservoir saturation and fluid movement.
- The surveillance and production objectives are achieved using the optimum completion approach.

Recommendations

The technology presented has proven useful and should be considered to maximize well performance. The following recommendations are a result of this work:

1. Select strategic locations for the application of the reentry window technology.
2. Improve the technology such that fewer runs are necessary during the intervention process.
3. After drilling the pay zone with polymer-based mud, perform clean out treatment to increase wellbore productivity.
4. Ensure the reentry window is of sufficient size to accommodate the logging tool.
5. Improve the technology in a way to be able to run it in an existing well.

Acknowledgments

This article was presented at the SPE Annual Technical Conference and Exhibition, San Antonio, Texas, October 16-18, 2023.

References

1. Vento, M. and Durst, D.: "Why Multilateral Cemented Junction Wells Can Help Economics for Development Projects in Oil and Gas Shale Reserves," SPE paper 178171, presented at the SPE/IADC Middle East Drilling Technology Conference and Exhibition, Abu Dhabi, UAE, January 26-28, 2016.
2. Sharma, H.K. and Almasri, A.: "Successful Intervention through Multilateral Completion Window for Logging and Wellbore Treatment," SPE paper 210334, presented at the SPE Annual Technical Conference and Exhibition, Houston, Texas, October 3-5, 2022.
3. Al Ansari, N. and Racine, B.: "A Successful Deployment of Level 4 Multilateral Isolation Completion System," SPE paper 197581, presented at the Abu Dhabi International Petroleum Exhibition and Conference, Abu Dhabi, UAE, November 11-14, 2019.

About the Authors

Yousef W. Ameen

M.S. in Petroleum Engineering, University of Southern California

Yousef W. Ameen is a Senior Petroleum Engineer working in the Hawiyah Unit of Saudi Aramco's Southern Area Reservoir Management Department (SARMD). He has 8 years of experience in reservoir management, production engineering, and drilling and workover engineering.

In 2015, he received his B.S. degree in Petroleum Engineering from the University of Tulsa, Tulsa, OK, and in 2020, Yousef received his M.S. degree in Petroleum Engineering from the University of Southern California, Los Angeles, CA.

Abdulrakeeb Almasri

B.S. in Civil Engineering, Sana'a University

Abdulrakeeb Almasri is a Senior Business Development Account Representative in Halliburton's Completion Tool Department at Halliburton Saudi Arabia. He is a subject matter expert for completion and multilateral completions with more than 18 years of experience.

As a completion design expert, Abdulrakeeb has working experience in well completion design and evaluation for standard well completions, multilateral well completions, and smart well completions.

He received his B.S. degree in Civil Engineering from Sana'a University, Sana'a, Yemen.

Abdullah Alsaleh

B.S. in Petroleum Engineering, Louisiana State University

Abdullah Alsaleh is a Petroleum Engineer in working in the Hawiyah Unit of Saudi Aramco's Southern Area Reservoir Management Department. He has 7 years of experience in the oil industry related to reservoir management, drilling, and production engineering.

Abdullah has authored more than five publications along with U.S. patents related to his work.

He received his B.S. degree in Petroleum Engineering from Louisiana State University, Baton Rouge, LA.

Mortada A. Alkadem

M.S. in Petroleum Engineering, King Fahd University of Petroleum and Minerals

Mortada A. Alkadem is a Senior Production Engineer working in the Hawiyah Production Engineering Unit of Saudi Aramco's Southern Area Production Engineering Department. He joined Saudi Aramco in 2012, and has over 11 years of experience in production engineering and reservoir management.

Mortada received his B.S. degree in Petroleum Engineering from the University of Leeds, Leeds, U.K., and his M.S. degree in Petroleum Engineering from King Fahd University of Petroleum and Minerals (KFUPM), Dhahran, Saudi Arabia.

Use of Logging while Drilling Data and Machine Learning to Predict Maximum Borehole Diameter for Multistage Completion

Khaqan Khan, Dr. Murtadha J. AlTammar, Rima T. Alfaraj and Rayan A. Alidi

Abstract /

Stress-induced borehole wall failure during the drilling of oil and gas wells can lead to an overgauged wellbore. Borehole instability can lead to an excessively enlarged wellbore and can increase the risk of drilling difficulties, and can also cause integrity issues for completions. For instance, there is a high probability of poor cementing or compromised zonal isolation across overgauged wellbore sections in cased and cemented completions or it can result in a loss of packers sealing in open hole multistage completions. Both of these inadequacies of poor cementing and insufficient packer sealing can jeopardize well stimulation operations. Therefore, knowing the accurate wellbore shape and diameter is critical for multistage well completion requirements.

While wireline multi-arm mechanical caliper tools can be run in an open hole after drilling to gain the direct measurement of a hole size, such measurements are not always possible due to prevailing drilling difficulties. Under such circumstances, making completion decisions become even more difficult with a higher risk of failure. Moreover, a solo wireline logging run to acquire caliper data requires additional cost, including rig time.

The objective of this article is to predict the synthetic caliper log using logging while drilling (LWD) measurements (notably azimuthal density and petrophysical properties) with the help of artificial intelligence (AI) and machine learning algorithms that can be used in place of wireline caliper data, thereby saving rig and logging costs, and thereby reducing overall field development expenditure.

This article presents the results of a machine learning algorithm used to predict the mechanical caliper logs using LWD data. Available LWD data for different wells were used to build a robust machine learning algorithm in Python. Different logging parameters from LWD were tested to quantify their sensitivity toward the caliper data and then predict the maximum hole diameter (Cmax) for different wells. The LWD data combines different parameters that have a direct effect on the caliper log with the machine learning model combining them for different wells to train the model and then predict the caliper log based on these parameters.

The parameters used in the prediction are gamma ray, four azimuthal photoelectric factors, sonic data, porosity, formation bulk density, four azimuthal formation densities, and mineralogy. The methodology is tested for horizonal wells drilled using a 5⅞" drill bit. The predicted caliper is compared with the measured caliper data so that it satisfies completion requirements for both multistage and cased hole completions.

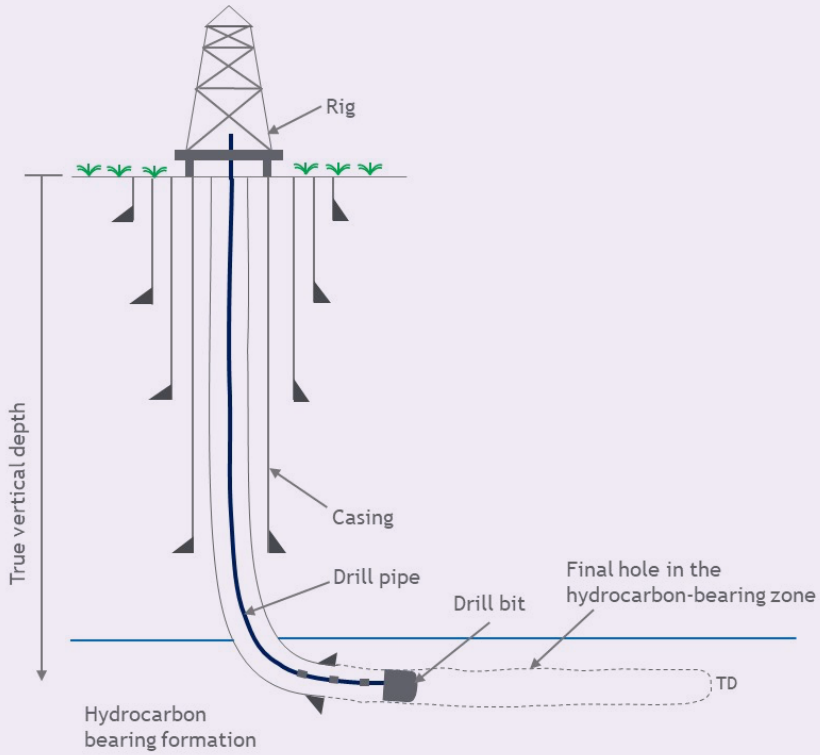
Introduction

Oil and gas extraction from subsurface rock formations requires drilling of wells using drilling rigs mounted on the ground surface or offshore rig platforms. The drilling process generates rock debris, which are carried to the surface with the help of circulating mud. As the bit advances further, the void (hole) created by the drill bit is filled with the drilling mud, which is lighter than the rock excavated. As a result, unbalanced Earth stresses are redistributed at the wellbore wall, which can cause compressive wellbore wall failure causing an enlarged wellbore.

The severity of wellbore wall failure depends on several factors, including the state of in situ Earth stresses, wellbore geometry, rock strength properties, formation pore pressure, and the density of the drilling mud. Depending on the depth of the hydrocarbon-bearing formation and other geological complexities, a well can have several hole sizes before it reaches its target depth, Fig. 1.

A steel pipe (casing) is lowered in each of these hole sections and cement slurry is pumped from the bottom up through the annular space between the pipe and the formation to ensure proper well integrity during production life of the well. The final hole size in the hydrocarbon-bearing formation can be completed using either a cased and cemented pipe, which is later perforated to access hydrocarbons or it may be completed

Fig. 1 *A schematic showing a horizontal well drilled into a hydrocarbon-bearing formation at a given true vertical depth below ground surface.*



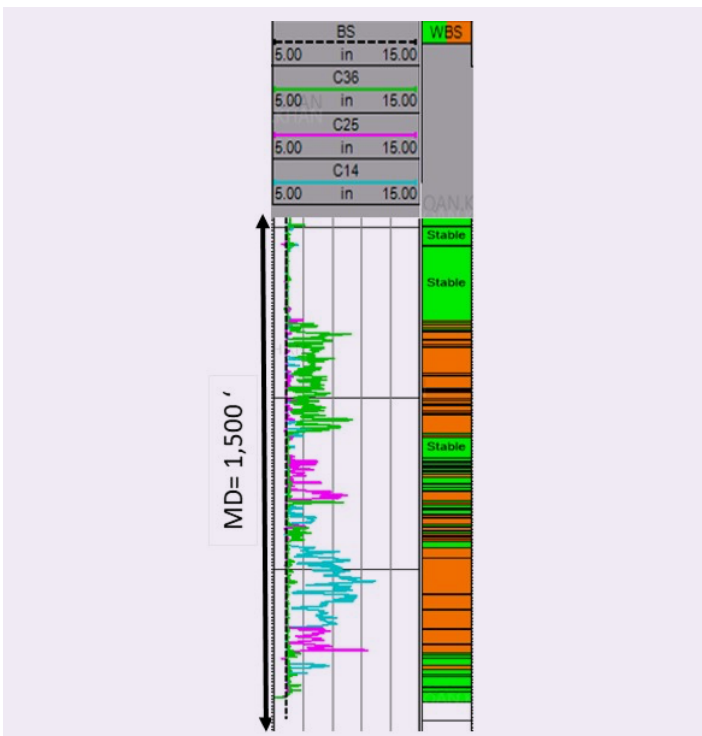
using a multistage open hole packers assembly. The open hole space between the set of packers can be stimulated through an injection port in each stage allowing hydrocarbons to flow to the surface.

An excessively enlarged wellbore wall cannot only pose a risk of drilling difficulties, but can also cause integrity issues for completions[1-3]. For instance, an overgauged wellbore may cause poor cementation in cased hole completions or improper sealing of packers in an open hole multistage fracturing (MSF) completions, which can jeopardize zonal isolation and well stimulation operations. In addition, the borehole diameter data is also used to calculate cement volume for well completion. Moreover, other measurements such as formation density are also affected by an excessively enlarged wellbore, and borehole diameter data is used to apply data corrections. Therefore, knowing the accurate wellbore diameter is crucial for a number of oil and gas well construction requirements.

Based on borehole diameter measurements, Fig. 2 shows an example of stable and unstable wellbore zones in a well. A multi-arm mechanical caliper tool was run across the open hole section to measure the shape of the wellbore. The caliper tool has six pads, which are separated by an in-plane angular displacement of 60°, continuously measures six independent hole radii at a resolution of 0.5 ft along the wellbore. After necessary data correction for tool eccentricity, the combined lengths of opposite pads provide three hole diameters (C14, C25, and C36) of the wellbore, Fig. 2 (first track from left).

A black dashed line in the caliper track represents bit size used to drill the well. Stable zones (green shaded regions) are

Fig. 2 *An illustration of wellbore stability using multi-arm caliper data (three diameters) over an interval of 1,500 ft in a well showing stable (green shade) and unstable (orange shade) zones.*



characterized when all three calipers indicate the hole size close to bit size. On the other hand, the wellbore is termed unstable when at least one of the hole diameters indicates a significantly enlarged wellbore as shown by caliper diameters. To ensure proper sealing of packers in open hole MSF completions, the maximum hole diameter should be equal to or less than 6.2”

Fig. 3 *A comparison of the calculated average borehole diameter from LWD measurements (DC_AVG) and Cmax from wireline measurements in three horizontal wells. The bit size (BS) is shown as black dash line. The first track from the left shows the gamma ray logs along the depth in the wellbore.*

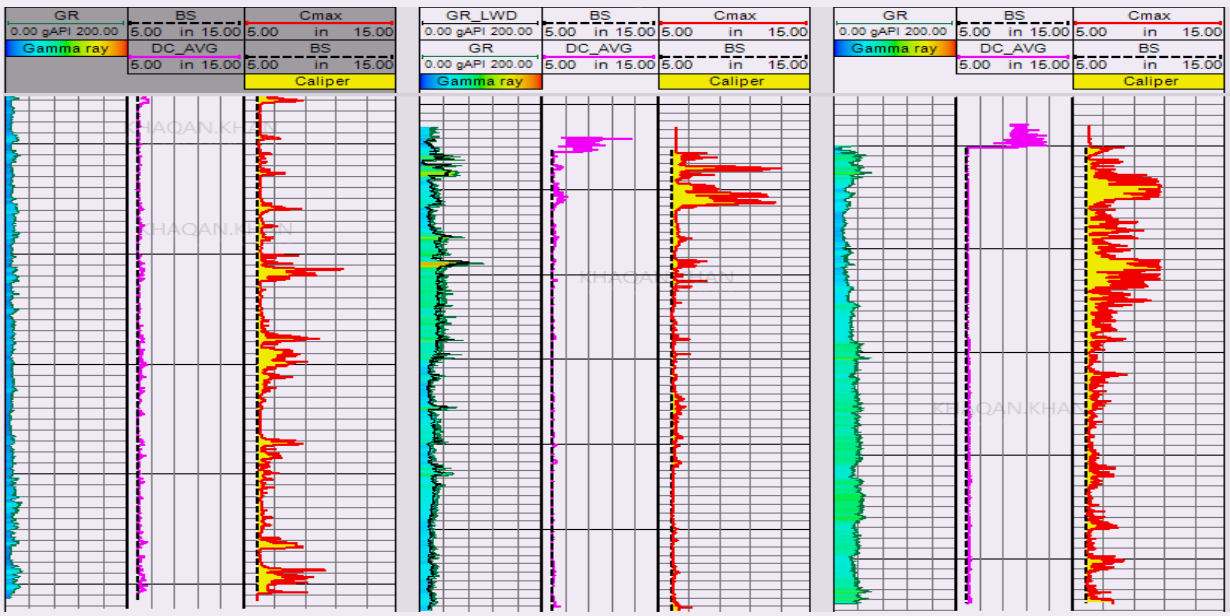
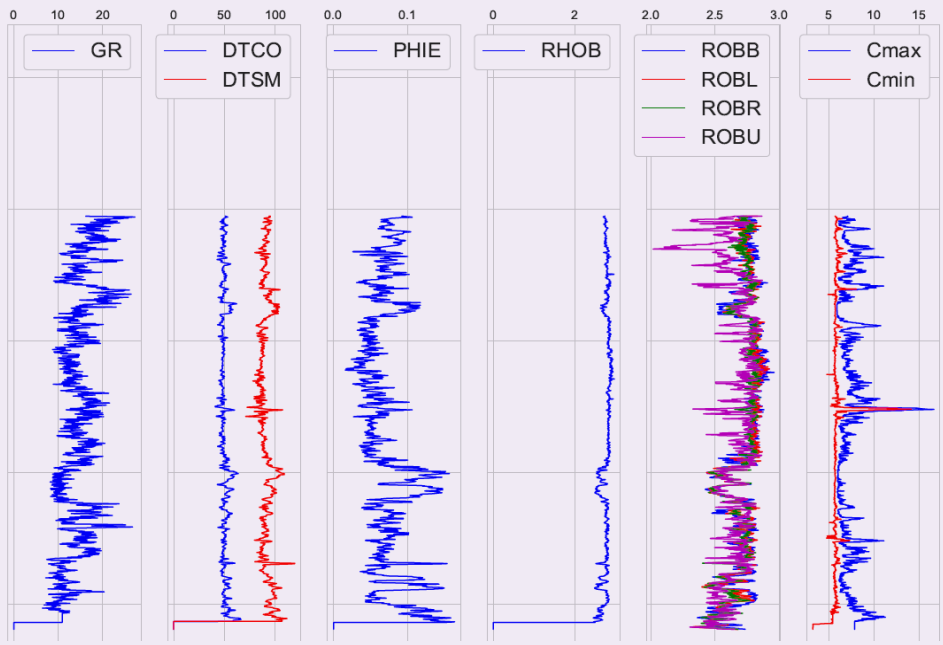


Fig. 4 *The log input data used in building the machine learning model. The input data also included four azimuthal photoelectric factors and volume fraction of dolomite, but these are not shown in this figure. In the model predictions, the wireline caliper data (Cmax and Cmin) were not included in the input.*



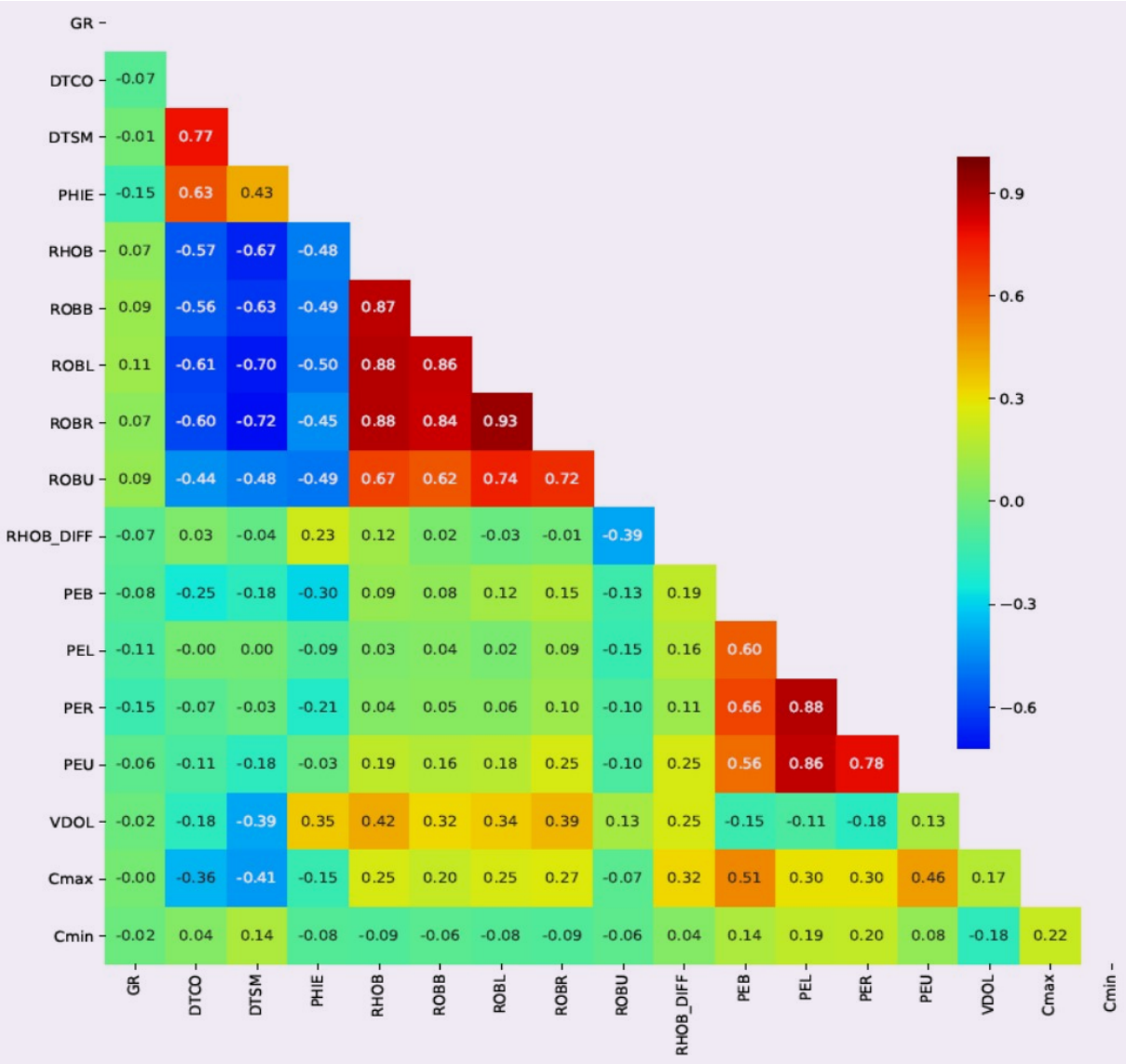
in a 5⅞" bit size for the currently available packers' technology.

Existing Techniques and their Limitations

Wireline and logging while drilling (LWD) are two broader categories of measurements to acquire downhole data in oil and gas wells. Wireline caliper tools are mechanical devices with multiple arms to measure hole shape and size. In their simplest form, such caliper tools can have at least four arms (a set of two arms 180° apart while the other set of two arms are orthogonal to the first arm) measuring two diameters on the wellbore wall. Other forms of these tools (6-arms providing three diameters or 8-arms providing four diameters at each depth) are also available in the industry. From the measured hole diameters, the maximum hole diameter calculated using multi-arm wireline caliper data (Cmax) and minimum (Cmin) hole diameters can be calculated at each depth. All data used in the current study use a 6-arm multi-arm caliper tool, i.e., three diameters, providing more accurate information of the hole shape.

The multi-arm caliper tools are run in the open hole after the drillstring is tripped out. While wireline caliper tools provide direct measurement of the hole size, these measurements are not only time-consuming, but may not always be possible, due to prevailing drilling difficulties or the risk of a stuck pipe. Apart from wireline, caliper data from other LWD measurements (density, resistivity, and acoustic) are also used in the industry; however, LWD-based calipers have several limitations. For instance, these measurements only provide an average caliper during drilling and may not be a true representative of the actual hole size required at the time of running completions. Consequently, for the placement of packers in open hole completions, a maximum hole diameter is required to identify stable wellbore zones to

Fig. 5 *A summary of different input parameters for the model with their correlation coefficients with other input parameters, including measured caliper data.*



achieve proper zonal isolation between successive stages.

In addition, drilling operations in the reservoir section can take several days in horizontal wells. Once the LWD sensor passes a certain depth, subsequent wellbore deterioration over time across this depth is seldom measured. Figure 3 shows a comparison of an average LWD density caliper (magenta curve in the second track from the left) and the wireline caliper (red curve in the third track from the left) in three horizontal wells. The caliper data is scaled from 5" to 15" and also displays the bit size used to drill the well, which is 5⅞" in this case. The yellow fill between the wireline caliper and the bit size indicates the extent of an overgauged wellbore.

The figure clearly demonstrates that LWD caliper underpredicts the hole diameter over most of the interval. The objective of this article is to build a machine learning algorithm capable of predicting a synthetic mechanical caliper using LWD measurements (notably azimuthal density and other petrophysical properties). The predicted caliper can be used in place of the LWD density caliper when wireline caliper data is missing to help reduce completion integrity risks.

Machine Learning Algorithm for Predicting Maximum Hole Diameter

Available LWD data from different wells were used to build the algorithm in Python. The algorithm is first trained using a range of LWD parameter data for different horizontal wells to quantify their sensitivity toward the measured wireline caliper data. The first step was to consider similar parameters in each well that will be used to train the data, the second step is cleaning, combining and splitting the data into training and testing datasets. The input parameters used in the model training include the gamma ray, four azimuthal photoelectric factors and four formation bulk densities, sonic travel-time, formation porosity and density, mineralogy, and measured wireline caliper data.

The azimuthal photoelectric and densities correspond to top, bottom, right, and left quadrants in the horizontal wellbore so that these measurements can reflect any borehole wall deterioration. Different modeling scenarios were used to find the model that can best fit the data to the actual caliper data. The model was trained using the XGBoost regressor modeling technique to predict the maximum caliper log data as this model showed the highest prediction score among others. The workflow steps used in the process are:

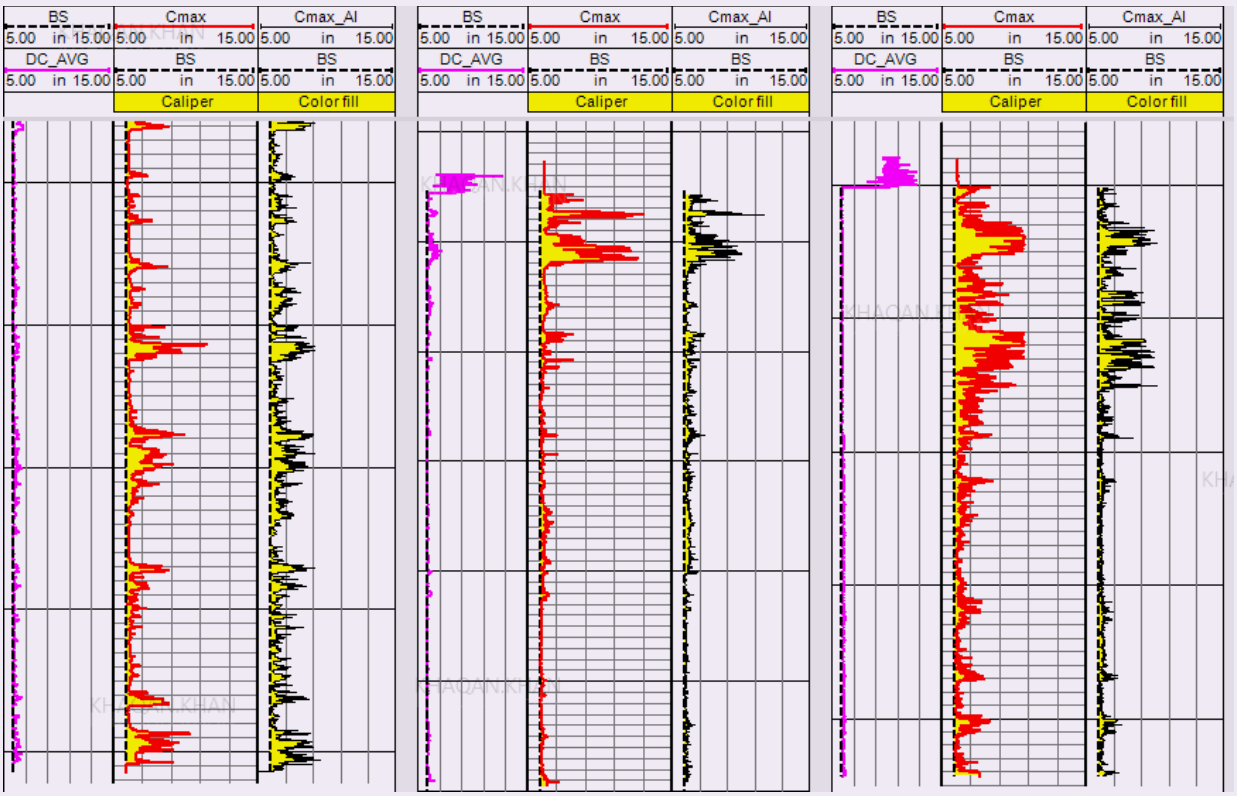
- Collect the LWD well data.
- Select the common parameters available in each well to use for training.
- Clean data in each well.
- Remove all missing entries from the dataset.
- Visualize the data of each well, Fig. 4.
- Combine the data of each well in one dataset for training.
- Set the data to have only 15 parameters in common: gamma ray (GR), four azimuthal photoelectric factors, compressional travel-time (DTCO), shear travel-time (DTSM), effective rock porosity (PHIE), formation bulk density (RHOB), azimuthal density data, including density at the bottom of the borehole (ROBB), density at the right side of the borehole (ROBR), density on the left side of the borehole (ROBL), density at the top of the borehole (ROBU), volume fraction of dolomite (VDOL), and Cmax, Fig. 5.

Table 1 *A summary of the root mean square error (RMSE), mean absolute error (MAE), and average absolute percentage error (AAPE) of the predicted and measured Cmax for a total of 17 wells in the training dataset where data from 16 wells was used for model training and the remaining one well was used for prediction.*

#	Well	Error between Measured and Predicted Maximum Hole Diameter		
		RMSE (in)	MAE (in)	AAPE (%)
1	D1	0.395	0.242	3.561
2	D2	0.664	0.495	7.278
3	D3	0.324	0.196	2.951
4	D4	0.687	0.387	5.148
5	D6	0.607	0.397	5.534
6	D7	0.839	0.642	8.834
7	D8	0.371	0.192	2.758
8	D9	1.103	0.900	12.637
9	D12	0.502	0.375	5.693
10	D14	0.769	0.476	6.269
11	D15	1.090	0.714	8.947
12	D20	0.783	0.455	6.087
13	D21	0.282	0.165	2.545
14	D22	0.670	0.503	7.925
15	D23	0.236	0.186	3.050
16	D24	0.341	0.240	3.852
17	D25	0.456	0.341	5.378
Mean:		0.595	0.406	5.791

- Use correlation coefficients to visualize the relationship between the LWD parameters and the caliper log.
- Set the 15 above-mentioned parameters as the x-variable that will be used in the model training.
- Set the caliper log (maximum logging data) as the y-variable that will be used in the predicting model.
- Divide the wells into training and testing wells — 17 wells were used for training and three as a blind well for testing.
- Train the model using available algorithms in Python.
- Predict the caliper log using a trained model.
- Test the model for selected wells to confirm robustness of the predictive model.
- Blind test the model predictions by comparing the Cmax from wireline data and the artificial intelligence (AI) predicted Cmax_AI caliper for selected wells.
- More details about the methodology and its application in different rock types can be found in AlTammar et al. (2022)[4] and (2023)[5].

Fig. 6 *A comparison of the average hole diameter from LWD (magenta curve), Cmax from the wireline data (red curve), and Cmax_AI predicted by the machine learning model (black curve).*



Model Validation Using Blind Wells Tests

The objective of predicting the caliper log for horizontal wells was to eliminate running wireline logs to help save logging and rig time cost to overall reduce field development cost. The methodology is tested for horizontal wells drilled using a 5⅞" drill bit along Shmin stress direction. The predicted caliper is compared with measured caliper data so that it satisfies requirements for both MSF and cased hole completions.

The trained model was used to predict the Cmax for different wells using the same input parameters that were used in building the model, excluding the measured wireline caliper data. The predicted Cmax using AI (Cmax_AI) was compared with the measured wireline Cmax, Fig. 6. As can be seen, the hole diameter predicted using AI model (black curve) compares very well with the measured hole diameter (red curve) using caliper tools whereas the LWD-based caliper (magenta curve) significantly underestimates the actual Cmax. The predicted caliper was used in several wells to make a completion decision, which were successfully stimulated without encountering any completion integrity issue.

Table 2 shows the average error of a predicted caliper (Cmax_AI) compared with the Cmax from the wireline for three wells, which are chosen for blind testing of the model. In the same table, the average error of the LWD density caliper (DC_AVG) compared with the Cmax from the wireline is also shown. Clearly, the predicted caliper is more accurate than the LWD caliper data. Well-2 had a largely stable wellbore across most of the logged interval, therefore, average errors from LWD and predicted calipers compared with Cmax are comparable. Moreover, in Wells-1 and 3 where the hole experienced more significant enlargements, the predicted caliper data is statistically more accurate and reliable than the LWD data when compared with the Cmax.

Satisfying Well Completion Requirements

The predicted Cmax_AI should meet the threshold limit for completion requirements, which is a wellbore overgauge limit of 0.3" or less for multistage open hole completions and less than or equal to 1" for cemented liner completions[6] to address the

Table 2 *The comparison of the average caliper of a predicted caliper and LWD caliper compared to the Cmax from the wireline for three blind wells.*

Well	Avg. Error (Cmax and Cmax_AI)	Avg. Error (Cmax and DC_AVG)
Well-1	-2.00%	10.60%
Well-2	-5.00%	3.60%
Well-3	3.90%	7.00%

integrity of completions during well stimulation. These requirements were tested using data from a LWD caliper, the Cmax from wireline caliper data, and the predicted Cmax_AI caliper.

Figure 7 shows the color-coded output of this analysis for three wells for open hole completions. The green shade represents the depths along the wellbore where the full integrity of the packers can be ensured, and therefore, provide adequate zonal isolation. On the other hand, the yellow fill indicates depths where the wellbore is overgauged more than the allowable limit, and therefore, not suitable for placing packers. The output for the LWD caliper, the wireline Cmax and Cmax_AI are displayed in Track-1, Track-2, and Track-3, respectively. It can be seen that the output based on Cmax_AI is closer to output from the wireline Cmax, whereas output from the LWD caliper has poor correlation with output of the Cmax. Subsequently, data from the Cmax_AI can be used with reliable results as an input for completion requirements.

Figure 8 shows the results of the integrity risk for the cemented liner completions using a similar color-coded output, where the green color shows minimal risk (wellbore overgauge 1" or less), and the red color shows a severe risk of liner integrity (hole enlarged more than 2") with intermediate colors indicating medium (yellow color) and high risk (magenta color) zones. Again, output based on the Cmax_AI closely matches with that from the Cmax over most of the logged section suggesting Cmax_AI can be used as a substitute of the wireline caliper data. The output from the LWD caliper underestimates the hole enlargements, and therefore, are not suitable for making decisions on completion integrity; however, the LWD caliper may still be useful for other applications such as monitoring hole conditions in real-time operations for making decisions on adjusting mud weight, etc.

Results of Field Implementation

The validated model was subsequently used to predict Cmax_AI using the acquired LWD data in several horizontal wells. No wireline caliper data was acquired in these wells. The predicted caliper was used to identity zones for the placement of packers in open hole MSF completions, or to provide a liner integrity risk assessment for cemented completions for optimizing perforation intervals.

Figure 9 is one example from these wells showing the predicted caliper and placement of the packers' flag. The predicted caliper suggests a largely stable wellbore enabling the completion of the well with eight stages in an open hole MSF completion. The well was successfully stimulated with excellent production results without having any integrity issues.

Fig. 7 *A comparison of stable wellbore for packers' placement depths (green shade) where the full packers integrity can be ensured using a LWD caliper (Track-1), the Cmax from wireline data (Track-2), and the predicted Cmax (Cmax_AI, Track-3) for three wells. Track-4 shows the lithology along the wellbore.*

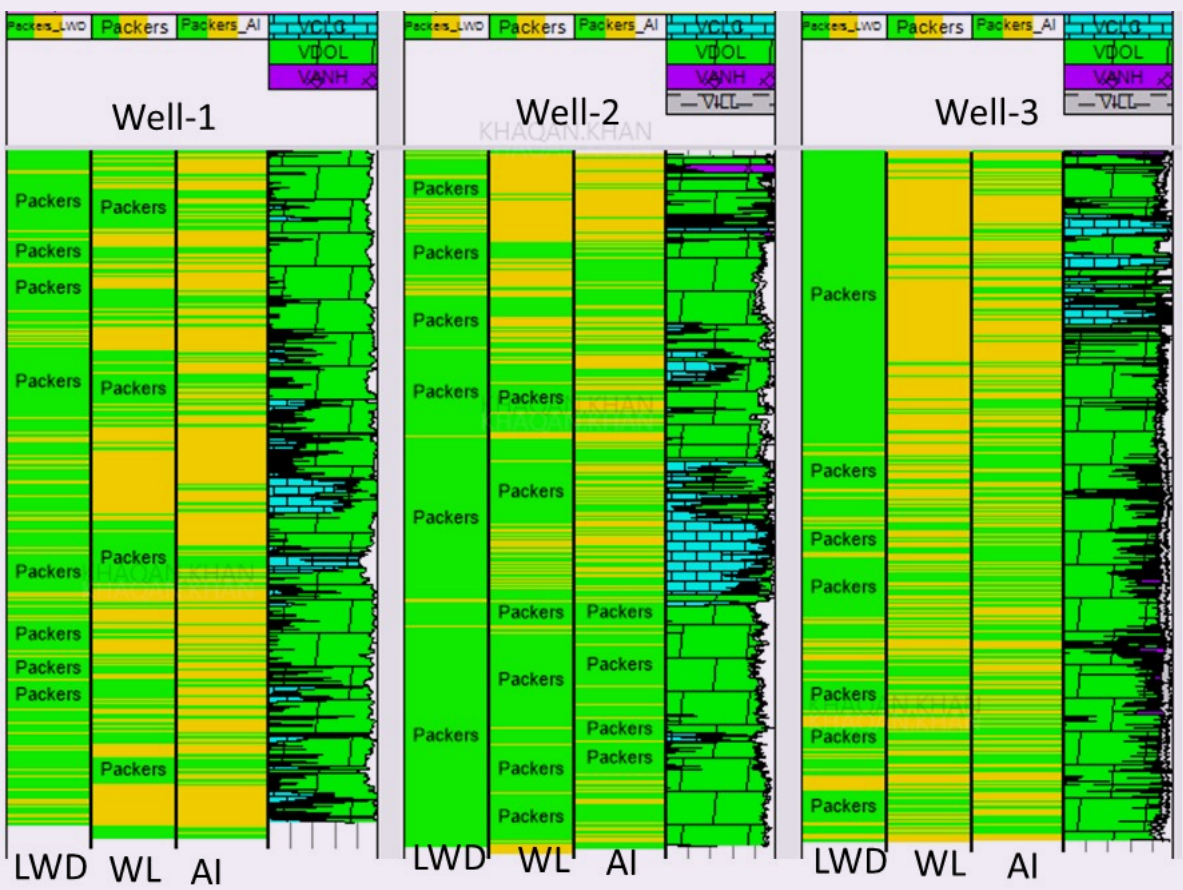
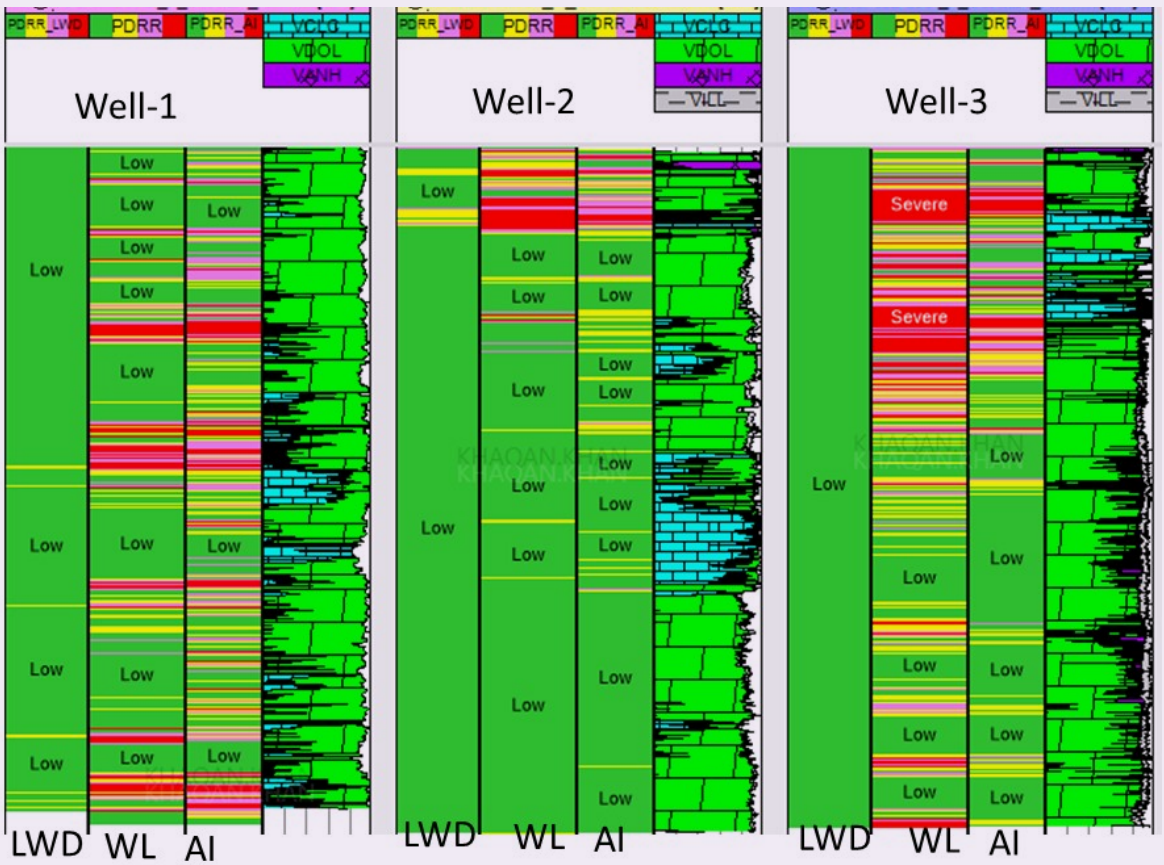


Fig. 8 *A comparison of liner integrity risk matrix based on LWD caliper (Track-1), Cmax from wireline data (Track-2), and predicted Cmax (Cmax_AI, Track-3) for three wells. Track-4 shows the lithology along the wellbore.*



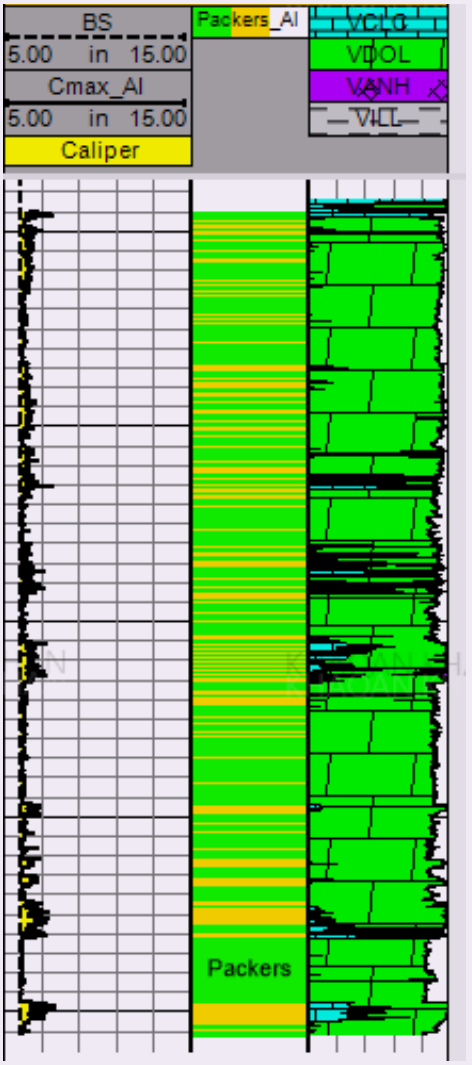
Conclusions

1. Wireline multi-arm caliper data is routinely used to calculate the Cmax, which is a critical input for making decisions in multistage completions for oil and gas wells.
2. Consequently, running multi-arm caliper tools bear extra data acquisition and rig time costs. Apart from cost, such tools cannot always be run in challenging drilling conditions due to the risk of stuck pipe, creating more uncertainties in well completion decisions.
3. This article presented an alternate innovative approach based on AI and machine learning to predict the Cmax using LWD data. The methodology, using the XGBoost machine learning algorithm, built a model utilizing different parameters from LWD data and measured wireline Cmax from a set of 17 horizontal wells.
4. The predicted caliper was rigorously tested using actual field data with excellent results, comparing very well with the measured wireline caliper data.
5. The synthetic caliper, based on validated machine learning models, is currently being used in place of a wireline caliper for well completion design. The analysis has been applied in more than 20 horizontal wells so far. Among these wells, several wells have already been stimulated without facing any well or completion integrity issue resulting in significant cost savings.
6. We also concluded that the DC_AVG from LWD significantly underestimates the actual borehole measurements, and therefore, cannot be used for well completion. Moreover, it can still be used as a qualitative assessment of wellbore stability during drilling.

Acknowledgments

This article was presented at the SPE/IATMI Asia Pacific Oil and Gas Conference and Exhibition, Jakarta, Indonesia, October 10-12, 2023.

Fig. 9 *An example showing the predicted Cmax using machine learning (black curve, Track-1 from left) and the stable zones for placement of packers (Track-2 from left) in a horizontal well enabling the completion and stimulation of the well using eight stages of open hole MSF completion.*



References

1. Ottesen, S. and Kwakwa, K.A.: "A Multidisciplinary Approach to In Situ Stress determination and Its Application to Wellbore Stability Analysis," SPE paper 21915, presented at the SPE/IADC Drilling Conference, Amsterdam, the Netherlands, March 11-14, 1991.
2. Chen, X., Tan, C.P. and Haberfield, C.M.: "A Comprehensive, Practical Approach for Wellbore Instability Management," *SPE Drilling and Completion,* Vol. 17, Issue 4, December 2002, pp. 224-236.
3. Kiran, R., Teodoriu, C., Dadmohammadi, Y., Nygaard, R., et al.: "Identification and Evaluation of Well Integrity and Causes of Failure of Well Integrity Barriers (A Review)," *Journal of Natural Gas Science and Engineering*, Vol. 45, September 2017, pp. 511-526.
4. AlTammar, M.J., Khan, K., Alfaraj, R.T., Altwaijri, M.H., et al.: "Prediction of Borehole Caliper Log Using Machine Learning for Multistage Frac Completions," paper ARMA-IGS-2022-077, presented at the International Geomechanics Symposium, Abu Dhabi, UAE, November 7-10, 2022.
5. AlTammar, M.J., Khan, K., Alfaraj, T.T., Alidi, R.A., et al.: "Use of Machine Learning to Predict Maximum Borehole Diameter for Multistage Frac Completions," paper URTEC-3852484, presented at the SPE/AAPG/SEG Unconventional Resources Technology Conference, Denver, Colorado, June 13-15, 2023.
6. Arshad, W. and Khan, K.: "Understanding the Key Factors Affecting Well Integrity in Horizontal Well Multistage Hydraulic Fracturing," SPE paper 213677, presented at the Middle East Oil, Gas and Geosciences Show, Manama, Kingdom of Bahrain, February 19-21, 2023.

About the Authors

Khaqan Khan

M.S. in Geotechnical Engineering, King Fahd University of Petroleum and Minerals

Khaqan Khan is a Geomechanics Subject Specialist with the Gas Geomechanics Studies Unit of Saudi Aramco's Gas Strategy & Technical Support Department. Since joining the company in 2012, his role has been to assist various aspects of field development activities focused on well planning, drilling, completions and stimulation.

Prior to joining Saudi Aramco, Khaqan worked with SLB, GeoMechanics International Inc. (GMI), and King Fahd University of Petroleum and Minerals (KFUPM).

During a career spanning more than 25 years, he has managed and technically led several consulting projects in the Middle East and elsewhere, focusing on the geomechanics aspects of reservoir management and field development.

Khaqan has written and coauthored several articles on the subject, including four U.S. patents, and has been actively involved in teaching and mentoring junior staff.

He received his M.S. degree in Geotechnical Engineering from KFUPM.

Dr. Murtadha J. AlTammar

Ph.D. in Petroleum Engineering, University of Texas at Austin

Dr. Murtadha J. AlTammar is a Lead Petroleum Engineer working with the Production Technology Team of Saudi Aramco's Exploration and Petroleum Engineering Center – Advanced Research Center (EXPEC ARC).

Previously, Murtadha worked in the field for 18 months as a Completion and Production Engineer with the Southern Area Gas Production Engineering Division.

He received the 2011 SAPED Significant Achievement Award for leading a well intervention campaign, and also the 2017 EXPEC ARC Best-in-Class Young Researcher Award. Murtadha was an invited speaker at the 2017 American Rock Mechanics Association (ARMA) Hydraulic Fracturing Workshop in San Francisco, CA.

He has been a technical reviewer for many journals. Murtadha has also been a member of organizing several technical committees for the Society of Petroleum Engineers (SPE) and ARMA conferences.

He received his B.S. degree in Petroleum Engineering from the Colorado School of Mines, Golden, CO. Murtadha received his M.S. degree and Ph.D. degree in Petroleum Engineering, specializing in hydraulic fracturing mechanics, from the University of Texas at Austin, Austin, TX.

Rima T. Alfaraj

B.S. in Petroleum Engineering, Colorado School of Mines

Rima T. Alfaraj joined Saudi Aramco in 2020, starting her career working as a Research Engineer with the Production Technology Team of Saudi Aramco's Exploration and Petroleum Engineering Center – Advanced Research Center (EXPEC ARC).

Rima explored different areas of the industry by working for one year as a Reservoir Engineer with the Gas Reservoir Management Department and as a Production Engineer when she worked for six months with the Northern Area Gas Production Engineering Department.

Her area of research focuses on rock characterization and wellbore stability, which includes understanding the properties of the rock, improving parameter estimation, and data calibration.

In 2020, Rima received her B.S. degree in Petroleum Engineering from the Colorado School of Mines, Golden, CO.

Rayan A. Alidi

M.S. in Petroleum Engineering, Colorado School of Mines

Rayan A. Alidi is currently the acting Manager for the Gas Reservoir Management Technical Studies Division of Saudi Aramco's Gas Strategy and Technical Support Department, where he leads a team of multidisciplinary subject matter experts that support the development of nonassociated gas reservoirs. He has 15 years of experience.

Since joining Saudi Aramco, Rayan has been involved in multiple applied projects dealing with reservoir stimulation, rock mechanics, and formation damage mitigation.

He received his B.S. degree in Petroleum Engineering with a minor in Geology from the University of Oklahoma, Norman, OK. Rayan then received his M.S. degree in Petroleum Engineering from Colorado School of Mines, Golden, CO, where he conducted research on how to improve the design of mud weight to support drilling operations.

Fracture Network Characterization Beyond Wellbores: A New Approach to Identify Water Corridors through Advanced Resistivity Analysis

Ida Bagus Gede Hermawan Manuaba, Mohammad K. Aljishi, Gagok I. Santoso and James T. Dolan

Abstract /

Carbonate rocks are often characterized as containing complex porosity systems from primary to secondary, and even intertwined multiporous systems. Consequently, this creates a challenge for petrophysicists and geologists with identifying the impact of such a complex system on a wells' productivity. This article studies delineating fracture network proximity and architecture beyond the wellbore and successfully identifying water corridors for completion enhancement.

This article presents a novel methodology for integrating wellbore centric micro-electrical borehole imaging with an ultra-high resolution bed boundary mapper (UHR-BBM)[1, 2]. The approach integrates the quantification and categorization of fractures around the wellbore acquired through a resistivity image, and fluid network in a radius of up to 30 ft around the wellbore derived from the UHR-BBM. The process encompasses a workflow starting from invasion profile determination to the UHR-BBM geosignals enhancement with fracture details prior to ultimately mapping their network extension and fluid characterization.

Advanced borehole analysis provided new insight into textural variations and lithofacies when analyzing the fractured zone, opening a gateway to incorporating geological features into the petrophysical analysis. Accordingly, it was observed that fractures could contribute an additional percentage of secondary porosity, improving the productivity index of such formation. Consequently, through conducting the aforementioned analysis, some of the fractures were featured as water driving factors when their proximity beyond the wellbore was uncovered. Moreover, resistivity analysis concluded that the water driving factors could have implications when the true resistivity affects the modeling process. Ultimately, the completion design shall be altered to isolate such zones, enhancing hydrocarbon recovery with minimized water cuts, as will be shown in one of the examples.

This methodology utilizes a new technique of incorporating shallow and deep measurements to quantify fracture systems, access their proximity to the wellbore, and determine their potential impact on the well's performance. This analysis facilitates a new approach to well completion design optimization, prolonging the life of the well and enhancing productivity.

Introduction

An analysis of the carbonate porosity system is quite complicated due to some layers being characterized by sporadic dolomitic intervals[3]. Additionally, some of the zones are characterized by widespread karst systems, which has important implications for water production management and completion design. Logging-while-drilling (LWD) data, including high resolution borehole images, are often used to characterize these fracture and karst systems for completion optimization purposes. It is important to note that LWD data acquired has a relatively shallow depth of investigation, therefore, cannot be used for fracture network mapping beyond the borehole.

On the contrary, azimuthal resistivity bed boundary mappers (BBMs) provide a means of identifying resistivity contrast of up to 30 ft around the wellbore, enabling the detection of water zones and corridors beyond the wellbore.

Geological Features Classification

The analysis revealed several geological features from the real-time interpretation. Subsequently, the memory data yielded superior quality due to omitting telemetry transmission limitations of the real-time image quality, facilitating the detection of a broader range of geological features.

In this analysis, we classified the geological features into eight classifications: (1) Bed boundary, (2) conductive fracture, (3) discontinue conductive fracture, (4) karst, (5) litho-bound fracture, (6) fault, (7) resistive fracture, and (8) vugular fracture.

Bed Boundaries

Bed boundaries identify transitions in layer properties, whether stratigraphic or structural dip change. The sedimentary dip is important in geosteering, geological mapping, and well design. Figure 1 shows that the bed boundary can be easily picked with a larger vertical section scale, e.g., 1:2. Consequently, finer features, such as fractures, faults, and karst, cannot be well-defined at this scale.

Fracture/Litho-Bound Fractures

Fractures represent natural breaks in rocks that can affect their physical properties and permeability. A litho-bound fracture is a type of fracture confined or limited by lithological boundaries, such as changes in rock type or compositional variations within a rock.

In a carbonate system, litho-bound fractures can occur due to variations in the rock's composition, texture, and depositional environment. For example, a litho-bound fracture in a carbonate sequence may occur where the rock transitions from a porous, well cemented limestone to a dense, poorly cemented dolomite. Figure 2 shows an example of litho-bound fractures crossing a

Fig. 1 *An example of the bed boundary dips on UHR images (green dashed line).*

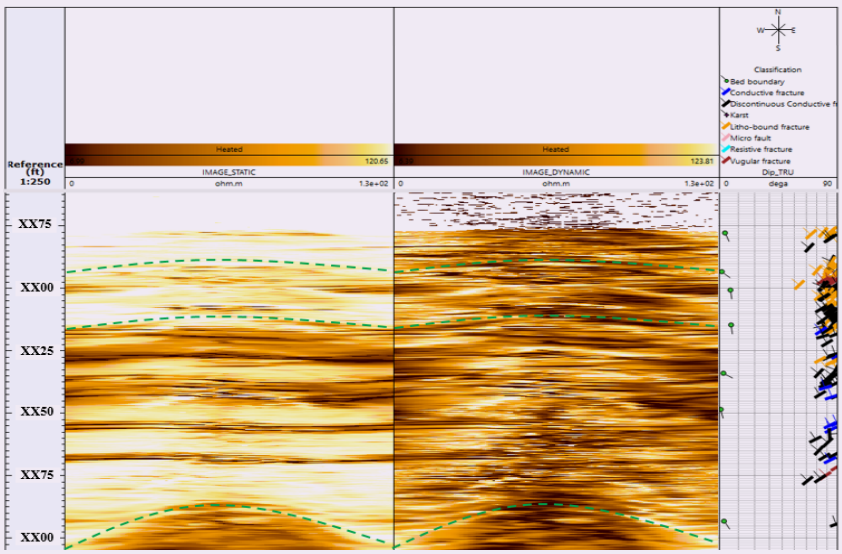
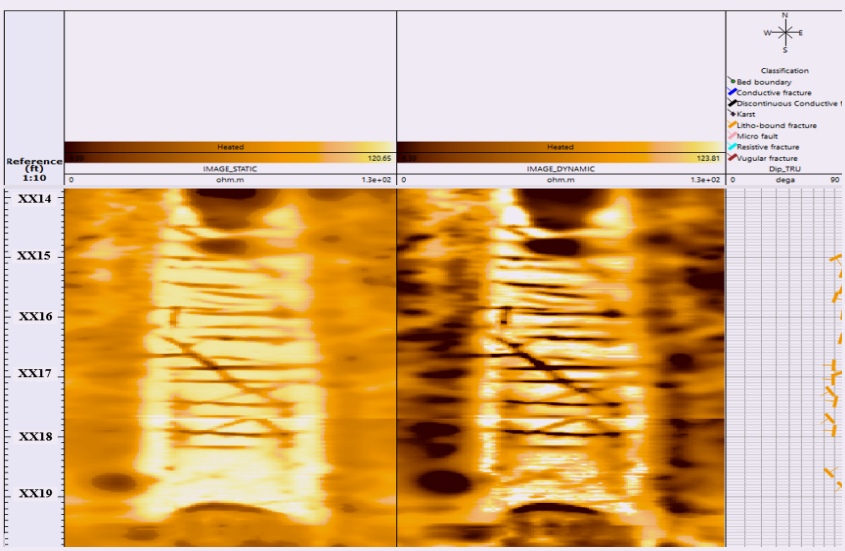


Fig. 2 *An example of litho-bound fractures. Litho-bound fractures can also occur due to sedimentary structures, such as bedding planes, laminations, or cross-bedding.*



highly laminated sedimentary sequence.

Conductive/Discontinuous Conductive Fractures

A conductive fracture is a type of fracture characterized by its high permeability, allowing efficient movement of fluids with relative ease. Conductive fractures are characterized by their ability to transmit fluids within rocks. These fractures can be highly conductive due to the presence of open voids or channels within the rock structure, Fig. 3.

A discontinuous conductive fracture is a fracture that does not extend continuously through the rock. These fractures can exist as isolated fractures or as fracture sets that are not interconnected, Fig. 4. Their limited connectivity restricts their impact on fluid flow through the rocks.

Vugular Fractures

In contrast, a vug is a small cavity or pore space within the rock, which may or may not be connected to other pore spaces.

Fig. 3 *An example of conductive fractures, which completely cross the wellbore image.*

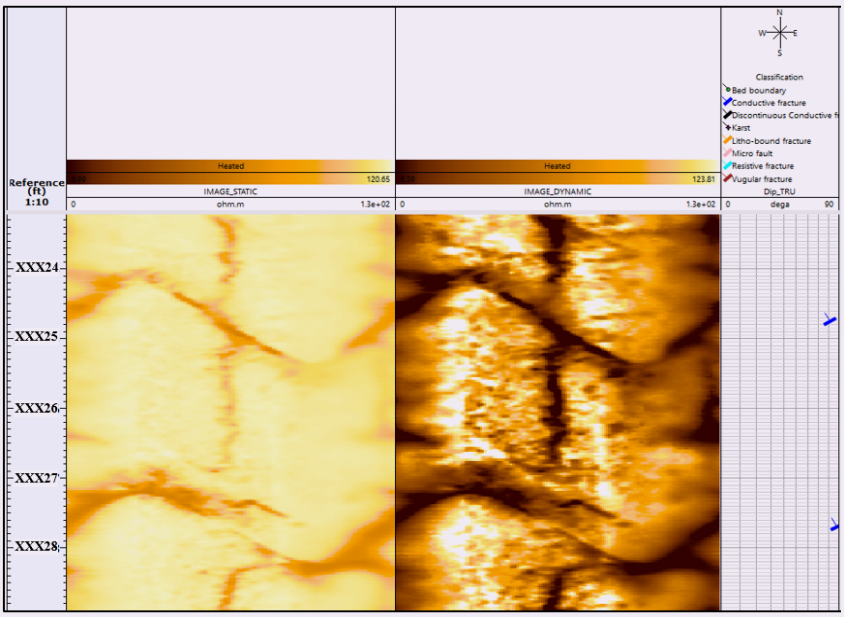
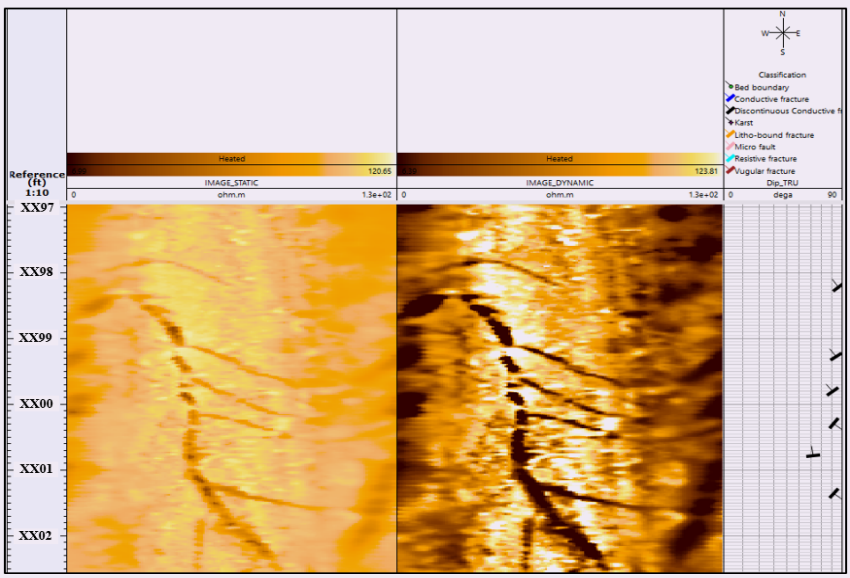


Fig. 4 *An example of discontinuous conductive fractures; it does not extend to the other layer.*



Vugs can occur naturally through the dissolution or erosion of the rock, or they can be created by the introduction of fluids or gases under pressure.

Vugs can also greatly enhance the porosity of the rock, but they may not be as interconnected as fractures. So, their impact on fluid flow and production may be more limited. Figure 5 is a vivid example of fractures taking the shapes of vugs, generally showing conductive features.

Technology Review

Wellbore Centric Micro-Electrical Borehole Imaging Processing

The laterolog resistivity borehole imager provides ultra-high resolution (UHR) images that detect features as thin as 0.5”[4]. The tool uses monitored button electrodes and toroidal antennas to produce focused laterolog resistivity measurements with azimuthal sensitivity, made at four depths of investigation to produce a standard 56-sector image with an axial resolution of l” for each of the four spacings: shallow, medium, deep, and extra-deep[5].

The multiple depth images are beneficial in cases of irregular boreholes and breakouts. The shallower images are mostly affected by borehole irregularities, while the deeper images are more sensitive to formation resistivity. Furthermore, the tool provides UHR imaging capability by utilizing an array of eight button electrodes (0.4” diameter buttons) on a removable sleeve.

Fig. 5 *An example of vugular fractures. These can occur naturally through the dissolution or erosion of the rock. In general, it has a conductive zone.*

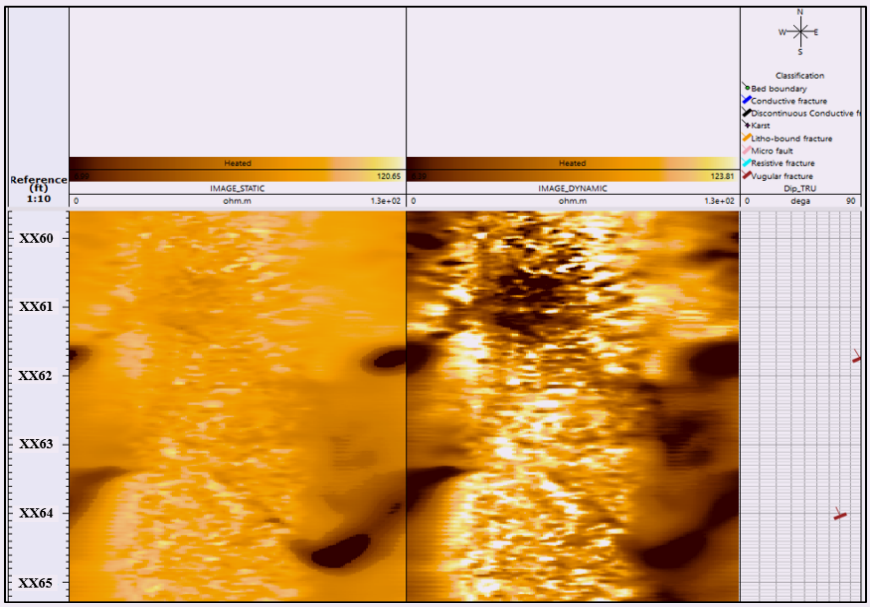
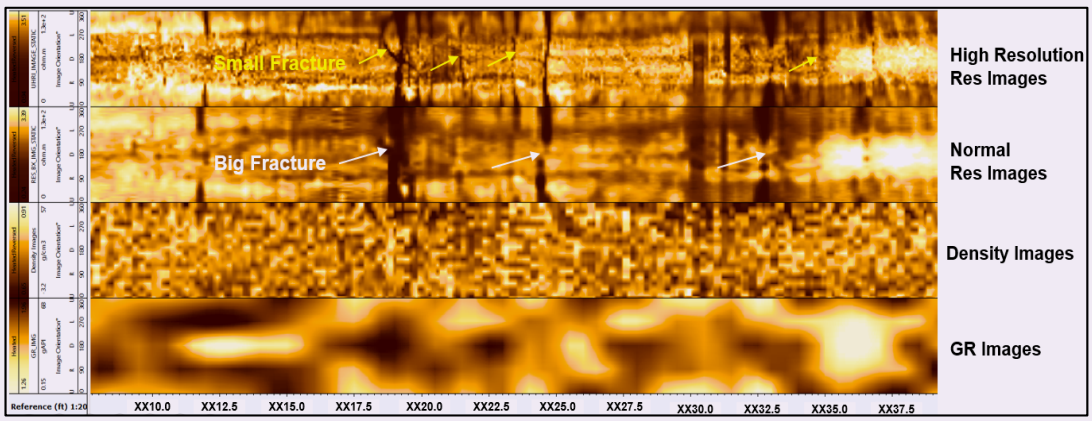


Fig. 6 *A comparison of four distinct resolutions of borehole imaging are presented, showcasing the versatility and capabilities of the laterolog resistivity borehole imager. UHR is required to resolve features below 1”.*



The resulting 160-sector image (pixel size 0.2*0.1") provides high resolution resistivity images comparable to those acquired by wireline tools. This level of resolution facilitates detailed quantitative evaluation of porosity, texture, facies, and fractures. In Fig. 6, four distinct resolutions of borehole imaging are presented, showcasing the versatility and capabilities of the laterolog resistivity borehole imager.

UHR-BBM

The technology of azimuthal resistivity BBM has been well described[6, 7]. The latest development of azimuthal propagation technology has six transmitters and four receivers that provide the directional measurements to enable multilayer inversions that map layer by layer while drilling. While five of the transmitters are axial, the sixth is transverse, and as such, has a sensitivity to anisotropy around the borehole[8].

New additions to the tool hardware and software provide additional and deeper azimuthal measurements that allow for new inversion methods to map around the wellbore[9]. The deterministic parametric inversion runs at sample points in a 1D layered formation model. It is defined with several formation parameters, including dip, layer thickness, horizontal resistivity, and anisotropy[8]. Figure 7 shows the progress of the technology revolution starting from simple near boundary mapping to the advanced UHR-BBM.

Water Corridor — Intertwined Multiporous Systems

The type of carbonate rock known for having several linked pores or voids at various scales that together form a complex and heterogeneous pore space network is referred to as an intertwined multiporous carbonate system. Calcite, aragonite, and dolomite are several minerals that make up a carbonate rock with a variety of textures and structures that are impacted by their deposition and diagenetic history.

This can contain a range of pore sizes that contribute to primary and secondary porosity, from micropores with a diameter of less than one micrometer to macropores with a diameter of several millimeters. Due to the complex geological event

Fig. 7 *The technology evolution from the first time BBM was invented in 2004, enhanced with HR-BBM in 2012, and then became UHR-BBM in 2021.*

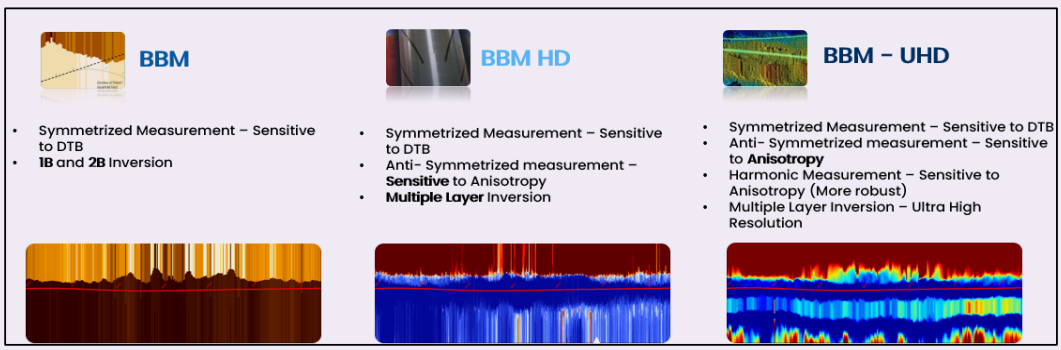
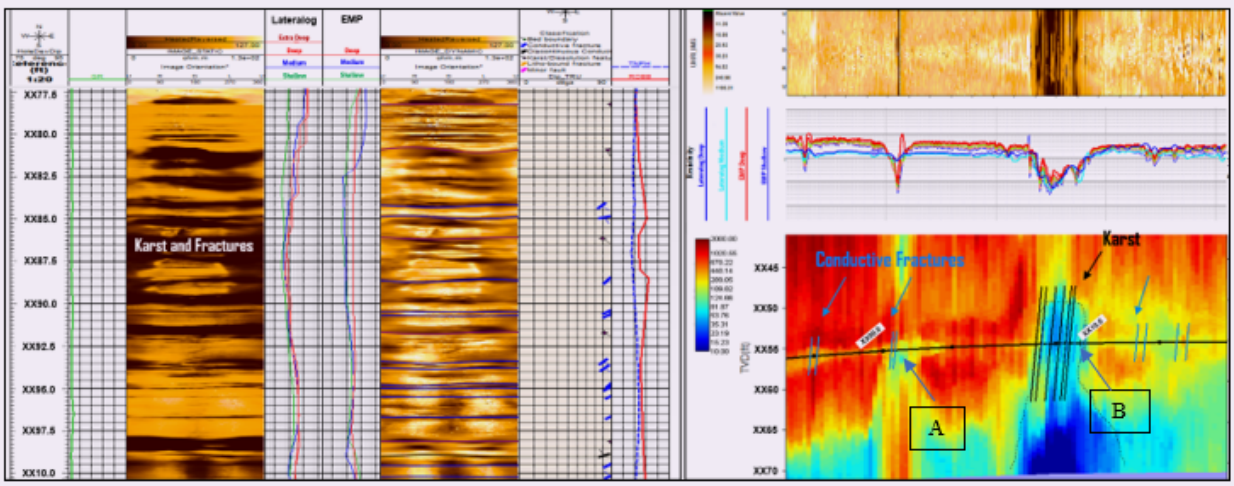


Fig. 8 *The presence of two water zones mapped below the wellbore using the BBM tools.*



that has altered the rock, the porosity and the permeability of interconnected multiporous systems can be very changeable, thereby challenging to characterize their properties accurately.

Figure 8 shows the presence of two water zones mapped below the wellbore using the BBM tools. Zone A displays a conductive boundary on the BBM inversion, indicating a contact point with the wellbore. This corresponds to a drop in the deep LWD electromagnetic propagation (EMP) resistivity, which has a depth of investigation (DOI) spanning several feet. Conversely, the shallower reading laterolog resistivity (DOI of several inches) exhibited minimal response, suggesting no water breakthrough into the wellbore during drilling.

Zone B reveals a more pronounced conductive zone in the inversion (representing lower resistivity in blue) intersecting the wellbore, accompanied by a significant drop in both EMP and laterolog resistivity curves. These observations indicate water breakthroughs during the time of drilling. Such valuable information can be applied to optimize the completion design and isolate this specific zone.

Examples of wellbores intersecting fractured and karst zones are shown in Fig. 9 and Fig. 10. In both examples, the conductive zones with fractures and karst zones are annotated, correlating to the same features on the ultra-high resistivity image. The karst zone in Fig. 9 is large enough to cause a drop in the electromagnetic resistivities that extend several feet into the formation. In Fig. 10, the BBM mapped a conductive zone close to the wellbore and where the conductive zones intersected the wellbore the well experienced lost circulation.

Fig. 9 *An example of the trajectory crossing a multifractured zone and karst. At the karst section, it shows a vertical connectivity of conductive fluid mapped by BBM.*

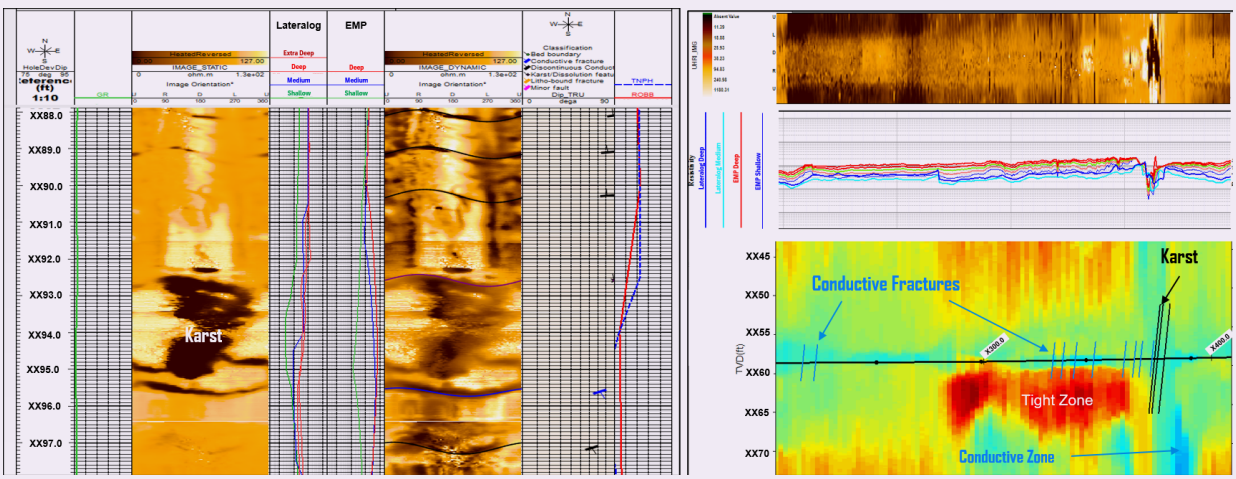


Fig. 10 *An example of the trajectory crossing a zone that experienced lost circulation. The conductive zone mapped by the BBM indicated some layer after being swept by the drilling fluid (conductive).*

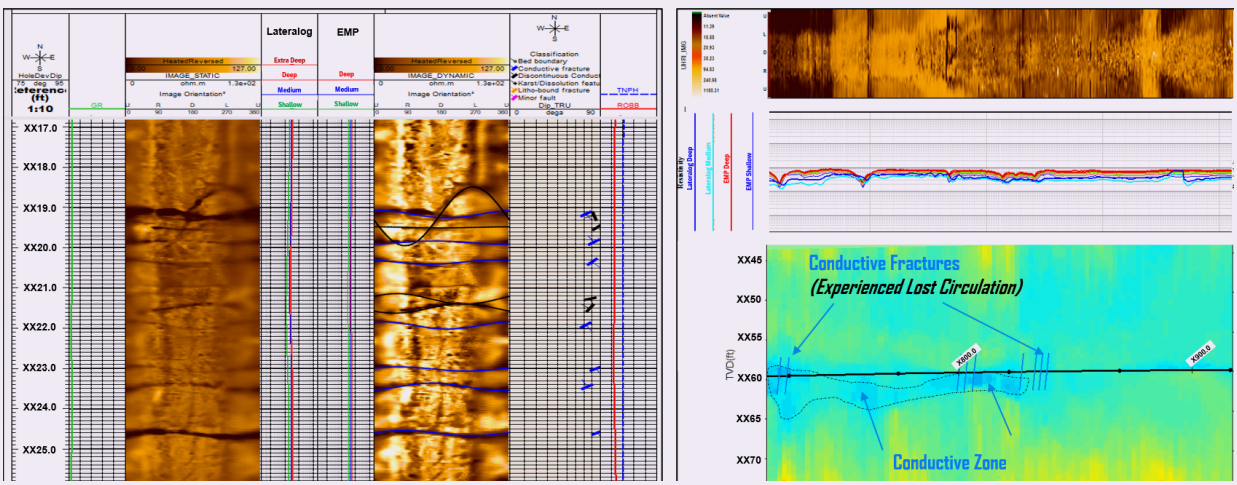
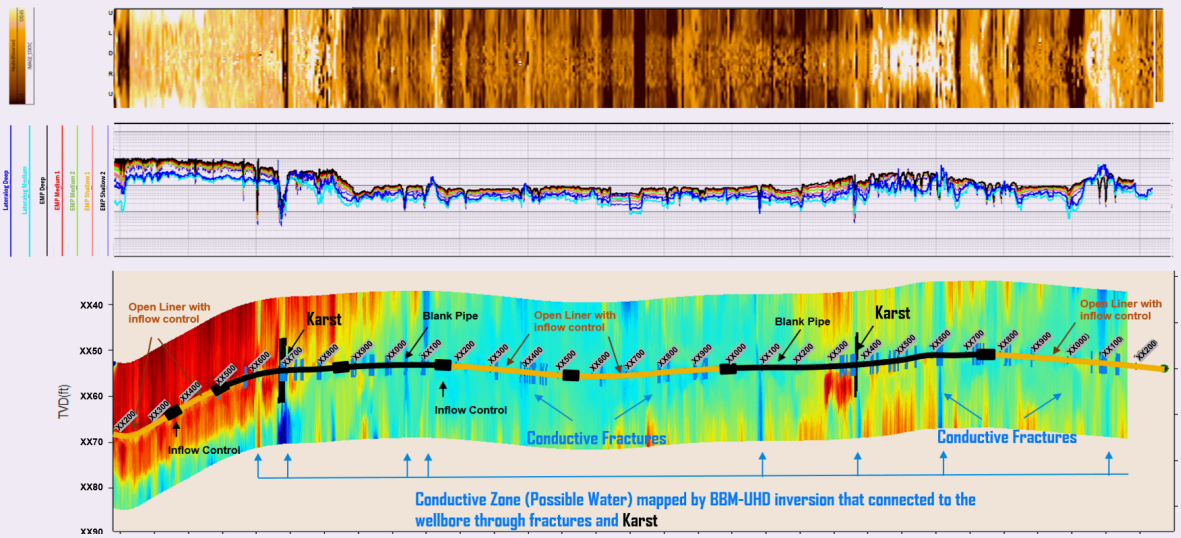


Fig. 11 *This indicates the whole interval of a horizontal section with completion design. The completion was optimized based on the water corridor finding.*



Completion Design

Based on the interpretation and analysis, certain fracture zones are identified as providing high permeability pathways. Optimizing completion and inflow control device placement based on fractures is an important aspect in maximizing the productivity of fractured rocks. One effective approach to achieve this is by utilizing a comprehensive fracture and rock model incorporating a high resolution BBM and high resolution resistivity images, Fig. 11. The optimization of the completion design is optimized from different zones in the rock structure, which can help to prevent early water breakthroughs and improve the overall sweep efficiency.

By strategically placing completion equipment and optimizing the flow paths, the productivity and performance of the fractured rock can be significantly improved.

Conclusions

This article provides a valuable insight in carbonate characterization, expanding our understanding vicinity from the near wellbore extended up to 30 ft away from the wellbore. While traditionally used mainly for fracture and geological information, borehole images when integrated with BBMs allows us to extend our understanding of layer by layer scale enabled by the high resolution resistivity contrast.

Future studies shall be geared toward a 3D mapping technology for a full understanding of fluid movement around the wellbore and away from the borehole. By encompassing 360° perspectives, these advanced techniques will enable a full understanding of fluids behavior inside the layers, and ultimately, facilitate more accurate management decisions.

Acknowledgments

We would like to thank Mustafa A. Mubarak, SLB senior geologist, for his support in supplying all geological interpretations for this study.

This article was presented at the SPE Annual Technical Conference and Exhibition, San Antonio, Texas, October 16-18, 2023.

References

1. Xiu, H., Sun, K., Gremillion, J., Mirto, E., et al.: "An Advanced Ultra-High Definition Directional Electromagnetic Propagation Logging Tool for Mapping while Drilling and Multilayered Formation Evaluation," paper presented at the SPWLA 63rd Annual Logging Symposium, Stavanger, Norway, June 11-15, 2022.
2. Dong, C., Dupuis, C., Morriss, C., Legendre, E., et al.: "Application of Automatic Stochastic Inversion for Multilayer Reservoir Mapping while Drilling Measurements," SPE paper 177883, presented at the Abu Dhabi International Petroleum Exhibition and Conference, Abu Dhabi, UAE, November 9-12, 2015.
3. Al-Mudhhi, M., Ma, S.M., Al-Hajari, A., Lewis, K., et al.: "Geo-Steering with Advanced LWD Technologies — Placement of Maximum Reservoir Contact Wells in a Thinly Layered Carbonate Reservoir," paper presented at the International Petroleum Technology Conference, Doha, Qatar, November 21-23, 2005.
4. Allouche, M., Chow, S., Dubourg, I., Ortenzi, L., et al.: "High Resolution Images and Formation Evaluation in Slim Holes from a New Logging-while-Drilling Azimuthal Laterolog Device," SPE paper 131513, presented at the SPE EUROPEC/EAGE Annual Conference and Exhibition, Barcelona, Spain, June 14-17, 2010.
5. Hermawan Manuaba, I.B.G., Aljishi, M., van Steene, M. and Dolan, J.: "LWD Laterolog vs. Electromagnetic Propagation Measurements: Which is Telling the True Resistivity?" IPTC paper presented at the International Petroleum Technology Conference, Bangkok, Thailand, March 1-3, 2023.
6. Li, Q., Omeragic, D., Chou, L., Yang, L., et al.: "New Directional Electromagnetic Tool for Proactive Geosteering and Accurate Formation Evaluation while Drilling," paper presented at the SPWLA 46th Annual Well Logging Symposium, New Orleans, Louisiana, June 26-29, 2005.
7. Omeragic, D., Li, Q., Chou, L., Yang, L., et al.: "Deep Directional Electromagnetic Measurements for Optimal Well Placement," SPE paper 97045, presented at the SPE Annual Technical Conference and Exhibition, Dallas, Texas, October 9-12, 2005.

8. Sun, K., Thiel, M., Mitro, E., Tan, S., et al.: "New Generation of Ultra-High Definition Directional Propagation Resistivity for Real-Time Reservoir Characterization and Geosteering-while-Drilling," SPE paper 204739, prepared for presentation at the SPE Middle East Oil and Gas Show and Conference, event canceled, November 28-December 1, 2021.

9. Xu, Y., Omeragic, D., Thiel, M., Dua, R., et al.: "A Novel High Definition Inversion of Deep Directional Electromagnetic Measurements while Drilling Enhances Layered Reservoir Mapping," paper presented at the SPWLA 59th Annual Logging Symposium, London, U.K., June 2-6, 2018.

About the Authors

Ida Bagus Gede Hermawan Manuaba

M.S. in Petroleum Engineering, Heriot Watt University

Ida Bagus Gede Hermawan Manuaba is a Lead Petroleum Engineer/Petrophysicist working in the Southern Area Petrophysics Unit of the Saudi Aramco's Reservoir Description and Simulation Department. He has over 25 years of experience in the oil and gas industry. Previously, Ida Bagus worked for several leading service providers, including Western Atlas, Baker Hughes, Precision Energy Services, and Weatherford, holding roles such as Wireline Engineer, Logging while Drilling (LWD) Engineer, and Directional Driller.

He specializes in LWD technologies and interpretation, serving as a subject matter expert. Ida Bagus has taught a Well Log Applications and Operations course at the Aramco Upstream Professional Development Center, and has published a number of articles.

In 2016, he obtained his Society of Petroleum Engineers (SPE) certification. Ida Bagus served as Secretary General in the Indonesian Petroleum Engineers Association-KSA chapter (IATMI-KSA) from 2017 to 2019 and was elected as President, serving from 2019 to 2021.

He received his Engineers Professional Program accreditation from PPI (Persatuan Insinyur Indonesia) in 2022.

In 1997, Ida Bagus received his B.S. degree in Petroleum Engineering from Bandung Institute of Technology, Bandung, Indonesia. He received his M.S. degree in Petroleum Engineering from Heriot-Watt University, Edinburgh, Scotland, U.K.

Mohammad K. Aljishi

B.S. in Petroleum Engineering, Louisiana State University

Mohammad K. Aljishi is a Petroleum Engineer working in the Southern Area Petrophysics Unit of Saudi Aramco's Reservoir Description and Simulation Department. With over five years of experience in the oil and gas industry, he leads formation evaluation efforts for major oil fields, optimizing the development plans using advanced logging data.

With expertise spanning drilling, production engineering, and formation evaluation, Mohammad demonstrates versatile proficiency in multiple industry domains. He has contributed significantly to innovative solutions, coauthoring patents related to sidetracking operations and formation damage removal methods, and publishing several papers.

Mohammad is an active member of several professional societies, including the Society of Petroleum Engineers (SPE) and the Society of Petrophysicists and Well Log Analysts (SPWLA). He was awarded his SPE certificate in 2022. Mohammad is currently serving as the Vice President for Planning and Strategy in the SPWLA Saudi Arabia Chapter, where he guides the vision of the chapter and planning of technical events.

In 2018, Mohammad received his B.S. degree in Petroleum Engineering from Louisiana State University, Baton Rouge, LA.

Gagok I. Santoso

B.S. in Naval Architecture Engineering, Sepuluh Nopember Institute of Technology

Gagok I. Santoso is Geosteering and Reservoir Domain Champion at Schlumberger, Saudi Arabia. He has more than 21 years of experience working in Schlumberger well construction, and has held various technical and leadership positions with the company, including 15 years as a Geosteering and Reservoir Mapping Subject Matter Expert. Gagok currently provides technical support and services for Well Placement Services to Saudi Aramco.

He has worked on various projects related to drilling measurements and geosteering in Southeast Asia, China, West Africa, the Middle East, the U.S., and the North Sea.

In 1999, Gagok received his B.S. degree in Naval Architecture Engineering from the Sepuluh Nopember Institute of Technology, Surabaya, Indonesia.

James T. Dolan

M.S. in Geology, Victoria University of Wellington

James T. Dolan is a Principal Petrophysicist at SLB. His current assignment is as Domain Champion supporting logging while drilling (LWD) petrophysics, geosteering, and reservoir mapping services for offshore projects in Saudi Arabia. Of his 23 years in the industry, 20 have been with SLB.

Since joining SLB, James has had worked as a LWD Field Engineer, Geosteering Engineer, and Petrophysicist. He has extensive experience in both conventional and unconventional reservoirs and has held several assignments in Australasia, Scandinavia, Europe, and Saudi Arabia.

James received his M.S. degree in Geology from Victoria University of Wellington, Wellington, New Zealand.

There is more.

Performance of Matrix Acid Stimulation Corrosion Inhibitors: Effect of Treatment Conditions and Acid Additives

Ali A. Al-Taq, Abdullah A. Al-Rustum, Ali H. Alsalem and Dr. Luai A. Alhamad

Abstract / Hydrochloric (HCl) acid solutions at 15 wt% to 28 wt% are commonly used in the stimulation of water, gas, and oil wells to remove formation damage and restore/enhance well productivity/injectivity. A corrosion inhibitor is one of the most imperative additives added to the acid system to inhibit its corrosivity, maintain its integrity, and avoid associated safety and economic problems. In addition to the corrosion inhibitor, several additives are commonly used in acid recipes for different purposes and objectives.

Hydraulic Fracturing of Highly Azimuthally Deviated Horizontal Wells Enhanced by Wellbore Notching

Dr. Murtadha J. AlTammar, Dr. Khalid M. Alruwaili, Hussain K. Al-Dakheel, Dr. Gallyam Aidagulov and Dr. Mustapha Abbad

Abstract / Multistage hydraulic fracturing is an effective stimulation method, as it communicates wellbore to larger reservoir volume. Nevertheless, there are cases where the formation cannot be fractured within the completion pressure limitations. This problem can be addressed by placing weak points, such as perforations and notches, so fractures could initiate at a lower pressure. This article discusses this remedy applied in horizontal open holes that are highly deviated from the minimum horizontal stress (σ_h).

Overcoming the Obstacle of Reservoir Stimulation through ICD Completion — The World's First Approach of Valvular Conduit for Inflow and Outflow Control Devices

Ikhsan Nugraha, Ahmed Siham, Danang R. Widjaja and Hussain A. Al Nasir

Abstract / Horizontal wells often require production control along the open hole. This is achieved by installing appropriate inflow control device (ICD) configurations that introduce higher restrictions across flow dominant zones and less restrictions across poorer quality zones, respectively. Although these restrictions are designed to allow normalized production across the entire horizontal section, they can adversely impact the control of injection rates across the horizontal section during acid stimulation jobs.

An Innovative Machine Learning Method for Predicting Well Performance in Unconventional Reservoirs with a Relatively Small Dataset

Dr. Hui-Hai Liu, Jilin J. Zhang, Cenk Temizel and Moemen A. Abdelrahman

Abstract / The machine learning method, now widely used for predicting well performance from unconventional reservoirs in the industry, generally needs large datasets for model development and training. The large datasets, however, are not always available, especially for newly developed unconventional plays. The objective of this work is to develop an innovative machine learning method for predicting well performance in unconventional reservoirs with a relatively small dataset.

Notes



Aramco
Journal
of Technology